INSTITUTO POTOSINO DE INVESTIGACIÓN CIENTÍFICA Y TECNOLÓGICA, A.C.

POSGRADO EN CIENCIAS APLICADAS

Adsorption of inorganic priority pollutants in water by tailored lignocellulosic and carbonaceous adsorbents.

Tesis que presenta

Litza Halla Velázquez Jiménez

Para obtener el grado de

Doctor en Ciencias Aplicadas

en la opción de

Ciencias Ambientales

Director de la Tesis:

Dr. José René Rangel Méndez

San Luis Potosí, S.L.P., Febrero de 2014

IPICYT

Constancia de aprobación de la tesis

La tesis *"Adsorption of inorganic priority pollutants in water by tailored lignocellulosic and carbonaceous adsorbents"* presentada para obtener el Grado de Doctora en Ciencias Aplicadas en la opción de Ciencias Ambientales fue elaborada por **Litza Halla Velázquez Jiménez** y aprobada el **veintiocho de febrero de dos mil catorce** por los suscritos, designados por el Colegio de Profesores de la División de Ciencias Ambientales del Instituto Potosino de Investigación Científica y Tecnológica, A.C.

Dr. José René Rangel Méndez
Director de la tesis

Dr. Felipe Alatriste Mondragón
Miembro del Comité Tutoral

Dra. María Catalina Alfaro de la Torre
Miembro del Comité Tutoral

Dr. Ramón Fernando García de la Cruz
Miembro del Comité Tutoral

I

Créditos Institucionales

Instituto Potosino de Investigación Científica y Tecnológica, A.C.

Acta de Examen de Grado

El Secretario Académico del Instituto Potosino de Investigación Científica y Tecnológica, A.C., certifica que en el Acta 024 del Libro Primero de Actas de Exámenes de Grado del Programa de Doctorado en Ciencias Aplicadas en la opción de Ciencias Ambientales está asentado lo siguiente:

En la ciudad de San Luis Potosí a los 28 días del mes de febrero del año 2014, se reunió a las 12:30 horas en las instalaciones del Instituto Potosino de Investigación Científica y Tecnológica, A.C., el Jurado integrado por:

Dr. Felipe Alatriste Mondragón	Presidente	IPICYT
Dra. María Catalina Alfaro de la Torre	Secretario	UASLP
Dr. José René Rangel Méndez	Sinodal	IPICYT
Dr. Ramón Fernando García de la Cruz	Sinodal externo	UASLP

a fin de efectuar el examen, que para obtener el Grado de:

DOCTORA EN CIENCIAS APLICADAS
EN LA OPCION DE CIENCIAS AMBIENTALES

sustentó la C.

Litza Halla Velázquez Jiménez

sobre la Tesis intitulada:

Adsorption of inorganic priority pollutants in water by tailored lignocellulosic and carbonaceous adsorbents

que se desarrolló bajo la dirección de

Dr. José René Rangel Méndez
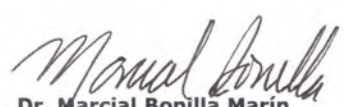
El Jurado, después de deliberar, determinó

APROBARLA

Dándose por terminado el acto a las 15:30 horas, procediendo a la firma del Acta los integrantes del Jurado. Dando fe el Secretario Académico del Instituto.

A petición de la interesada y para los fines que a la misma convengan, se extiende el presente documento en la ciudad de San Luis Potosí, S.L.P., México, a los 28 días del mes de febrero de 2014.

Dr. Marcial Bonilla Marín
Secretario Académico

Mtra. Ivonne Lizette Cuevas Vélez
Jefa del Departamento del Posgrado

INSTITUTO POTOSINO
DE INVESTIGACION
CIENTÍFICA Y TECNOLOGICA, A.C.

IPICYT
SECRETARIA ACADEMICA

Página en Blanco que se utilizará para colocar la **COPIA DEL ACTA DE EXAMEN**.

Dedicatorias

Dedico este trabajo a mis padres y hermano, por su apoyo incondicional y porque han contribuido a la culminación de esta meta propuesta.

A mi esposo, por permitirme crecer juntos con momentos inolvidables y enseñanzas que se reflejan en lo personal y profesional.

A mis compañeros y amigos que siempre han estado presentes cuando los necesito: Alma, Javier, Carlos, Eduardo, Héctor, Erika, Maricruz, Jorge, Claudia, Emilia, José Luis, Cesar, Guillermo, Megan y todos que no fueron nombrados aquí, pero que también ayudaron a cumplir esta meta. Por todos los buenos y malos momentos que hemos pasado juntos.

¡MUCHAS GRACIAS A TODOS CON LOS QUE TENGO EL HONOR DE COMPARTIR LA VIDA!

Agradecimientos

Table of Contents

Chapter 2

CHEMICAL CHARACTERIZATION OF RAW AND TREATED AGAVE BAGASSE AND ITS POTENTIAL AS ADSORBENT OF METAL CATIONS FROM WATER.

Abstract

xi

List of Tables

xiii

List of Figures

Resumen

Adsorption of inorganic priority pollutants in water by tailored lignocellulosic and carbonaceous adsorbents

En México se conocen 17 entidades del país que poseen fuentes de abastecimiento de agua con altos niveles de cadmio, plomo, fluoruro y zinc, que exceden el límite permisible establecido por la NOM-127-SSA1-1994. Diversos tratamientos para eliminar o reducir estos contaminantes han sido usados, sin embargo, involucran la mayoría de las veces altos costos de operación y mantenimiento. No obstante, el uso de adsorbentes diseñados específicamente para remover estos elementos representa una alternativa viable y con gran futuro en procesos de tratamiento de agua.

El bagazo de *Agave salmiana* (sub-producto de la industria mezcalera) puede ser usado como adsorbente para remover iones metálicos contenidos en agua. Sin embargo, la capacidad de adsorción de este material puede ser incrementada modificando químicamente su superficie, para aumentar los grupos funcionales implicados en la remoción de estas especies iónicas. Por otra parte, la alúmina activada es generalmente usada para remover fluoruro (F^-) de abastecimientos de agua por su gran afinidad y capacidad de adsorción. No obstante, el uso de este adsorbente no es recomendado debido a que provoca afección a la salud humana por el desprendimiento de aluminio. El carbón activado representa una alternativa para remover fluoruro del agua, pero su baja capacidad de adsorción debido a la pobre afinidad por este anión sugiere modificar su superficie carbonosa con oxo(hidróxidos) metálicos.

Este trabajo de investigación fue dividió en dos partes. La primera buscó incrementar la capacidad de adsorción de Cd(II), Pb(II) y Zn(II) del bagazo de *Agave salmiana*, así como elucidar el mecanismo de adsorción y el efecto que generan dichos iones metálicos adsorbidos en la matriz lignocelulósica. Los resultados demostraron que el bagazo de agave modificado con NaOH o HCl 1M y con HNO_3 0.5M aumentó la capacidad de adsorción, encontrándose en todos los casos que se adsorbe Pb>Zn>Cd a pH 5 y 25°C. Ácidos orgánicos como el tartárico, oxálico u cítrico no incrementaron la capacidad de adsorción, excepto para Pb(II). Técnicas como la espectroscopia de infrarrojo y titulaciones ácido-base demostraron que los grupos carboxílicos (-COOH) son los principales sitios que adsorben a los iones metálicos. Además, fue posible regenerar el bioadsorbente hasta un 45% con HNO_3 0.1N. Se encontró que los compuestos solubles del agave contribuyen hasta en un 60% del total de la capacidad de adsorción, mientras que la celulosa, hemicelulosa y lignina aportan el resto a este material. Análisis termogravimétricos revelaron que los iones Cd y Pb aumentan la temperatura de descomposición del bagazo debido a que crean complejos termoestables con la matriz lignocelulósica, mientras que los iones Zn la disminuyen. Estos resultados ayudaron a concluir que el mecanismo de adsorción de los iones metálicos involucra el intercambio iónico y complejación, y que la pirolisis del material lignocelulósico se debe a reacciones de descarboxilación y eliminación de grupos –OH de la celulosa.

La segunda parte de esta investigación se enfocó a modificar carbón activado comercial con Zr(IV) para remover fluoruro. Se usó ácido oxálico (OA) para controlar el

tamaño de partícula de las especies formadas de este ion metálico. Se encontró que la relación óptima Zr/OA (1.05) originó 3 veces más capacidad de adsorción a F$^-$ que el material original o modificado solo con Zr(IV). Titulaciones potenciométricas mostraron que el material modificado posee carga positiva a pH<7, mientras que la espectroscopia infrarroja demostró que Zr^{4+} interactuó con los grupos carboxílicos de la superficie del carbón activado. La espectroscopia fotoelectrónica de rayos X demostró que los iones Zr interactuaron con los iones oxalato, y se encontró por medio de microscopia y análisis de volumen de poro que se anclaron en la superficie del carbón partículas de los complejos Zr-oxalato inferiores a 2 nm. El mecanismo de adsorción de fluoruro sobre el carbón activado modificado involucró intercambio iónico entre grupos –OH y los complejos de Zr-oxalato.

Palabras clave: adsorción, bagazo, carbón activado, iones metálicos, fluoruro.

Abstract

Adsorption of inorganic priority pollutants in water by tailored lignocellulosic and carbonaceous adsorbents

In Mexico there are 17 states with water supplies that exceed the maximum concentration limits of cadmium, lead, fluoride and zinc, as established by the Official Mexican Standard NOM-127-SSA1-1994. Several water treatment techniques have been applied to reduce or eliminate these pollutants from water, however, they involve high operational costs and maintenance. The use of specific adsorbents designed for removal of these elements represents an alternative with high potential to be applied in the near future for water treatment processes.

Agave salmiana bagasse (a sub-product from mescal industry) can be used as adsorbent material for the removal of metallic ions from water. However, the adsorption capacity can be improved by a chemical modification of its surface, to increase the functional groups involved in the removal of those ionic species. On the other hand, activated alumina is typically used to remove Fluoride (F^-) from water supplies because of its high affinity and specific adsorption capacity. However, the use of this adsorbent is no longer recommended due to the affectation to humans' health by aluminum leaching. Activated carbon is an alternative to remove fluoride from water, but, it has low adsorption capacity due to the poor affinity for this anion, which could be enhanced by the modification of its surface with metal oxy(hydroxides).

This research was divided in two parts. The first one looked to increase the adsorption capacity of *Agave salmiana* bagasse to remove Cd(II), Pb(II) and Zn(II) ions, as well as to elucidate the adsorption mechanism and the chemical effect that generates those metal ions adsorbed by the lignocellulosic matrix. The results demonstrated that agave bagasse modified with 1M NaOH or HCl, and with 0.5 M HNO_3 enhanced the adsorption capacity; finding in all cases was the adsorption of Pb>Zn>Cd at pH 5 and 25°C. Organic acids like tartaric, oxalic or citric did not improve the adsorption capacity, except in the case of Pb(II). Infrared spectroscopy and acid-base titrations demonstrated that carboxylic groups (–COOH) were the main adsorption sites for metallic ions. It was also possible to regenerate the bioadsorbent around 45% using 0.1N HNO_3. It was found that soluble agave compounds contributed up to 60% to the total adsorption capacity, while cellulose, hemicellulose and lignin provided the remainder. Thermogravimetric analyses revealed that Cd and Pb ions increased the agave bagasse thermal decomposition due to the development of thermo stables complexes with the lignocellulosic matrix, while Zn ions decreased it. Those results helped to conclude that the adsorption mechanism of metal ions involved ion-exchange and complexation; and the pyrolisis of the lignocellulosic material was due to decarboxylation reactions and the elimination of –OH groups from cellulose.

The second part of this research was focused on the modification of commercial activated carbon with Zr(IV) for fluoride removal. Oxalic acid (OA) was used to control the particle size of zirconyl species formed. It was found that the optimum Zr/OA ratio (1.05) gave 3 times higher fluoride adsorption capacity than the original material or that modified

just with Zr(IV). Potentiometric titrations showed that the modified material had positive charge at pH>7, while the infrared spectroscopy demonstrated that Zr^{4+} interacted with carboxylic groups contained in the activated carbon surface. Photoelectronic X-ray spectroscopy demonstrated that Zr ions interacted with oxalate ions and, it was found by microscopy and volumetric analyses that it was possible to load >2 nm particles of Zr-oxalate complexes on the carbonaceous surface. The fluoride adsorption mechanism of modified activated carbon was found to involve ion-exchange between –OH groups and Zr-oxalate complexes.

KEY WORDS: adsorption, bagasse, activated carbon, metallic ions, fluoride

Thesis Outline

Chapter 1 presents a general review about the adsorption process and the main components of lignocellulosic materials as possible biosorbents of metal ions in aqueous solution. The physical and chemical characteristics of activated carbon are also presented in this chapter, and the importance of tailoring this adsorbent to increase its affinity for anions in aqueous streams is highlighted.

Chapter 2 reports the chemical modification of raw *Agave salmiana* bagasse to increase its adsorption capacity for Cd(II), Pb(II) and Zn(II) ions in aqueous solutions. Besides, the analytic techniques helped to elucidate the way that those metal ions interact with the binding sites of the adsorbent where also described.

Chapter 3 reports the results of chemical and thermogravimetric analyses of agave bagasse main fractions (hemicellulose, cellulose, and lignin) when Cd(II), Pb(II) and Zn(II) ions are loaded in these components. A possible mechanism for metal ion uptake is presented.

Chapter 4 discusses the fluoride adsorption mechanism when using Zr(IV) during the impregnation of commercial activated carbon, and the effects that oxalic acid (as complexing agent) plays to control the particle size of zirconyl species.

Finally, the general remarks and conclusions of this research are presented in Chapter 5 and Chapter 6, respectively. The references consulted through this research are listed at the end of this manuscript.

1
CHAPTER

INTRODUCTION

1.1 WATER POLLUTION WITH INORGANIC IONS: AN OVERVIEW

Water is the most essential substance for all life forms on earth, and a precious resource for human civilization. Nevertheless, its pollution due to the presence of several contaminants has been a major concern during decades. The presence of inorganic pollutants contained in drinking water and water supplies have been more strongly regulated since a close relationship with the increase on illnesses and diseases over global population has been recently demonstrated. Worldwide, some 780 million people stick lack access to improved drinking water sources [1], and it is urgent to implement basic water treatment where infrastructure does not exist.

The international water regulations depend on national or regional standards developed from scientific basis as well for environmental, social, economic and cultural conditions. The World Health Organization (WHO) provides international guidelines and standard settings on water quality and human health, and they are followed in most of the nations. According to the WHO, the priority chemical pollutants that are considered to be regulated in drinking water, and in the best of the cases removed are aluminium (Al), ammonia (NH_3), arsenic (As), antimony (Sb), barium (Ba), boron (B), bromide (Br), cadmium (Cd), chloride (Cl), cooper (Cu), chromium (Cr), cyanide (CN^-), fluoride (F^-), iron (Fe), lead (Pb), manganese (Mn), mercury (Hg), molybdenum (Mo),nickel (Ni), nitrite and nitrate, selenium (Se), silver (Ag), sodium (Na), sulfate (SO_4^{2-}), uranium (U), zinc (Zn), among others [1]. Natural and anthropogenic activities are responsible for the increase of these inorganic pollutants in the environment, but only few are of immediate health concern. In addition, current water and wastewater treatment technologies and infrastructure are reaching their limit for providing adequate water quality to meet human and environmental needs. For this reason, the need for technological innovation that can

provide clean and affordable water at low cost with environmental-friendly processes that may reduce the volume and toxicity of non-desirable inorganic elements, is a very relevant challenge of the 21st century. By the development of new technological advances, the emphasis here is on the origin and potential health effect of heavy metals and fluoride, and the importance of their removal from drinking water and water supplies.

1.1.1 Heavy metals

'Heavy metals' is general a collective term applying to the group of metals and metalloids with an atomic density greater than 4.5 g cm^{-3}, and include a block of elements from group 3 to 16 of the periodic table. [2]. Although this definition is a vague term, it is widely recognized and usually applied. Many of these metals are not specifically toxic, and some of them are essential for living organism, independently that a certain concentration may be toxic in some of their forms [3]. Heavy metals such Al, Cd, Sb, Cr, Cu, Hg, Ni, Pb, As and Zn are commonly associated with pollution and toxicity problems. Several industrial processes, mining, agriculture and some domestic processes use and release them from burning of fossil fuels, incineration of wastes, automobile exhausts, fertilizers, among others. These processes have introduced substantial amounts of potentially toxic concentrations of heavy metals into atmosphere, aquatic and terrestrial environments. Table 1.1 shows the diverse discharge metal-containing wastewater from several anthropogenic sources.

In Mexico, organizations like Secretaria del Medio Ambiente y Recursos Naturales (SEMARNAT), Procuraduria Federal de Protección al Ambiente (PROFEPA), Secretaria de Salud (SSA), among others, have regulated and set the maximum allowed concentrations for the discharge of toxic metals in sewers and municipal wastewater, as well as for drinking water guidelines. The limits established for Cd, Pb and Zn with these national organizations and other international organisms are given in Table 1.2.

When metals are in contact with aqueous solutions, they tend to dissolve and form ionic species. In the ionic form, concentrations of metals in water supplies exceed the standards and constitute a severe health hazard that includes accumulation in living species and magnification throughout the food chain.

Although adverse health effects have been known for long time, exposure to metals continues and it is even increasing in some areas around the world. High Pb exposure levels causes encephalopathya, cognitive impairment, behavioral disturbance, kidney damage, anemia and toxicity to the reproductive system; and chromium is widely

recognized to exert toxic effects in its hexavalent form and it is associated with a higher incidence of respiratory cancers [4, 5]. Cadmium may cause kidney and skeletal damage, as well can produce some types of cancer and mutagenic effects, while an excess of zinc produces low levels of copper and iron in blood that affect the immunological system and the cholesterol levels, as well mental depression and renal problems. Acute mercury exposure may give arise to lung problems, eczema, nervous system damage and neurobehavioural disorders including dyslexia, attention deficit hyperactivity disorder and intellectual retardation. In other hand, arsenic leads to gastrointestinal, lung and bladder problems, besides skin cancer and other skin lesions such hyperkeratosis and pigmentation changes known as *arsenicosis*. Excessive copper concentrations can lead to weakness, lethargy and anorexia, as well as damage to the gastrointestinal tract.

Table 1.1 Significant anthropogenic sources in the environment [5].

Source	Metals	Pollution arising
Metalliferous mining	Cd, Cu, Ni, Cr, Co, Zn	Acid mine drainage and slag heaps
Fertilizers	Cd, Cr, Mo, Pb, U, V, Zn	Run-off, surface and groundwater contamination, plant bioaccumulation
Industrial sludge	Zn, Cu, Ni, Pb, Cd, Cr, As, Hg	Land spreading threat to grounds and surface water
Metallurgical industries	Pb, Mo, Ni, Cu, Cd, As, Te, U, Zn	Manufacture, disposal and recycling metals.
Waste disposal	Zn, Cu, Cd, Pb, Ni, Cr, Hg	Landfill leachte, contamination of groundwater and surface water
Electronics	Pb, Cd, Hg, Pt, Au, Cr, As	Aqueous and solid metallic wastes
Paints and pigments	Pb, Cr, As, Ti, Ba, Zn	Aqueous waste from manufacture, paint deterioration and soil pollution
Batteries	Pb, Sb, Zn, Cd, Ni, Hg	Waste battery fluid, soil and groundwater pollution

Table 1.2 Permissible limits (mg L^{-1}) for Cd, Pb and Zn in water discharges and drinking water for human use.

Metal	SEMARNAT NOM-001-ECOL-1996[a]	NOM-002-SEMARNAT-1996[b]	SSA NOM-127-SSA1-1994[c]	WHO[d]	EPA[e]
Cd	0.01	0.50	0.005	0.001	0.002
Pb	5.0	1.0	0.01	0.003	0.005
Zn	2.0	6.0	5.0	-	-

[a]Offical Mexican Standard NOM-001-ECOL-1996 that establish the limit maximum permissible for wastewater discharge in national waters and properties [6].

[b]Offical Mexican Standard NOM-002-SEMARNAT-1996 that establish the limit maximum permissible for contaminant for wastewater discharge in urban and municipal sewers [7].

[c]Offical Mexican Standard NOM-127-SSA1-1994 that establish "Environmental health, water for human use-permissible limits and treatments that must be regulated the drinking water [8].

[d]WHO, Guidelines for drinking water quality [1]

[e]U.S EPA 40 CFR Parts 141-143, National Primary Water Regulations [9]

An important characteristic of the biological behavior of a metal is the affinity to certain organic groups. Depending of the oxidation state, heavy metals can be highly reactive, since they have a great affinity to functional groups such carboxyl, thiol, amino, phosphate, hydroxyl and carbonyl. Lead and cadmium possess high affinity to –SH groups, because they have high charge/ionic ratio, while zinc does not exhibit this behavior. Furthermore, these metals can change their preference to bind N, S or O atoms, depending of the solution pH, size and geometry of the binding site. Besides, Cd, Pb and Zn ions can replace essential metals (Na^+, Ca^{2+}, Mg^{2+}) in living organism, affecting enzymes and inhibit the function of proteins rich in cysteine (S^{2-}) [3 ,4]. On the other side, proteins can contribute significantly to metal bioaccumulation in human organism due to the functional groups of aminoacids (hydroxyl, carboxyl, sulfhydryl, amine, imine, amide, among others), as well as carbohydrates (involving galactose, arabinose, xylose, rhamnose, glucuronic acid) that content –COOH and –OH groups, mainly. These organic functional groups also have metal binding properties.

The metal interaction and the preference for these and others organic groups depend mainly on the physical and chemical properties of metal ions. The more importants

are given below [10], while the physic-chemical properties of Pb, Cd and Zn are listed in Table 1.3.

1. *The atomic weight.* The metal affinity is correlated to stereo-chemical effects; large ions could better fit a binding site with two distant functional groups.

2. *The electronegativity.* More electronegative metal ions are more strongly attached to the negative surface of the biosorbents.

3. *The ionic radius.* A smaller ionic radius implies more molecules can be sorbed onto a fixed surface area of a biological material.

4. *The covalent index.* Defined in 1973, it is defined by the expression $X_m^2(r+0.85)$, where X_m is the electronegativity, r is the cationic crystal radius and 0.85 stands for the contribution of N or O donors to the bond distance. In general, the higher the covalent index of a metal ion, the higher its potential to form covalent bonds with biological material.

Table 1.3 Physical and chemical properties of Pb, Cd and Zn metal ions [6].

Parameter	Pb^{2+}	Cd^{2+}	Zn^{2+}
Atomic weight	207.2	112.4	65.38
Ionic radius ($\mathring{A}$)	1.21	0.97	0.74
Covalent Index	6.61	5.20	4.54
Electronegativity of the atom	2.33	1.69	1.60

Aside heavy metals, other priority pollutants also considered for its removal from drinking water and aqueous streams are some anions, like fluoride. This anion is found to be strongly regulated by water quality and human health standards. In the next section fluoride origins and sources when it is present in aqueous environments will be presented, as well as the importance to maintain its concentration levels under permissible limits.

1.1.2 Fluoride

Fluoride occurs in the environment mainly as mineral like sellaite (MgF_2), fluorspar (CaF_2), cryolite (Na_3AlF_6) and fluorapatite [$3Ca_3(PO_4)_2Ca(F,Cl_2)$]. As fluorspar it is found in sedimentary rocks and as cryolite in igneous rocks. Besides, fluoride is a minor element of the earth's crust representing just 0.065% by weight, and only the isotope ^{19}F is found in nature. Some of the physicochemical properties of fluoride are given in Table 1.4.

Table 1.4 Physicochemical properties of fluoride [11].

Property	Value
Atomic weight	19
Stable isotope	^{19}F
Ionic radius (F⁻)	1.19
F-F distance (Å)	1.43
Electronegativity of the atom	4.0

When conditions favor the dissolution of fluoride-containing minerals, the anion can be present in drinking water as a negative charge ion (F⁻). Other sources of fluoride are the anthropogenic discharges from industrial, commercial and/or domestic activities, which include emissions from brickworks, aluminium smelters, iron and steel production, fossil fuel burning, ceramic industries and phosphate fertilizers plants. In addition, many sources of exposure to fluoride for human include food, air, medicaments, cosmetics, organo-fluoro compounds, among others.

In most potable waters, F⁻ comprises over 95% of the total fluoride and the magnesium-fluoride complex (MgF^+) is typically the next prevalent form [12]. Its relationship to human health is quite extensive and includes on chronic exposure with adverse effects on teeth and bones (dental and skeletal fluorosis), DNA structure (genetic mutations, birth defects) and illnesses spread (cancer, Alzheimer disease, renal and neurological damage) The excess concentrations of fluoride can also interfere with carbohydrates, lipids, proteins, vitamins and mineral metabolism [13].

Fluoride contained in drinking water is considered hazardous once it exceeds 1.5 mg L^{-1}, which was established by the World Health Organization (WHO), and this limit has been adopted in Mexico and in most of the nations around the world. The vast majority of fluoride related to health problems occur as a result of the groundwater ingest that was in contact with the geological fluoride rich substrate. Groundwater constitutes 97% of global freshwater and it is used for drinking by more than 50% of the world population. It is estimated that more than 200 million people worldwide rely on drinking water with fluoride concentrations that exceed the WHO guideline and serves as the only economically viable option for many communities. High fluoride concentrations in groundwater, up to more than 30 mg L^{-1}, can be found in many parts of the world, and is endemic in at least 25 countries across the globe [14, 15]. The most affected areas are parts of China, India, Sri

Lanka, Turkey, South Africa, and in less proportion in rural and semi-urban areas of United States of America, central Europe, northern Mexico and central Argentina. This problem is exacerbated by the need to drink more water because of the heat and dry climates, and the limited water resource in Third World countries where populations have little choice in the source of their drinking water and food. Even in developed nations, defluoridation of public drinking water has been a contentious issue that ends in more stringent fluoride limits [16]. It is important to point out that although anthropogenic sources of F^- in the environment have occasionally been the cause of human health problems, the vast majority of fluoride related to health problems occurs as a result of ingesting this element from natural sources like groundwater [13, 17].

1.2 TECHNOLOGIES FOR REMOVAL OF METAL IONS AND FLUORIDE FROM WATER SUPPLIES

Several techniques have been developed in order to bring down metals and fluoride concentrations to safe limits in water supplies and drinking water. The efficiency of any treatment technique depends on the conditions of the effluent, treated volume, the objective concentrations and the nature of the mechanism involved. The selection of the most suitable treatment also depends on the flexibility and reliability of the water treatment plant, environmental impact, as well as economic parameters such as the capital investment and operational costs (energy consumption and maintenance). Finally, the technical applicability, the water treatment plant simplicity and cost-effectiveness are key factors that play major roles in the selection of the most suitable treatment system for inorganic effluent.

Physico-chemical treatments can be generally grouped into precipitation/coagulation, membrane processes, ion-exchange and adsorption techniques. The coagulation-precipitation methods involve precipitation or co-precipitation of metals and fluoride by using reagents like lime, aluminium, calcium and magnesium salts, as well some polymers and chitin. This methodology creates a colloidal suspension in order to promote chemical dissolution and particle destabilization that creates flocs that are removed by sedimentation or filtration. However, residual concentrations of reagents employed in the treated water and formation of toxic sludge limits its use. Membrane techniques imply the use of semi-permeable membranes as an interface between the polluted aqueous streams and the membrane, where a high pressure flow is passed through the membrane. This phenomenon allows the filtration of impurities of the aqueous

effluent. There are several types of membrane filtrations such ultrafiltration (UF), nanofiltration (NF) and reverse osmosis (RO). Besides, electro-treatments such as electrodialysis, membrane electrolysis and electrochemical precipitation have also been applied for removal of fluoride and metals with high efficiency. Nevertheless, membranes and electro-treatments have been investigated less extensively due to the high operational cost caused by membrane price and the elevated energy consumption. Ion-exchange is a non-traditional technology that can be successfully applied, and it consists in exchanging the pollutant to be removed from the solution at the same time that it is replaced for a non-toxic compound from the resin. There are several commercially exchangers resins, depending on the contaminant to remove and on the conditions of the water. The resins are named depending whether the kind of ion to be exchanged is cationic or anionic. Nonetheless, the relatively high cost of any ionic exchanger makes difficult its application.

Adsorption is characterized by the use of adsorbents that concentrate the metal ion or fluoride on their surface. Several materials have been tested to remove those contaminants and include activate carbon, metal oxides, activated alumina, fly ash, clay, minerals and soils, natural materials, among others. In despite of the overview of methods and techniques for metal and fluoride removal, the adsorption process is widely used and seems to be a more attractive method, offering satisfactory results at low-cost with a simplicity of design and operation. Several materials have been assessed for metal and fluoride removal from water, and they will be discussed in the following section.

1.2.1 ADSORPTION AND MATERIALS USED AS ADSORBENTS

As was discussed previously, adsorption is a mass transfer process by which a substance (adsorbate) is transferred from a liquid phase to the surface of a solid (adsorbent), and becomes bound by physical and/or chemical interactions. The accumulation can also involve liquid-liquid or gas-liquid phases interfaces.

If adsorption occurs as a result of van der Waals forces is termed "physical adsorption" or "physisorption". A physisorbed species is not attached to a specific site at the surface, and usually predominates at low temperatures. It is characterized by a relatively low energy of adsorption (20-40 kJ mol^{-1}), which means that the adsorbate is not held strongly to the adsorbent. If the adsorbate is retained by chemical interaction with the adsorbent, the phenomenon is referred to as "chemisorption". The chemisorbed molecules are not free to move on the surface since they form strong localized bonds at the active centers of the adsorbent. Chemisorption exhibits high energies of adsorption (20-200 kJ

mol^{-1}) and it is favored at high temperatures. Another adsorption process that may occur is known as "exchange adsorption", in which ions from the adsorbate are attached to charged sites of the adsorbent surface by electrostatic attractions [17]. Theoretically, the adsorption process in solid materials normally takes three essential steps:

1) Diffusion or transport of the adsorbate molecules to the external surface of the adsorbent from the bulk solution across the boundary layer surrounding the adsorbent particle, called external mass transfer.

2) Adsorption of fluoride ions on the material surface.

3) The adsorbed molecules of adsorbate probably exchange with the structural elements inside the solid adsorbent, depending on the adsorbent chemistry or a possible transference to the internal surface of the porous material (intraparticle diffusion).

Table 1.5 Review of adsorbents used to remove metal ions and fluoride from water.

Source of adsorbent	Type of adsorbent	Pollutant removed	Reference
Agricultural waste	Oat biomass	Cr	[19]
	Rice bran	Pb, Cd, Cu, Zn	[20]
	Tamarindus india fruit shell and Pumice stone	F	[21, 22]
Industrial by-products	Red mud	Ni, F	[23, 24]
	Blast-furnace slag	Cu, Zn	[25]
	Fired clay chips	F	[26]
Activated carbon	Activated carbon from peanut shells	Pb, Cd, Cu, Ni, Zn	[27]
	Commercial activated carbon	F	[28]
Natural materials	Clays and soils	F, Cu, Ni, Zn	[29, 30]
	Chitosan	F, Cd	[31, 32]

The success of an adsorbent in water treatment depends on the concentration and kind of pollutants in the influent, the volume of water to be treated and the adsorption capacity of the adsorbent in such conditions. The most important factors for screening an

adsorbent for water treatment are their high mechanical strength and surface area, a diverse chemical surface where metal ions and F^- can be attached, their chemical stability and the low cost to develop and apply them in water treatment processes [18]. There are several material used to remove metal ions and fluoride from water, as can be seen in Table 1.5. When using natural materials, industrial or agricultural wastes, the adsorption process is called "biosorption". This process will be discussed in the next section.

1.2.1.1 BIOSORBENTS

Biosorption technology offers an efficient and cost-effective alternative compared to traditional chemical and physical remediation and decontamination techniques [33]. The "bio" prefix denotes the involvement of a biological entity (living organism, component or product produced or derived from living organism, etc.). Coupling of "bio" to a physic-chemical expression like "sorption" (term used for both absorption and adsorption processes) means the removal of substance from solution by biological material. "Biosorption" is the most common form of sorption used in traditional clean-up technologies, that could use living or dead biomass (defined as "biosorbents", independently of their chemical state). A great number of research has been focused in the performance of different biosorbents for the removal of different metals ions and anionic pollutants like fluoride under various experimental conditions, in aqueous solutions. Results have shown that the performance of such materials depends on pH and the presence of other ions in the aqueous solution. In addition, the screening of biosorbents to be use in possible water treatment processes include the cost of processing materials, the pollutant selectivity and the regeneration of the material. Cost is a very important factor when considering materials for use as biosorbents. It is generally recognized that a material can be deemed as "low cost" if it requires little processing, it is abundant in nature, or it is a by-product or waste material from industry [34]. Numerous low cost natural materials, particularly of cellulosic nature, have been proposed as a potential biosorbents for metal uptake. These includes moss peat, algae, leafs, coconut shells, sugar cane bagasse, rice hull, plant biomass, seaweed, orange peel, apple and tamarind seeds, fungus, among others; that have shown to be capable of concentrating different metal ions from aqueous solutions [35]. Likewise, wood sawdust and/or bark from some trees species have been reported as effective for heavy metal uptake [35, 36]. The use of large quantities of wastes generated from processing agricultural products, food/and or wood, may constitute an attractive option for water treatment.

1.2.1.1.1 LIGNOCELLULOSIC MATERIALS AND THEIR COMPOSITION

The agricultural wastes are also known as "lignocellulosic materials" because the main components are cellulose, hemicellulose and lignin. Other components that lignocellulosic materials also contain in minor proportion are extractives, lipids, proteins, simple sugars, water hydrocarbons, ash and many more compounds that enclose a variety of functional groups (acetamido, carbonyl, phenolic, amido, amino, sulphydryl, carboxylic, ester, etc.) that facilitates metal binding during the adsorption process [36].

In general, the plant cell wall of biosorbents such lignocellulosic materials is a highly-organized composite which molecular composition and arrangements is a cross-linked matrix of fibers, and differ among species, tissues, individual cells, and regions of the wall around protoplasm [33]. Cell wall components are linked by covalent and ionic bonds, as well by hydrogen bonding and hydrophobic interactions. Cellulose, hemicellulose and lignin are linked together by calcium bridges which play an important role in heavy meal removal from aqueous solution, because metal ions exchange with calcium ions from the material. Figure 1.1 shows a schematic model of the conformation of cellulose, hemicellulose and lignin in a primary plant cell wall, showing the structural arrangement of main components.
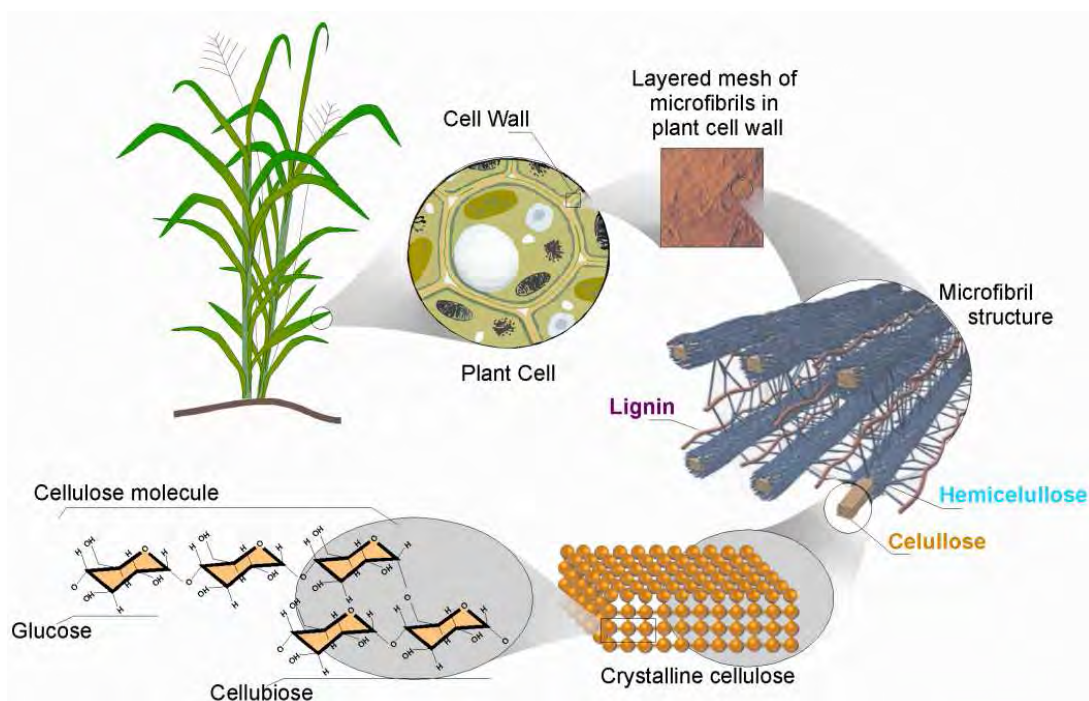
Figure 1.1 Schematic model of main components in biomass, adapted from [37].

1.2.1.1.1.1 CELLULOSE

Cellulose constitutes the most abundant and renewable polymer resource available worldwide. The molecular structure of cellulose as a carbohydrate polymer comprises a repeating β-D-glucopyranose units which are covalently linked through acetal functions between the OH group of the C_4 and C_1 carbon atoms (β-1,4-glucan), see Figure 1.2. Cellulose is a large, linear-chain polymer with a large number of hydroxyl groups (three per anhydroglucose (AGU) unit). This biolopymer is naturally found as arrays of microfibers, with variable length (0.2-2 μm) and diameters (5-30 nm), which depends on the number of constituent AGU units (degree of polymerization, DP) and varies with the origin of the cellulose raw material. Cellulose has a ribbon shape which allows it to twist and bend in different directions, so the molecule is moderately flexible. There is a relatively strong interaction between neighbouring cellulose molecules in dry fibers due to the presence of hydroxyl (-OH) groups, which stick out from the chain and form intermolecular hydrogen bonds. This molecular structure gives cellulose its characteristic property of hydrophilicity, chirality and degradability. Chemical reactivity is largely a function of the high donor reactivity of OH groups [5]. Cellulose in a plant consists of parts with crystalline (organized) structure, and parts with a not well-organized amorphous structure [38].
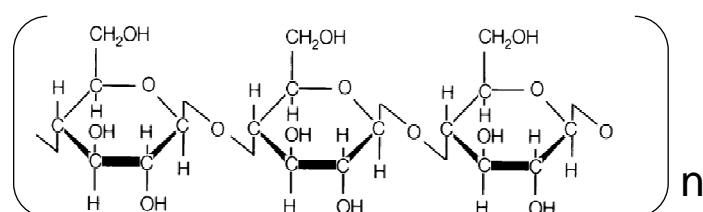
Figure 1.2 Chemical structure of cellulose.

1.2.1.1.1.2 HEMICELLULOSE

Hemicellulose is a complex carbohydrate structure that consists of different polymers such pentoses (like xylose and arabinose), hexoses (like mannose, glucose, galactose) and uronic acids (like 4-o-methlglucuronic, D-glucuronic and D-galactouronic acids), see Figure 1.3b. The backbone of hemicellulose is etiher a homopolymer or heteropolymer with short branches linked by β-(1,4)-glycosidic bonds and occasionally β-(1,3)-glycosidic bonds with other substances of acetyl feruoyl and glycouronyl groups [5, 39]. Hemicellulose has lower molecular weight that cellulose, and branches with short

12

lateral chains that consist of different sugars, which are easy to hydrolyze. In addition, hemicellulose serves as connection between the lignin and the cellulose fibers, and gives the whole cellulose-hemicellulose-lignin network more rigidity.
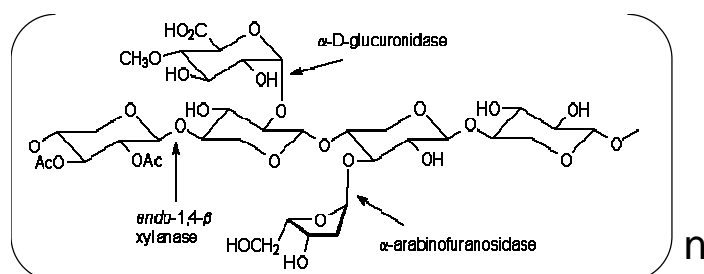
Figure 1.3 Chemical structure of hemicellulose

1.2.1.1.1.3 LIGNIN

Lignin is, after cellulose and hemicellulose, one of the most abundant polymers in nature. It is a complex, large molecular structure in the primary cell wall that contains cross-linked polymers of phenolic monomers, and imparts structural support, impermeability and resistance against microbial attack and oxidative stress [40]. Three phenyl propionic alcohols exist as monomers of lignin: coniferyl alcohol (guaiacyl propanol), coumaryl alcohol (*p*-hydrxylphenyl propanol) and sinapyl alcohol (syringyl alcohol). Alkyl-aryl, alkyl-alkyl and aryl-aryl either bonds link these phenolic monomers together. The amorphous heteropolymers are also non-water soluble and optically inactive, all this makes the degradation of lignin very difficult [37]. Herbaceous plants such as grasses have the lowest contents of lignin, whereas softwoods have the highest one [39].
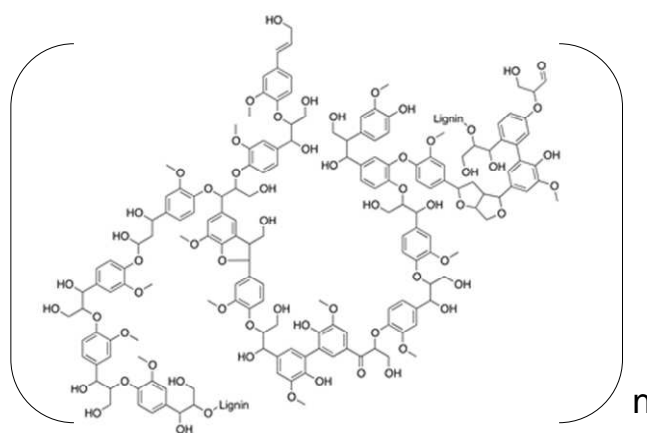
Figure 1.4 Chemical structure of lignin.

13

1.2.1.1.2 CHEMICAL MODIFICATION FOR HEAVY METALS UPTAKE

Several adsorption studies have been focused on untreated lignocellulosic material for heavy metals uptake from aqueous solution [41], because some of the advantages include little processing, good adsorption capacity, selective adsorption of heavy metal ions, low cost, free availability and easy regeneration. However, the application of untreated lignocellulosic materials as biosorbents can bring several problems such as low adsorption capacity, high chemical oxygen and biological chemical demand (COD and BOD, respectively) as well as high values of total carbon (TOC) due to the release of soluble compounds that contains the lignocellulosic materials. The increase of COD, BOD and TOC can cause depletion of oxygen content in water and can threaten the aquatic life [42]. Therefore, lignocellulosic materials and most of the biomasses used as biosorbents need to be modified or treated before being applied for the decontamination of toxic metals. Modification methods use different kind of modifying agents such as base solutions ($NaOH$, $CaOH$, Na_2CO_3), mineral and organic acids (HCl, HNO_3, H_2SO_4, tartaric acid, citric acid, oxalic acid), organic compounds (ethylenediamine, formaldehyde, epichlorohydrine, methanol), oxidizing agents (H_2O_2), among others, that have the purpose of removing soluble organic compounds, eliminating coloration of the aqueous solution and increasing the efficiency of metal adsorption. The chemical modifications include esterification of carboxyl and phosphate groups, methylation of amino groups, and hydrolysis of carboxylate groups [43, 44]. Esterification is usually performed through the reaction of the biomass with acidic methanol (reaction 1), where an ester is formed and the carboxyl groups are blocked. Esterification of phosphate groups is accomplished by treating the biomass with a triethyl phospite/nitromethane mixture (reaction 2). Methylation of amino groups is achieved by a reaction of the biomass with a mixture of formaldehyde/formic acid (reaction 3). Finally, the formation of carboxylate moieties from esters is carried out by exposing the biomass to $NaOH$ solutions (reaction 4).

$$RCOOH + CH_3OH \longrightarrow RCOOCH_3 + H_2O \qquad (1)$$

$$RO-\underset{\underset{O}{\|}}{\overset{\overset{O^-}{|}}{P}}-\bar{O} \quad \xrightarrow[CH_3NO_2]{(CH_3CH_2)_3PO_3} \quad RO-\underset{\underset{O}{\|}}{\overset{\overset{H_3CH_2CO}{|}}{P}}-OH \qquad (2)$$

$$RCH_2NH_2 \xrightarrow{\text{HCHO/HCOOH}} RCH_2N(CH_3)_2 + CO_2 + H_2O \qquad (3)$$

$$RCOOCH_3 \xrightarrow{\text{NaOH}} RCOO^- Na^+ + CH_3OH \qquad (4)$$
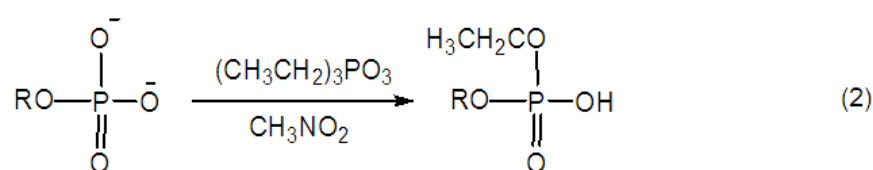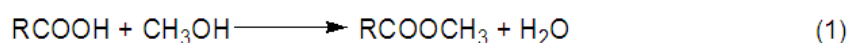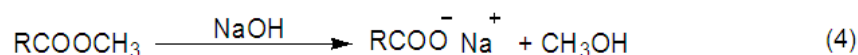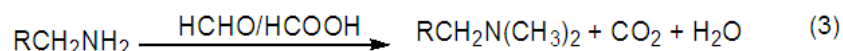
Hence, the chemical modifications of lignocellulosic materials increase the stability of biomass and the concentration of functional groups involved in metal recovery will significantly facilitate the application of bioadsorbents in water treatment. The adsorption (bioadsorption) mechanisms will be discussed in the next section.

1.2.1.1.3 ADSORPTION OF METAL IONS IN AQUEOUS SOLUTION

In water, metal cations are surrounded by water molecules that form inner or outer sphere complexes, and the process is called "hydrolysis". Hydrolysis refers to the reaction between water and other chemical species. In this reaction, one or both of the O-H water bonds are broken and hydrogen, oxygen, or hydroxyl group is incorporated into one or more of the final products: an aqueous complex [42]. A typical hydrolysis reaction is shown in reaction 5, where M^{n+} refers to the metal cation.

$$M^{n+} + xH_2O \rightleftharpoons [M(H_2O)_x]^{n+} \rightleftharpoons [M(H_2O)^{x-1}OH]^{(n-1)+} + H^+ \qquad (5)$$
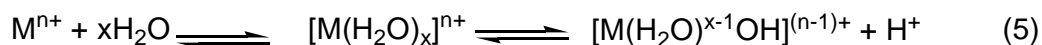
As can be seen in reaction 5, hydrogen ions are released and consequently the solution pH is lowered during the hydrolysis process. This reaction also shows that the metal cation is not "free", but instead surrounded by water molecules. Besides, in many aqueous systems metals like Cu, Cd and Zn are hydroxylated or complexed (e.g. to Cl) depending on the pH and the medium composition. Many research studies assumed that these and others hydrolyzed metals are entirely present as divalent cations, although this assumption is not true [45].

In despite that lignocellulosic materials or any kind of bioadsorbent may be chemically modified or not, the adsorption mechanism can be attributed to two main terms: intrinsic adsorption and coulombic interaction [46]. The coulombic term results from the electrostatic energy of interactions between the bioadsorbent and metal ion. The charge on both substrates is responsible for the intensity of the attraction, and can be observed from the adsorption of cationic species (mostly all metal ions) found in the biosorbents. The intrinsic adsorption is determined by the bioadsorbent surface area, which plays an important role in the adsorption capacity. Although the adsorption process is a surface

reaction, most of the lignocellulosic materials contain pores and the adsorption process is affected by this surface property. A large surface area is preferable for providing large adsorption capacity. Therefore, porosity in the lignocellulosic materials (treated or not) may increase the metal uptake by diffusional paths in the adsorbent that increase the adsorption area [33].

Most adsorption studies have employed simple closed batch systems. The results of those studies are adsorption isotherms that asses lignocellulosic capacity over metal ion removal from aqueous solution. The adsorption capacity in equilibrium (q_e), accumulated in the bioadsorbent surface, is plotted against the equilibrium (final) metal concentration (C). Such equilibrium adsorption isotherms can be used to compare different adsorbents and affinities of several metal ions for the same bioadsorbent. In simple terms:

$$q_e = \frac{V(C_0 - C)}{w} \qquad (6)$$

where V is the volume (L) of solution contacted with the adsorbent, C_0 and C are the initial and final metal concentration (mg L^{-1}) and w is the mass of bioadsorbent. Many researchers have studied simple adsorption systems and single metals under different parameters varying biomass density, pH, metal concentration, presence of competing ions, among others. In addition, batch adsorption studies can provide useful information of the relative efficiency of biosorbents and important physicochemical factors that affect the adsorption process, although they usually provide no information on adsorption mechanism.

A variety of models have been used to describe the adsorption of metal ions (or other pollutants) by bioadsorbents and other kind of materials. Langmuir or Freundlich models are probably the most widely used, however, other complex multicomponent models have been derived from them. However, these models were originally derived from gas adsorption in activated carbons, and some of the assumptions like all binding sites have the same affinity, do not often apply to bioadsorbents. Cell walls and other lignocellulosic components (as well other biomasses) have multiple binding sites, as was previously described that have different affinities for metal ions, and can change by pH and solution chemistry. The Langmuir model contains a number of assumptions which include that a) all binding sites possess an equal affinity for the adsorbate, b) adsorption is limited to formation of a monolayer, and c) the number of adsorbent species does not exceed the total number of surface sites. It is likely that none of these assumptions apply to biological systems. Its expression is given by:

$$q_e = \frac{q_{max}bC_e}{1+bC_e} \qquad (7)$$

where q_{max} (mg g^{-1}) is the maximum adsorption capacity of the adsorbate upon complete saturation of its surface, b (L mg^{-1}) is an affinity parameter related to the bonding energy of the adsorbate (metal ion) to the surface, and C_e is the equilibrium (final) concentration of the adsorbate remaining after the adsorption process.

The Freundlich model is also used to estimate the adsorption intensity of the adsorbents towards the bioadsorbent, and is given by:

$$q_e = K_F C_e^{1/n} \qquad (8)$$

where q_e (mg g^{-1}) is the equilibrium value of metal removed by the bioadsorbent, C_e is the equilibrium (final) concentration of the metal remaining after the adsorption process, K_F (L$^{1/n}$ mg/mg^{1-1n} g^{-1}) is an affinity parameter and $1/n$ is a dimensionless heterogeneity parameter, and also indicates the affinity of the metal ion towards the bioadsorbent.

There are other single-component adsorption models, based on different theoretical assumptions, like Reddlich-Peterson, Dubinin-Radushkevich and Radke-Prausnitz isotherm models.

1.2.1.2 ACTIVATED CARBON

Activated carbon (AC) is a term that includes a wide range of amorphous carbonaceous materials that exhibit a high degree of porosity and an extended interparticulate surface area [47]. They are obtained by combustion, partial combustion or thermal decomposition of a variety of carbonaceous materials. Active carbons have been prepared from coconut shells, wood char, lignin, petroleum, coke, bone char, peat, carbon black, sugar, fish, fertilizer waste, bituminous coal, etc. [48]; and are used in the removal of undesirable odor, color, taste, and other organic and inorganic impurities from domestic and industrial wastewater, solvent recovery, air purification, food-processing and chemical industries. 80% of the world production of activated carbons is used in liquid-phase applications, where wastewater treatments and decontamination of groundwater use mainly AC as primary treatment preceding another purification process, or as final tertiary or advanced treatment [49]. Carbon is the major constituent of activated carbons, and is present to the extent of 85-90%, and this also contains other elements such hydrogen (0.5%), nitrogen (0.5%), sulfur (1%) and oxygen (6-7%). The other remaining fraction represents the inorganic ash content. The oxygen content may vary between 1 and 20%, depending on the source of the raw material and the carbonization and activation process.

ACs are mainly prepared by pyrolisis of carbonaceous raw materials at temperatures lower than 1000°C. The preparation involves two main steps: carbonization of the raw material at <800°C in an inert atmosphere, and activation of the carbonized product between 950-1000°C. Thus, all carbonaceous materials can be converted into active carbons. During carbonization most of the noncarbon elements such O, H, N and S are eliminated as volatile gaseous products. The residual carbon atoms group themselves into stacks of aromatic sheets cross-linked in a random manner that leaves free interstices between sheets, given rise to pores that make AC an excellent adsorbent. Activation also defines the pore structure. Mesopores, micropores and ultramicropores are formed during activation, yielding large surface areas up to 2000 m^2 g^{-1}.

Physical or chemical activation are two options to activate carbons. The physical or thermal activation involves carbonization at 500-600°C to eliminate the volatile matter followed by a partial gasification using a mild oxidizing gas such CO_2, steam or fuel gas at 800-1000°C to develop porosity and surface area; while chemical activation involves inorganic additives such metallic chlorides such $ZnCl_2$ or H_3PO_4 into the precursor before carbonization, generally at temperatures (400-600°C) lower than physical activation. Ammonium salts, borates, calcium oxide, ferric and ferrous compounds, manganese dioxide, nickel salts, HCl, HNO_3 and H_2SO_4 have also been used for activation [48].

As previously mentioned, the staring material and the activation method to produce AC determine the physical and chemical properties of the carbonaceous material that will be discussed in the following sections.

1.2.1.2.1 PHYSICAL PROPERTIES
1.2.1.2.1.1   SURFACE AREA

The term *surface area* has been use since the development of the Langmuir and Brunauer-Emmett-Teller (BET) adsorption equations, and indicates in a convenient way the adsorption capacity of a porous solid in m^2 g^{-1}. The Langmuir equation defines a monolayer area, while BET determines a multiple coating. According to the classical BET method, the surface area of the adsorbent is usually measured by adsorption of nitrogen at 77K. The physisorption of N_2 on a porous solid resembled to that on non-porous surfaces, and could be calculated a value for a surface area, assuming that this internal surface was similar (identical) to the external surface of the non-porous solid [50]. The fundamental assumption of BET model is that the pressure applied activates the condensation of

gases, being responsible for the binding energy in multi-molecular adsorption. The BET equation is given below:

$$\frac{P}{V_a(P_0 - P)} = \frac{1}{V_m C} + \frac{C-1}{V_m C}(P/P_0) \qquad (9)$$

where P_0 is the saturation vapor pressure at the temperature used in the test, V_a is the amount of gas adsorbed at any given pressure P, V_m is the amount of substance adsorbed when one complete monolayer of gas coverage is attained, and C is a constant that depends on the isotherm shape. A plot $P/[V_a(P_0-P)]$ vs. P/P_0, and data over the range of 0.05 to 0.3 P/P_0 values are fitted to the best straight line using the linear least squares procedure. V_m and C values are then determined. Alternatively, the monolayer capacity can be expresses in grams of the adsorbate (m^2 g^{-1}), then, the specific area is given by:

$$S_{BET} = N n_m a_m 10^{-18} \qquad (10)$$

where S_{BET} is the surface area of the adsorbent, N the Avogadro's number, n_m is the number of moles of N_2 and a_m is the molecular area of N_2 (0.162 nm^2). The surface area includes adsorption into all porosities, characterized in terms of the volume of their various sizes (narrow or wider pores). The typical surface area of activated carbons is in the range of 800-1200 m^2 g^{-1}. High surface area does not necessarily mean high adsorption capacity because 1) only wetted surfaces adsorb ions, 2) sometimes the pollutant to be adsorbed is too large to enter the smallest pores, and 3) surface area, pore volume and surface chemistry are not usually correlated with species adsorbed.

1.2.1.2.1.2   PORE STRUCTURE

The porous structure is developed further during the activation process. The activation process enhances the volume and enlarges the diameters of the pores. The structure of the pores and their pore size distribution are largely determined by the nature of the raw material and the history of its carbonization. Active carbons are associated with pores starting from less than a nanometer to several thousand of nanometers. The pores are classified according to the International Union of Pure and Applied Chemistry (IUAPAC) into three groups: micropores (<2nm), mesopores (2-50 nm) and macropores (>50 nm). Each pore plays a specific role in the adsorption process. Micropores constitute a large surface area, and micropore's volume determines to a considerable extent the adsorption capacity of an AC. Macropores are not of considerable importance to the process of adsorption in AC because their contribution to the surface area of the adsorbent

is very small, and does not exceed 0.5 m^2 g^{-1}. They act as transport channels for the adsorbent into the micro- and mesopores.

To evaluate the pore size distribution, various methods have been employed using N_2 adsorption at -196 °C. The most common methods are the Dubinin-Radushkevich (DR), Barrett-Joyner-Halenda (BJH), Horvath-Kawazoe (HK), t plot, density functional theory (DFT) and the theoretical calculations based on the Grand Canonical Monte Carlo method (GCMC) [51]. DR plots are useful for finding the characteristic energy of adsorption to micropore structure, while BJH is used for mesoporous and small macropore size range. HK provides the micropore volume distribution of an active carbon, respectively. T plots determine the external surface area and micropore volume of microporous carbons. Finally, GCMC computes the relative positions of the layers until a thermodynamic (minimum energy) equilibrium is obtained to represent the pore volume distribution by size, while DFT provides a method to determine both microporosity and mesoporosity in a continuous distribution of pore volume. The information of theses analyses is usually expressed as a plot of pore volume vs. pore width.

1.2.1.2.2   CHEMICAL PROPERTIES
1.2.1.2.2.1 CARBON SURFACE GROUPS

AC's are associated with appreciable amounts of oxygen and hydrogen, as well as with atoms of sulfur, nitrogen and halogens. These heteroatoms are derived from the starting material and become part of the chemical structure as a result of the carbonization process, or they become chemically bonded to the surface during the activation or during subsequent treatments. Carbon-oxygen surface groups are the most important groups that influence the surface characteristics such as wettability, polarity, acidity, and physicochemical properties such as catalytic, electrical and chemical reactivity of these materials. AC is in general hydrophobic, but the presence of carbon-oxygen groups increases the hydrophilicity, since water molecules can form hydrogen bonds with the polar atoms of the carbon surface. Two types of carbon-oxygen surface groups (acidic and basic) have been recognized [47]. The acidic groups make the carbon surface hydrophilic and polar in character, and have been postulated to be carboxylic, lactone and phenolic groups. On the other hand, basic surface oxygen groups are pyrones, chromenes, ethers and carbonyls. Figure 1.5 summarizes the most important types of surface groups that can be present on carbon surfaces.
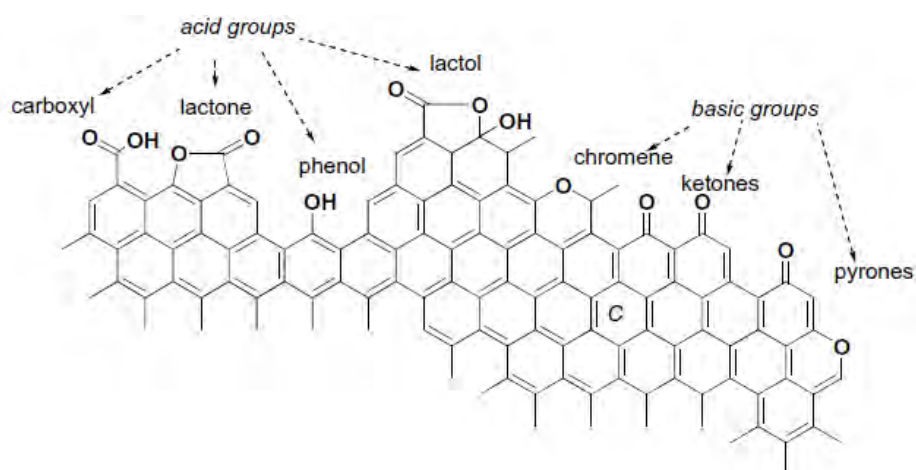
Figure 1.5 Acidic and basic oxygen functionalities on carbon surfaces [52].

The acidic groups exhibit different acid strengh following the next order: phenolic>lactones>carboxyl (and anhydrides) [50]. The acidity of any functional group is influences by its local chemical environment, that is, the size and shape of the polyaromatic layers, other neighboring groups and their charges.

The other effect that makes surface groups is related to the generation of localized electric charges all over the carbon surface, when acidic and basic groups ionizate in contact with aqueous solutions. Inozation of these surface groups depends strongly on the solution pH, and leads to build up a charge interface between the AC and the bulk of the solution. The formation of complexes occurs in addition to simple ionization/dissociation reaction of protons and hydroxyl ions. Pyrone-tipe basic group contains two non-neighboring oxygen atoms to constitute one basic site (see Figure 1.5). Upon contact with a proton in the aquoues media, the semiquinone oxygen is protonated to a hydroxyl, leaving a positive charge on the other oxygen:

(11)
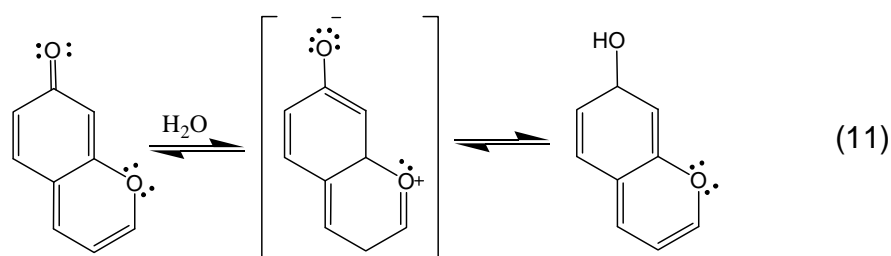
The two oxygen atoms are located at two different graphite rings, so as to favor resonance stabilization on the positive charge. The net positive charge gives rise to its

anion exchange capacity and basicity, as can be seen in equation 11. The chromene basic group (see Figure 1.5) reacts with a proton and O_2, and a positive charge is introduced to the aromatic ring that produced its basicity (see equation 12):

(12)
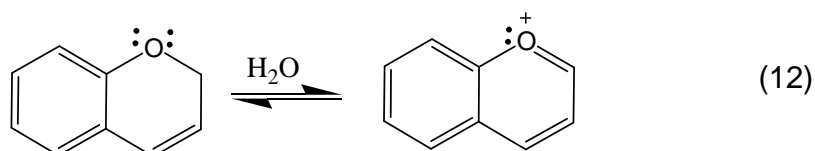
Besides the pyrone and chromene types, the basic behavior of carbon surface is also derive from the π basicity (or Lewis basicity) from the aromatic rings of graphene sheets: $C_\pi + 2H_2O \rightarrow C_\pi\text{-}H_3O^+ + OH^-$. However, the basicity from the aromatic rings is weak in comparing with those of oxygen-containign groups.

1.2.1.2.2.2   POINT OF ZERO CHARGE

The surface charge of AC is a function of the solution pH that is in contact with it. The pH at which the surface charge is zero is called the point of zero charge (pH_{ZPC}), also referred in the literature as *zero point of charge* (ZPC) [50]. At solutions pH higher than pH_{ZPC}, the sorbent is negatively charge and could interact with positive species, while at pH's lower than pH_{ZPC}, the solid surface is positively charged and may interact with negative species. The surface charge determines the capacity of the carbon for ion-exchange. In aqueous solution, the electrical double layer (or diffuse cloud) is dissociated in H^+ and OH^- to form a surface charge. Hydroxide ions (OH^-) compose the inner layer of the electrical double layer on a positively charge surface, whereas protons (H^+) form the inner layer on a negatively charged surface. Anion exchange occurs on the positively charge carbon surface via: $C_\pi\ldots OH^- + H^+ + A^- \rightarrow C_\pi\ldots A^- + H_2O$.

Cation exchange occurs on the negatively charged surface, and it is accompanied by acidification of the solution: $C_\pi\ldots H^+ + A^- \rightarrow C_\pi\ldots A^- + H^+$.

The extent of ionization in the aqueous solutions depends on the pH, and is given by the dissociation constant K. An acid "HA" and a base "B" (Bronsted acid and base) take part in the following equilibria, in water:

$$HA + H_2O \rightarrow A\text{-} + H_3O^+ \quad K_a = [H^+]\,[A^-]/[HA] \qquad (13)$$

$$B + H_2O \rightarrow BH^+ + OH^- \quad K_b = [BH^+]\,[OH^-]/[B] \qquad (14)$$
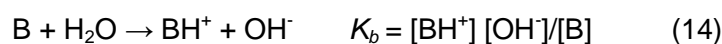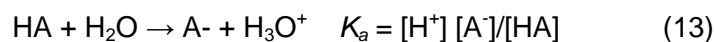
1.2.1.2.3 ANCHORAGE WITH METAL (HYDRO)OXIDES FOR ANION UPTAKE IN AQUEOUS SOLUTION

Activated carbon has proven to be an effective adsorbent for the removal of a wide variety of organic and inorganic pollutants. However, recent research has emphasized on modifying the physical and chemical attributes of carbon adsorbents to enhance the adsorption of diverse molecules that carbon usually cannot remove or that is not selective to. As was previously discussed, AC surface can display acidic or basic characteristics depending on the presence of surface functional groups.

Chemical, physical or biological modifications could be followed to modify the AC chemistry surface, which are further subdivided into their pertinent treatment techniques (see Figure 1.6).
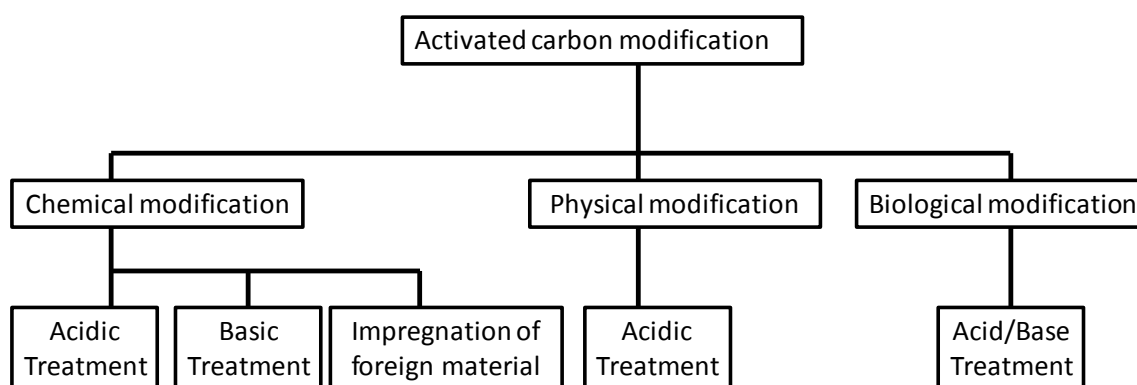
Figure 1.6 Types of modifications applied to activated carbons [53].

In terms of chemical modifications, several research has been focused on modifying AC with metal oxides. It has been reported that the most suitable way to load transition metals onto activated carbon surfaces would be as a metal oxide, for being the most thermodynamically stable form [54]. Metal oxides are employed to modify carbon materials to take advantage of its capacity to attract dissolved species such as metal cations, anions, neutral molecules and polymers [55]. In aqueous solutions, metal oxides develop a hydroxylated surface that can ionize to develop negative or positive charges as a function of the solution pH, see Figure 1.7. The hydroxylated surface of the metal oxides may also act as coordination sites for dissolved cations, or can be substituted by anions (surface coordination).
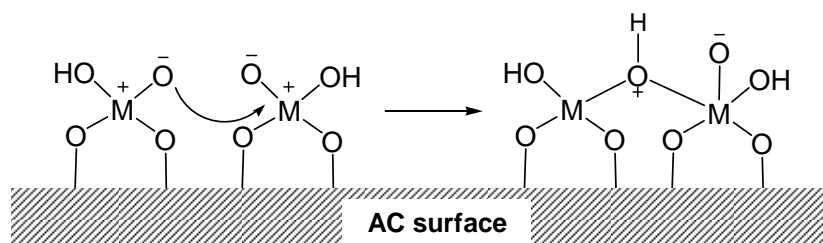
Figure 1.7 Charge development from a hydroxylated activated carbon (AC) surface.

Silver and/or Nickel impregnated AC for removing cyanide from aqueous solutions was developed by Adhoum et al [56]. It was found that silver impregnated AC has a cyanide removal capacity nearly two times that of nickel-impregnated AC, and four time that untreated AC. They conclude that uptake of cyanide on impregnated AC could be attributed to either adsorption, exchange with positively charged groups existed in the surface of AC and/or complexation in the forms of $Ag(CN)_2^-$ and $Ni(CN)_4^{2-}$. Huang and Vane [57] evaluated the effectiveness of pre-treating AC with a metallic salt solution to improve its arsenic removal capacity, where the adsorption capacity improved 10 times than untreated AC. They found that the arsenic removal was attributed to adsorption of ferrous ions and formation of arsenate complexes. Leyva Ramos et al [58] investigated the efficiency of aluminium-impregnated AC for removing fluoride from aqueous solution, which was prepared by impregnation with aluminium nitrate solution at fixed pH, followed by calcinations in an inert environment at temperatures above 300°C. They found that the impregnated AC had a fluoride adsorption capacity of three to five times that of virgin AC and that the solution pH affected the adsorption of Al(III) onto AC.

1.2.1.2.3.1 ADSORPTION OF ANIONS IN AQUEOUS SOLUTION BY METAL (HYDRO)OXIDES LOADED IN ACTIVATED CARBON

The specific mechanism for anion adsorption on modified-AC remains ambiguous. There are several factors that play significant roles in determining the adsorbability of anions onto modified-AC may depend in the specific selective binding sites developed after modification procedure. Aqueous anions adsorb on the electrically charged surface of oxides anchored on AC surface. The charge on metallic oxide particles results from the ionization upon contact with water of hydroxyl groups on their surface (M-OH) [55]:

$$M\text{-}O^- + H_3O^+ \leftrightarrow M\text{-}OH + H_2O \leftrightarrow M\text{-}OH_2^+ + HO^- \qquad (15)$$
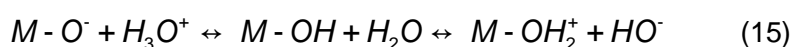
The charge on surface groups can be negative, positive or zero, depending on the pH_{ZPC}, that gives the surface a basic, acidic or neutral character. Acid-base properties of surface ligands are different from those of the ligand on the monomeric cation in solution. The surface charge on a metallic oxide is the result of acid-base equilibria, and it is a function of pH and the ionic strength of the solution. In general, metal (hydro)oxides exhibits specific binding affinity toward anions through Lewis acid-base interactions.

Besides, anion adsorption by ligand-exchange mechanism involves the release of a water dipole from the adsorption site [59]. In addition, the structure of the surface groups of metallic oxides plays an important role. They can be mono, di or tri-coordinated, and their proximity is also subjected to short-distance electrostatic interactions. The exact mechanism of anions removal is still not well documented, but a combination of protonation-deprotonation of surface sites has been suggested too.

1.2.2 ADSORPTION KINETICS

One of the most important factors in designing an adsorption system is predicting the rate at which adsorption takes place, referred as "kinetics of the adsorption". In adsorption process, the selection of an adsorbent, its configuration and attainment of equilibria are related to the "rate-limiting process". An understanding of the rate-limiting step will greatly help to decide the contact time to be allowed between the adsorbent and adsorbate, and the possible adsorption mechanism. As was described previously, there are essentially three consecutive steps in the adsorption process namely bulk diffusion, film diffusion and pore diffusion [47]. Any of these steps can be "rate-limiting" in adsorption, and can be predicted from kinetic models developed for this purpose that will be discussed in the next sections.

1.2.2.1 EMPIRICAL MODELS

The empirical models were developed to predict the overall adsorption rate but do not imply the physical mass transfer in the adsorption process.

The pseudo first-order model (or Lagergren's rate equation) is one of the most widely used rate equation to describe the adsorption of adsorbate from liquid phases, ad it is given by:

$$\log(q_e - q_t) = \log q_e - \frac{k_1 t}{2.303} \qquad (16)$$

where q_e and q_t are the amounts of adsorbate adsorbed on the adsorbent (mg g^{-1}) at equilibrium and time t (min), respectively, and k_1 is the rate constant of pseudo first order kinetics (min^{-1}).The pseudo first-order rate constant (k_1) and q_e values can be determined from the slop and the intercept of a plot t (min) vs q_t [60]. By contrast, the adsorption kinetics can also be described by a pseudo-second order process with the following equation:

$$\frac{t}{q_t} = \frac{1}{k_s q_e^2} + \frac{1}{q_e}(t) \qquad (17)$$

where q_e and q_t have the same meaning as mentioned previously, and k_2 (g mg^{-1} min^{-1}) is the rate constant for the pseudo second-order kinetics. A plot t/q_t vs t is expected to yield a straight line and the values q_e and k_s can be determined from the slope and intercept, respectively [61].

1.2.2.2 DIFFUSION MODELS

These models explain the mass transfer of solutes from solutions to solid adsorbents, and consider various resistances along the movement to the adsorbent particle. Such resistances are film and intraparticular diffusion (pore-volume diffusion and/or surface diffusion).

The intraparticular diffusion model is used to analyze the nature of rate-controlling step, and it is represented by the following Weber and Morris equation:

$$q_t = k_{ip} t^{1/2} + C \qquad (18)$$

where C (mg g^{-1}) is the intercept related to the thickness of the boundary layer and k_{ip} is the intraparticular diffusion rate constant (mg g^{-1} min$^{1/2}$). According to this model, if adsorption of a solute is controlled by the intraparticular diffusion process, a plot of q_t vs $t^{1/2}$ gives a straight line. The value C is determined from the slop of the previously plot. If the plot shows two stages, where the first shows a linear portion and the second one is a curve path followed by a plateau means that in the first stage the adsorbate is remove by the adsorbing surface binding sites of the adsorbent, while the second stage is attributed to a diffusion of the adsorbate from the surface site into the inner pores of the adsorbent [62]. The pore diffusion model (Bangham's model) has been used to describe pore diffusion during the adsorption model, given by:

$$\log(\frac{C_i}{C_i - q_t m}) = \log(\frac{k_0}{2.303V})\alpha \log t \qquad (19)$$

where C_i is the initial concentration of the adsorbate in solution (mg L^{-1}), V is the volume of the solution (mL), m is the weight of adsorbent (g L^{-1}), q_t (mg g^{-1}) is the amount of adsorbate retained at time t and α (less than 1) and k_0 are constants. A linear plot of log [$C_i/(C_i-q_t m)$] vs log t gives α and k_0 values from the slope and intercept, respectively. The Elovich equation is given as follows:

$$q_t = \frac{1}{\beta}\ln(\alpha\beta t) + \frac{1}{\beta}\ln(t) \qquad (20)$$

where α (mg g^{-1} min^{-1}) is the initial sorption rate and the parameter β (g mg^{-1}) is related to the extents of surface coverage and activations energy for chemisorption. The kinetic experimental data will be linear on q_t vs ln(t) plot if they follow an Elovich's equation. It was suggested that diffusion accounted for this model might be taken as evidence that the rate-determining step is diffusion in nature, and this equation should apply at conditions where desorption rate can be neglected [63].

1.2.3 ANALYTIC TECHNIQUES USED FOR ADSORBENT CHARACTERIZATION

Several analytical techniques have been used to identify and estimate the adsorbent's composition (or functional groups content), using several physical and chemical techniques that include potentiometric, thermometric and spectroscopic methods such IR, Energy-disperse and X-ray Photoelectron spectroscopy. A brief description of the procedures will be given in the next sections.

1.2.3.1 ACID-BASE TITRATION

Acid-base titration is of the earliest and simplest methods used to determine the nature and amount of surface acidic and base groups content in the adsorbents. Biosorbents can be characterized under such methodologies, as well as carbonaceous materials. This titration can be used to estimate the cationic exchange capacities and the diversity of functional groups present in the adsorbents. Besides, titration is able to identify and quantify the acid ionizable functional groups or binding sites that participate in pollutants uptake.

The acidic groups in the materials and their corresponding pK$_a$ values can be evaluated by identifying the inflection points of the titration curves by the first derivative and the searching for zero values on the second derivative. The number of weak acidic groups at 4<pH<7 (carboxylic, carboxylic groups linked to aromatic functions, and some proteic groups) and very weak groups attributed to cyclic compounds (phenolic, piranose) and amine groups (including the ionization of amino group) at pH>7 can be detected by simple acid-base titration. In addition, *pK$_a$* values at pH<4 can be attributed to strong acidic groups (like sulfur or phosphoric groups) [33]. The pH$_{ZPC}$ can also be determined indirectly from the acid-base potentiometric titration.

A specific methodology to characterize quantitatively acidic functionalities in activated carbons is the Boehm titration, that is based on the principle that oxygen surface groups differ in the strength of their acidity and hence can be neutralize by bases of different strengths like NaHCO$_3$ (which neutralizes carboxylic groups), Na$_2$CO$_3$ (which neutralizes lactonic and carboxylic acid groups), NaOH (that neutralizes all of three functionalities groups, giving total acidity) and C$_2$H$_5$ONa (which neutralizes carboxylic groups type aldehyde and cetone). Phenolic groups are quantified as the difference between the values obtained by Na$_2$CO$_3$ and NaOH.

1.2.3.2 FOURIER TRANSFORM INFRARED (FTIR) SPECTROSCOPY

Fourier-transform infrared spectroscopy (FTIR) in its various forms is an important tool that provides information about surface functional groups on adsorbents. Infrared radiation from 4000-400 cm^{-1} provides information about molecular vibration frequency of bonds between atoms of distinct elements. The radiation is adsorbed and converted by the adsorbent into energy of molecular vibration/rotation, and appears as spectra of multiple bands associated with the energy changes of atoms bonds characteristic of each functional group. Band positions in the spectra are presented as wavenumbers (ν) whose unit is the reciprocal centimeter (cm^{-1}). The adsorbent can be mixed with KBr to make pellets or just placed in close contact with a suitable reflecting element (AgCl, TiBr, Ge). Functional groups identified by Fourier-transform infrared spectroscopy include hydroxyl, carbonyl, nitrogen, phosphoric and sulfur content groups, carboxylic, phenolic, aromatic and some halogenated elements. Studies have used FTIR analyses to corroborate functional groups in biosorbents and activated carbons [63-64].

1.2.3.3 X-RAY PHOTOELECTRON SPECTROSCOPY

X-ray photoelectron spectroscopy (XPS) is an ultrahigh vacuum technique (10^{-9} Torr) used for surface characterization of solid and powder samples. Essentially, the technique measures the kinetic energy of electrons emitted from atoms under the influence of irradiation of the sample with X-rays. The kinetic energy of the emitted electron is related to the binding energy of electron, and it could be measured by a spectrometer. Furthermore, the penetration depth from which the photoelectron emerges is more than 10-15 nm from the surface, which makes the XPS technique ideal for surface chemical analysis as well as for the study of adsorbed species.

The binding energy of the electron is dependent upon the chemical environment of the atoms or atoms from which the electron has been emitted in form of peaks. In addition, it is useful for quantitative elemental analysis and can provide information of bonding from the measurement of chemical shift.

1.2.3.4 ENERGY-DISPERSIVE X-RAY (EDX) SPECTROSCOPY

The energy-dispersive X-ray spectroscopy is a technique used to identify elemental composition of materials. Each element has a unique atomic structure that can stimulate the emission of characteristic X-rays. A high-energy beam of charged particles (electrons or protons) interact with the sample, and the energy difference between the charged particles , mainly electrons, are excited from the inner shell of an atom of certain element. The vacancy or hole created by such effect is released in form of an X-ray. The number and energy of the X-rays emitted from the element is measured by an energy-dispersive spectrometer. This technique can be coupled with electron microscopes like the Scanning Electron or Scanning Transmission (SEM and STEM, respectively) [47].

1.2.3.5 THERMOGRAVIMETRIC ANALYSIS

Adsorbent surface contains a variety of functional groups that have different thermal stabilities, because they are formed at different sites associated with varying energies. For example, carbonyl groups decomposed at lower temperatures than phenolic or quinone groups. When the adsorbent is heat treated in vacuum or in an inert atmosphere, different surface groups decompose at different temperatures ranges. The surface groups that contain oxygen, nitrogen, phosphorous, sulfur, among others, decompose into volatile gaseous products, which are then analyzed by conventional

methods such as gravimetry, mass spectroscopy, gas chromatography and FTIR spectroscopy.

Thermal gravimetric analyses or thermogravimetric analyses (TGA) is a method in which changes in physical and chemical properties of materials are measured as a function of the temperature (with constant heating rate) or as function of time (with constant temperature and/or constant mass loss). This technique is used to determine selected characteristics of materials that exhibit either mass loss or gain due to decomposition, oxidation or loss of volatiles. The TGA instrument continuously weighs the sample as it is heated, and the basic instrument requirements for TGA are a precision balance and a programmable furnace. Numerous studies based on TGA have been focused on the main components of lignocellulosic biomass [65].

1.3 MOTIVATION OF THIS RESEARCH

Water pollution represents a serious health problem around the world. In Mexico, there are 17 estates that hold water supplies contaminated with lead, cadmium, zinc and fluoride that exceed the maximum concentration limits established by the Official Mexican Standard NOM-127-SSA1-1994. In order to bring down metal and fluoride concentration levels, several water treatment methods have been applied. Nevertheless, the capital investment and operational costs (energy consumption and maintenance) make hard its implementation. An alternative to these high-cost water treatment methods, the adsorption process is a more attractive technique that offers satisfactory results at a low-cost with a simplicity in design and widely operational applications.

The development of materials that can be used in adsorption processes for water treatment purposes is a key factor on the preparation of novel adsorbents. Many agro–based waste materials have shown to be good adsorbents for heavy metal removal from aqueous solutions. *Agave salmiana* bagasse is an agro-waste lignocellulosic material generated in the mezcal industry. Annually, 122 696 tons of mezcal agave bagasse are generated only in Oaxaca (Mexico) [66] without taking into account other states that also produce it, and its volume has been increased every year due to the high demand of mezcal beverage. Its disposal produces ecological impacts due to its low natural degradation rate. Moreover, agave bagasse is commonly eliminated by burning or it is dumped into rivers and streams. Faced with this problem, it is necessary to give a good use of this lignocellulosic material to prevent environmental problems. An alternative to this

problematic is to use the agro-waste material as bioadsorbent to remove heavy metal ions from aqueous streams.

Agave bagasse has been tested for Cr(III) removal, and can be used as bioadsorbent for other metal ions from aqueous solutions since its chemical surface possesses metal binding sites. The natural adsorption capacity of agave bagasse can be improved with several treatments or modifications using organic acid solutions to increase the number of active binding sites.

On the other hand, activated carbon has been proven to be an excellent material for water treatment processes. Its high mechanical strength, elevated surface area (800-2000 m^2 g^{-1}) and good permeability in flow-through systems make this material suitable for ionic species removal from water. Activated carbon has been tested for anionic species removal, like fluoride, from aqueous solutions; however, it does not exhibit a high affinity for this specie. A way to increase the adsorption capacity of this carbonaceous material for fluoride and other anionic species is loading metal oxides on its surface to make it more selective. These modified materials could be applied to bring down unsafe pollutants limit concentrations to allow an acceptable water quality for human health and for the environment.

1.4 MAIN OBJECTIVE

The purpose of this work is to modify raw *Agave salmiana* bagasse with organic acid solutions in order to increase its natural adsorption capacity for Cd(II), Pb(II) and/or Zn(II) from aqueous solutions, and to anchor Zr(IV) oxyhidroxides nanoparticles on commercial activated carbon for fluoride removal from aqueous streams.

1.5 SPECIFIC OBJECTIVES

a) To increase the active binding sites on raw *Agave salmiana* bagasse with organic acids to enhance its natural adsorption capacity for metal ions removal from aqueous solutions.

b) To quantify the agave bagasse main components (hemicellulose, cellulose and lignin), and to study the way that this fractions are affected with chemical treatments and metallic ions loaded into the lignocellulosic matrix.

c) To find the optimal modifying conditions to load Zr(IV) particles on commercial activated carbon surface by impregnation methodologies at room temperature, that could origin high adsorption capacity.

31

d) To characterize the modified and non-modified agave bagasse and activated carbon by physical and chemical analytical techniques in order to identify their main adsorption sites and surface area.

e) To conduct batch adsorption experiments with agave bagasse (modified or not) for Cd(II), Pb(II) and/or Zn(II) uptake, and with Zr(IV) modified activated carbon for fluoride removal, both in aqueous solutions.

f) To study the fluoride adsorption kinetic on Zr(IV) modified activated carbon and to evaluate its performance when competing anions are present in the same solution.

g) To elucidate the adsorption mechanism of metals and fluoride removal from aqueous solutions when using agave bagasse and modified activated carbon.

1.6 HYPOTHESIS

It is possible to modify raw agave bagasse with organic acids to enhance its oxygen-containing groups which are the main responsible of metal ions removal. Besides, activated carbons will be effective to remove fluoride from aqueous solutions by anchoring Zr(IV) particles on its surface, due to the high charge density of zirconium that tends to form stable fluoride complexes.

2
CHAPTER

CHEMICAL CHARACTERIZATION OF RAW AND TREATED AGAVE BAGASSE AND ITS POTENTIAL AS ADSORBENT OF METAL CATIONS FROM WATER

ABSTRACT

Lignocellulosic materials have a very complex configuration that contains a variety of active sites capable, in some cases, of adsorbing contaminants from water. Agave bagasse is a sub-product from the alcohol industry that has not been well studied, but that could have the potential to remove a variety of contaminants from aqueous solutions.

Raw and modified *Agave salmiana* bagasse were characterized, before and after they were tested to remove metal cations, by acid-base titrations, elemental analysis and ATR-FTIR. HCl, HNO_3, NaOH, tartaric, citric and oxalic acids were used to modify bagasse to determine if its concentration of active groups could be improved. These materials were then tested for the removal of Cd(II), Pb(II) and Zn(II) ions from water at pH 5, and desorption studies were performed at pH 2 and 4 at 25°C. The characterization techniques mainly identified carboxyl, hydroxyl, sulfur and nitrogen containing groups in bagasse. It was clear that mainly the carboxylic groups were responsible for metal uptake. Raw bagasse has an adsorption capacity of about 8, 14 and 36 mg g^{-1} for zinc, cadmium and lead, respectively, and this was improved approximately by 27-62 % upon modification with HNO_3 and NaOH. Treatments with citric, oxalic and tartaric acid did not have a significant effect in adsorption capacity. Raw agave bagasse has a very acceptable adsorption capacity of metal cations and it can approximately be regenerated in a 45%, since the biosorption mechanism involves ion exchange and complexation.

2.1 INTRODUCTION

Research in removal of heavy metals from aqueous streams by natural biosorbents has been conducted for several years. This technique has shown to be very promising over conventional treatment methods because of its low cost, high efficiency, easy regeneration of biosorbents, and possibility of metal recovery. The native exchange capacity and general sorption characteristics of these materials derive from their constituents: cellulose, hemicelluloses, pectin, lignin, and proteins; which contain a variety of functional groups that can adsorb certain contaminants in water [67].

Agricultural waste materials are abundant and have proven to be good low cost adsorbents due to their easy conversion to a value-added product. These biosorbents, mostly lignocellulosic residues, have a comparable metal adsorption capacity (mg g^{-1}) to other natural sorbents [42, 68-71]. Agave bagasse (*Agave salmiana*) is an abundant lignocellulosic waste material at the alcohol industry: as an example, about 350 000 tons per year are generated in the mezcal industry in Mexico. This residue produces ecological problems due to its low natural degradation rate, and because it is commonly eliminated by burning, thereby becoming a source of atmospheric pollution.

Recent studies by our research group have indicated that agave bagasse has a higher adsorption capacity for Cr(III) than sorghum or oat straw [41, 72, 73]. These results have encouraged us to continue exploring the potential of Agave bagasse to remove contaminants from water, such as Cd, Pb, and Zn that are usually found in wastewater [68,69]. Moreover, the concentration of binding sites in Agave bagasse could be increased, considering that the natural adsorption capacity of some lignocellulosic materials has been improved with treatments or modifications that include basic solutions (NaOH, Na_2CO_3, $Ca(OH)_2$), mineral and organic acid solutions (HCl, HNO_3, H_2SO_4, tartaric acid, citric acid, formic acid), organic compounds (formaldehyde, CH_3OH, epichlorohydrin), and oxidizing agents (H_2O_2, K_2MnO_4, propylene oxide) [42,43,]. For the purpose of this study, Agave bagasse was treated with mineral acids (HCl and HNO_3), NaOH, and organic acids (tartaric, citric and oxalic acid).

The aim of this work was to determine the chemical properties of raw and modified Agave bagasse, and to find out their potential to remove Cd (II), Pb (II), and Zn(II) from water. The results reported herein also suggest possible biosorption mechanisms of metallic ions.

2.2 MATERIALS AND METHODS

2.2.1 MATERIALS

Agave bagasse (*Agave salmiana*) was collected from a local distillery in San Luis Potosi, Mexico. It is important to mention that this material undergone a thermal and mechanical treatment, which was previously applied to the mature *A. salmiana* head (also known as "piña) to hydrolyze sugars and polymers, with a later milling of the agave heads. The bagasse was ground to a particle size of approximately 1 cm long and then rinsed several times with distilled water to remove impurities. It was dried overnight in an oven at 60°C, and then, stored in polyethylene bags. The adsorbent thus obtained was designated as raw agave bagasse (RAB). The bagasse was modified as follows: 25 g of RAB was soaked in 350 mL of 0.01, 0.505, or 1 M NaOH solution for 6 h at 25°C. Excess of NaOH was removed by rinsing with deionized water until a neutral pH was attained. The bagasse was then dried overnight in an oven at 60°C. The resultant material was designated as Na-AB. The same protocol was followed when treating bagasse with HCl and HNO_3, and treated samples were designated as HC-AB and HN-AB respectively.

The tartaric acid (L-$C_4H_6O_6$, Fermont) modification was conducted by a method previously described elsewhere by Wong *et al.* [75]. Na-AB, HC-AB and HN-AB were added separately to a 0.01 or 2 M organic acid solution at a ratio of 2 g of material/100 mL solution. Each mixture was stirred and heated for the time and temperature established by a fractional factorial experimental design shown in Table 2.1.

Table 2.1 Parametric settings for a 4-factor experimental design.[1]

Runs	[NaOH, HCl or HNO₃]/M	[Tartaric acid]/M	T/°C	t/min
1	1	0.01	60	120
2	1	2	100	120
3	1	2	60	10
4	0.01	0.01	100	120
5	0.01	0.01	60	10
6	0.01	2	100	10
7	0.01	2	60	120
8	0.505	1.005	80	65
9	1	0.01	100	10

[1] Statistic, versión 7.0, Statsoft, Inc. (2004)

Finally, the treated material was left to cool, washed several times with distilled water until a neutral pH was attained, and dried overnight in an oven at 60°C. These adsorbents were designated as TNa-AB, THC-AB and THN-AB: where T signifies tartaric acid treatment. The same procedure was followed when raw agave bagasse was treated with tartaric, oxalic or citric acid. These samples were named T-AB, Ox-AB and Cit-AB respectively.

2.2.2 ADSORPTION EQUILIBRIUM EXPERIMENTS

Individual stock solutions of 100 mg L^{-1} were prepared with analytical grade $Cd(NO_3)_2 \bullet 4H_2O$ (Fluka Chemika), $Pb(NO_3)_2$ (Sigma-Aldrich) and $Zn(NO_3)_2 \bullet 6H_2O$ (J.T. Baker). Samples of either 0.08 or 0.04 g of raw or modified agave bagasse were added to 40 mL of an individual metal solution (1 to 100 mg L^{-1}) in conical-bottom polypropylene tubes. The solution pH was adjusted daily to 5.0 ± 0.25 using 0.1N HNO_3 or NaOH. Experiments were monitored until equilibrium was achieved, which was determined when the concentration of adsorbate in solution remained constant. An alternative adsorption experiment was performed by contacting 0.08 g of RAB and an equimolar solution of Cd(II), Pb(II) and Zn(II) (1:1:1, 3.86×10^{-4} M). All of the experiments were conducted in duplicate. The concentrations of metal ions were determined by Inductively Coupled Plasma-Optical Emission Spectroscopy (ICP-OES) with a Varian 730-ES spectrophotometer. The adsorption capacity of the biosorbents (q_e, mg g^{-1}) was calculated as follows:

$$q_e = \frac{V(C_0 - C_e)}{w}$$
(21)

where V is the total solution volume, w is the amount of adsorbent, and C_0 and C_e are the initial and final (or equilibrium) metal concentration, respectively.

2.2.3 DESORPTION EXPERIMENTS

Agave bagasse materials were saturated with 80 mg L^{-1} of Cd(II), Pb(II) or Zn(II) at pH 5 and 25°C until equilibrium was achieved. They were then filtered and slightly rinsed with deionized water to remove any excess metal solution. The materials were then added to 40 mL of deionized water at initial pH of 2 or 4, and stirred for 72 h at 25°C. The pH of each solution was adjusted daily to 2 or 4 using 0.1N HNO_3. Finally, the concentration of metals, Ca, Na and K ions released was determined by ICP-OES and the desorption capacity was calculated by mass balance.

2.2.4 BIOSORBENT CHARACTERIZATION

Attenuated total Fourier transform infrared spectroscopy (Thermo Nicolet 6700 ATR-FT-IR) was used to determine both active groups and changes in vibrational frequencies in the functional groups of the raw and modified bagasse. The spectra were obtained within the wavenumber range of 600-4000 cm^{-1}, with a 4 cm^{-1} resolution. The influence of atmospheric water and CO_2 was always subtracted.

2.2.5 POTENTIOMETRIC TITRATIONS

Potentiometric titrations were carried out with an automatic titrator (Mettler-Toledo T70) and with an InLab DG111-SC pH electrode (Mettler-Toledo). A sample of 0.1 g of raw, pretreated or modified agave bagasse was dispersed in a 50 mL solution of 1 mM NaCl as background electrolyte. Titration was carried out by stepwise addition of 0.001 mL of 0.1 N NaOH to the flask while the solution was stirred under a N_2 atmosphere to exclude CO_2. After each addition of titrant, the system was allowed to equilibrate until a stable pH value was obtained.

2.2.6 ELEMENTAL ANALYSES

Elemental analyses of dried agave bagasse samples were performed using an Elemental Combustion System (COSTECH instruments). Samples of raw, treated or modified agave bagasse were ground to fine powder and 8 mg of each material (dry basis) were weighed on tin capsules and placed into the elemental furnace. The samples were burned in an excess of oxygen, and the mass of these combustion products (NO_2, CO_2 and H_2O) were used to calculate the percentage of C, H and N contained in each sample. The O content was calculated by difference to 100%, considering the ash content of each material.

2.3 RESULTS AND DISCUSSION

2.3.1 FTIR ANALYSIS OF AGAVE BAGASSE

The ATR-FTIR spectra of saturated materials are shown in Figure 2.1. The characteristic absorption bands in RAB indicated the presence of protonated carboxylic groups or ester groups around 1725 cm^{-1}, as well as alkyl chains (-CH_3 and -CH_2) and –OH groups at 2940 -2846 and 3360 cm^{-1}, respectively. Bands at 1410 and 1020 cm^{-1} confirmed the presence of acidic groups due to C-O and O-H of aliphatic and phenolic

structures respectively. These bands could be related to cyclic structures, such as cellulose or lignin. A new band close to 1530 cm^{-1} appeared when RAB is pretreated with acid or alkali solutions. This peak showed the presence of a carboxylate anion $((COO)_2^-)$ stretch vibration, and demonstrates the conversion of a salt or ester group to a carboxylic acid group by the following reactions [43, 76]:

$$R-C(=O)-O-CH_3 \xrightarrow{\text{NaOH}} R-C(=O)-O^{\ominus} + Na^{\oplus} \qquad (22)$$

$$R-C(=O)-O-Na \xrightarrow{H^{\oplus}} R-C(=O)-OH + Na^{\oplus} \qquad (23)$$
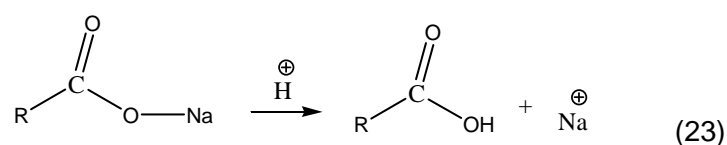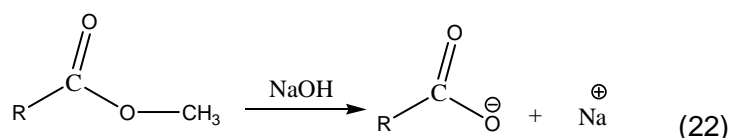
Modification with tartaric acid showed peaks around 1220 and 880 cm^{-1} related to sulfur-containing functional groups. Weak peaks around 983 and 1440 cm^{-1} were attributed to C-N-O and N-H respectively, but free –NH$_2$ groups are not clear due to band overlap between 3100 and 3680 cm^{-1}. The carboxylate ion absorbs strongly near 1714-1620 cm^{-1}, which indicates the chemical modification or introduction of carboxylic groups in the RAB pretreated structure. It is important to point out the presence of overtone or combination bands at 1720-2275 cm^{-1} attributed to aromatic structures related to cellulose or lignin (which contain a higher density of hydroxyl groups) [73].

TNa-AB and the metal-loaded TNa-AB display similar spectra: the absorbance around 1020 cm^{-1} is associated with stretching of alcoholic groups (-OH) and 2875 cm^{-1} related to CH$_3$ and CH$_2$ groups. The extent of band shifting in saturated agave bagasse with Cd(II), Pb(II) or Zn(II) gives an indication of the degree of interaction between functional groups and metal cations. There is no -OH shift among TNa-AB Pb and TNa-AB Zn except for TNa-AB Cd that has a $\Delta_{O-H}= 76$ cm^{-1}. This value may indicate that alcoholic groups could participate in Cd binding. Stretching vibrations of carbonyl (-C=O) and carbon-oxygen single bond (-C-O) were located around 1700 and 1210 cm^{-1} in all spectra, and this indicated the presence of carboxylic groups. The difference in bond stretching ($\Delta= \Delta_{-C=O} - \Delta_{-C-O}$) is related to the relative symmetry of these two carbon-oxygen bonds, and reflects the nature of carboxyl group binding status:
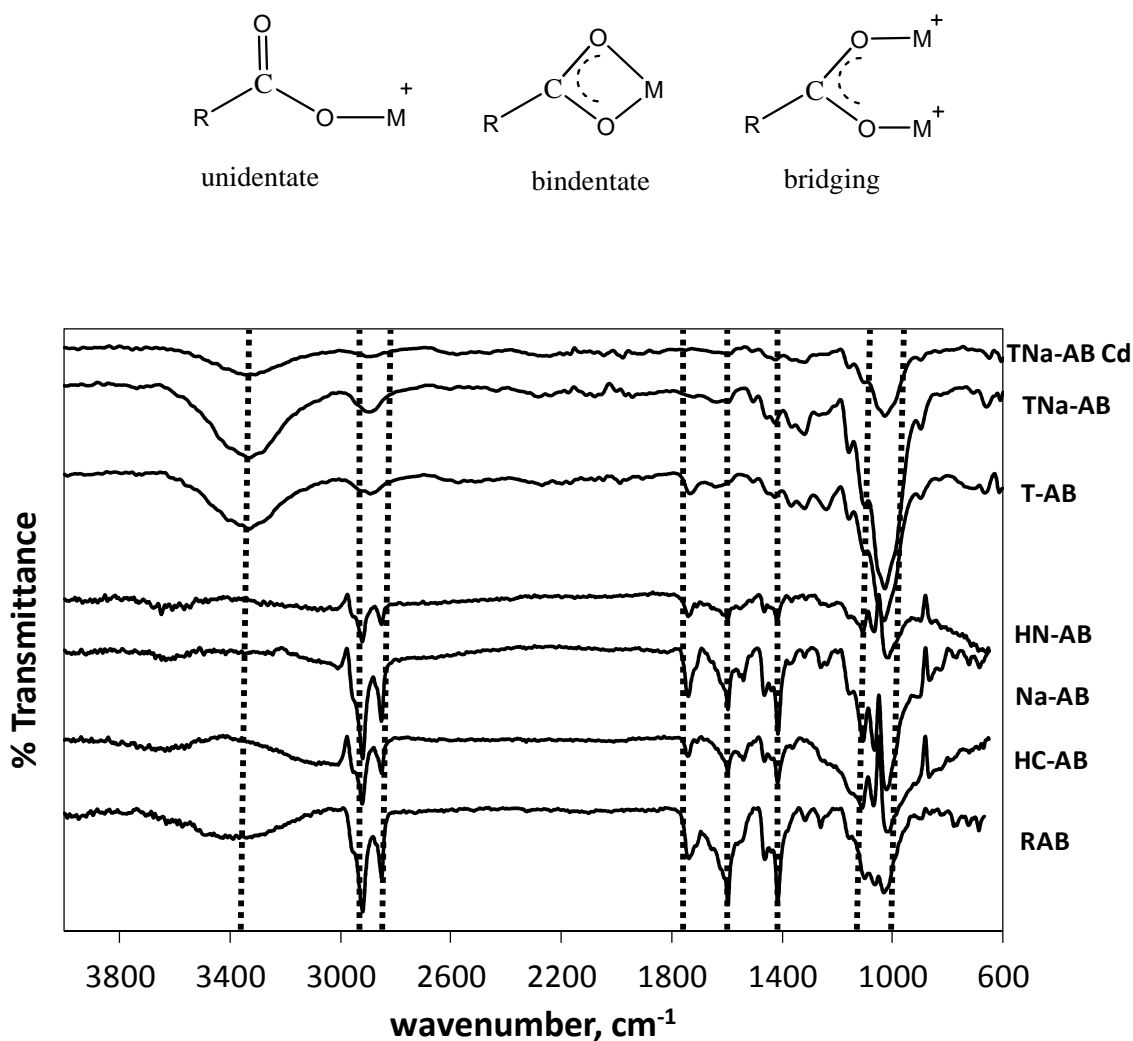
Figure 2.1 ATR-FTIR spectra for: RAB pretreated with HCl (HC-AB), HNO_3 (HN-AB) and NaOH (Na-AB); modified RAB with tartaric acid (T-AB) and pretreated RAB with NaOH prior modification with tartaric acid (TNa-AB) exposed to 80 mg L^{-1} of Cd (TNa-AB Cd) ions, at pH 5 and 25 °C.

The lower values of Δ in presence of metal ions clearly indicated more involvement of carboxylate groups forming complexes with metal ions, as was shown for TNa-AB Pb and TNa-AB Cd in Table 2.2 [77].

In general, similar spectra and shifting bands were found for THN-AB and THC-AB loaded with Cd, Pb and Zn separately. A peak at 1585 cm^{-1} (related to carboxyl asymmetrical vibration) was found in TNa-AB Pb. This peak is not present or is weaker in the others materials, suggesting that Pb bounds with carboxylate groups to form bridging

complexes. This band in the carboxylate anion decreases the frequency but not the strength of these complexes [78].

Table 2.2 Carboxyl stretching frequencies for TNa-AB materials.

Biosorbent	cm^{-1}		
	$\Delta_{C=O}$	Δ_{C-O}	$\Delta= \Delta_{C=O} - \Delta_{C-O}$
TNa-AB	1675	1214	461
TNa-AB Cd	1614	1211	403
TNa-AB Pb	1616	1217	399
TNa-AB Zn	1683	1207	476

2.3.2. POTENTIOMETRIC TITRATIONS TO DETERMINE BINDING SITES

Although the resulting agave bagasse biosorbents have a heterogeneous surface from the chemical modification, the diversity of the functional groups and their organic nature are suitable for an acid-base potentiometric titration. This titration was used to estimate the cationic exchange capacities and the diversity of functional groups present in the agave bagasse. Besides, the titration was able to identify and quantify the acid ionizable functional groups or binding sites that participate in metal uptake.

The acidic groups in the materials and their corresponding pK_a values were evaluated by identifying the inflection points of the titration curves by the first derivative and the searching for zero values was conducted on the second derivative (see Figure 2.2) [79]. The concentration of strong acidic groups, such as phosphoric or sulfonated groups at pH<4, was determined from the first peak, while the total concentration of acidic groups was determined from the final peak.

The number of weak acidic groups at 4<pH<7 (carboxylic, carboxylic groups linked to aromatic functions, and some proteic groups) and very weak groups attributed to cyclic compounds (phenolic, piranose) and amine groups (including the ionization of amino group) at pH>7 was calculated by difference [80,81].

The concentration of acidic groups in agave bagasse materials found in this study is summarized in Table 2.3.

a

b
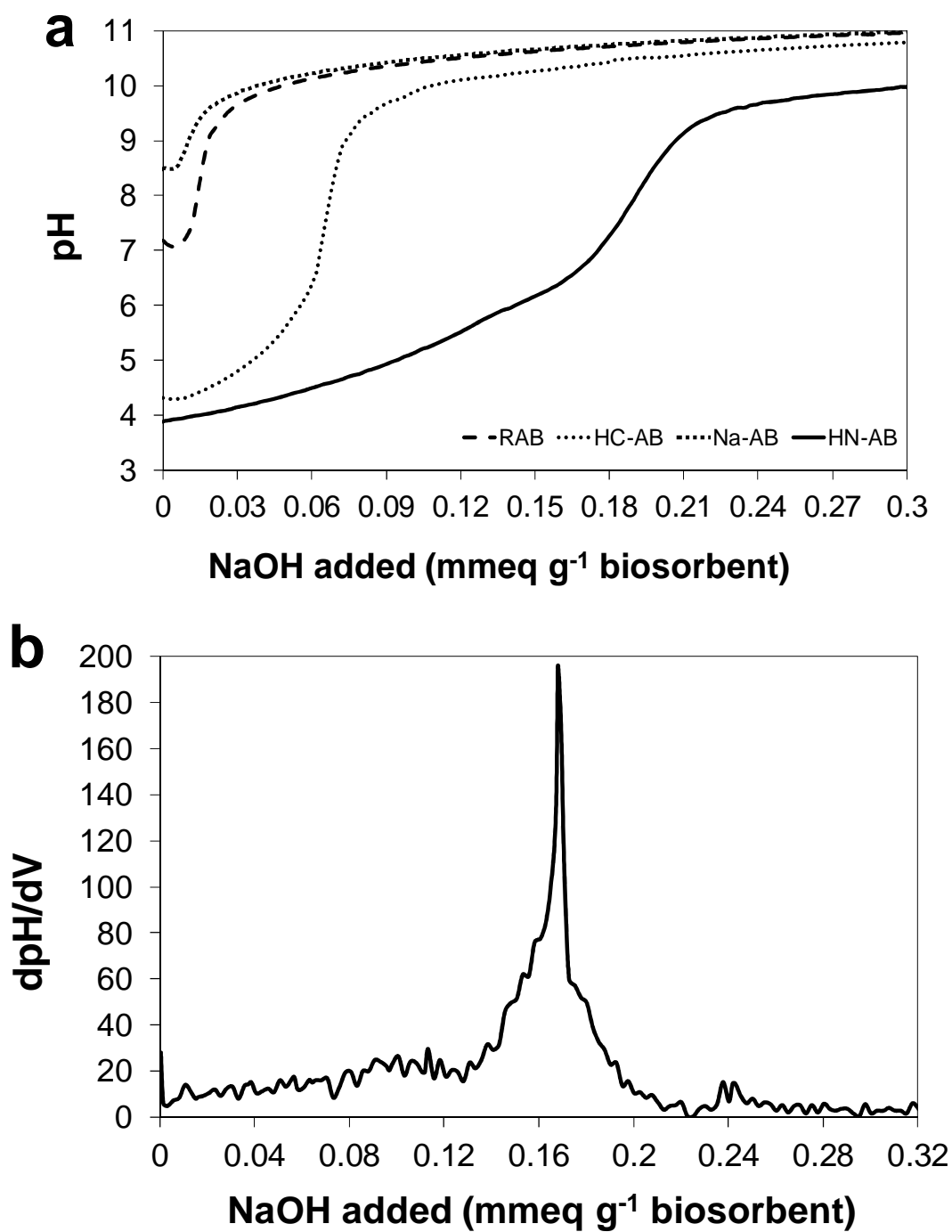
Figure 2.2 a) Potentiometric titration curves for Agave bagasse pre-treated with 1M NaOH (Na-AB) and HCl (HC-AB), and 0.505 M HNO_3 (HN-AB), and b) first derivative plot of average pH titration data for HN-AB.

Table 2.3 Quantity of acidic groups determined by potentiometric titration with 0.1 N NaOH at 25°C.

Biosorbent	Quantity of acidic groups (mmeq g^{-1} biosorbent)			
	Strong	Weak		*Total
		Very weak	-COOH	
RAB	0.0045	0.060	0.007	0.072
Na-AB	0.0095	0.284	a	0.293
HN-AB	0.0032	0.243	0.059	0.305
HC-AB	0.0045	0.353	0.053	0.412
T-AB	0.0045	0.562	0.033	0.6
Cit-AB	0.0045	0.562	0.032	0.6
Ox-AB	0.0045	0.615	0.036	0.656

* Total acidity was obtained at pH=10.8.   a Functional group not observed.

Although alkali treatment did not show the presence of carboxylic groups, it was shown that acids treatments enhanced the number of these functional groups. In spite of apparent pK_a values of pH<4 were not detected by titration, strong acidic groups (like sulfur groups) were confirmed by FTIR. This strong acidic group usually contributes to metal binding at low pH. Hydroxyl groups, among others, are considerably weaker than –COOH, and therefore may only interact with cations at pH>10 [80, 81].

An increase of weak acids was observed when RAB was modified only with organic acids, but the presence of carboxylic acids was not improved. This could be due in part to the fact that organic acids were used in secondary reactions with the bagasse. The residual organic acid concentration after the consumption by these reactions is the organic acid concentration left over for the modification. The possible secondary reaction that can take place in the bagasse is with the soluble fraction or lost compounds (26.9% w/w) of RAB, consisting of proteins, minerals, fats, gums, sugars, pectin, fatty acids, among others. Furthermore, the reported quantity of acidic values for weak functional groups suggested a structural re-adjustment of cellulose (fraction rich in -OH) derived from chemical modification, by loss of soluble and possible hemicellulose fractions during the modification process.

Although carboxylic groups are primarily responsible for metal uptake, the quantity of these functional groups remaining after exposure to Cd, Pb and Zn ions was

not observed. A minimum fraction of -COOH were found in bagasse modified with tartaric and citric acid for Pb uptake, as shown in Table 2.4. Therefore, the results corroborated that –COOH plays the major role in heavy metal biosorption in agave bagasse, and a possible bulk impediment may be affecting the adsorption of Pb ions by the remaining of weak groups.

Table 2.4 Evaluation of metal uptake of agave bagasse modified with tartaric acid (T-AB), citric acid (Cit-AB) or oxalic acid (Ox-AB), saturated with 80 mg L^{-1} of Cd, Pb or Zn ions at pH 5 and 25 °C.

| Biosorbent | Metal ion | Quantity of acidic groups (mmeq g^{-1} biosorbent) | | | *Total |
| | | Strong | Weak | | |
			Very weak	-COOH	
	Cd	0.0045	0.251	a	0.255
T-AB	Pb	0.0075	0.261	6.62e-5	0.262
	Zn	0.0075	0.261	a	0.268
	Cd	0.0045	0.554	a	0.558
Cit-AB	Pb	0.0015	0.521	8.08e-5	0.523
	Zn	0.0015	0.398	a	0.400
	Cd	0.0015	0.390	a	0.391
Ox-AB	Pb	0.0015	0.477	a	0.479
	Zn	0.0055	0.555	a	0.561
	Cd	0.0035	0.249	a	0.253
RAB	Pb	0.0002	0.238	0.0012	0.239
	Zn	0.0015	0.307	a	0.309

* Total acidity was obtained at pH=10.8.   [a] Functional group not observed.

2.3.3. ELEMENTAL ANALYSES OF AGAVE BAGASSE

Elemental analysis showed that RAB content was 0.42% N, 41.72% C, 1.69% H, and 49.26% O (considering 6.88% ash). Similarly, TNa-AB, THC-AB, THN-AB, Na-AB, HC-AB and HN-AB contained almost equal amount of carbon (C) and hydrogen (H), with some variations in nitrogen (N), oxygen (O) and ash content. The O content in HC-AB and HN-AB increased 4.9% compared to RAB, but slightly decreased (1%) for Na-AB. However, the ash content in these samples decreased nearly 33%. This behavior showed

that the modification increased the concentration of oxygenated groups (as carboxyl groups), and reduced the ash content due to the loss of the soluble and inorganic fraction contained into RAB. TNa-AB, THC-AB and THN-AB showed the same behavior, except that the oxygenated group density was improved 3.5, 12.6 and 10.0 % respectively. These contents suggested that oxygenated groups (like carboxylic groups) could be introduced into RAB's cellulose or lignin fractions, as shown in FTIR analysis and potentiometric titrations.

2.3.4. ADSORPTION CAPACITY OF AGAVE BAGASSE

The experimental sorption data of Cd(II), Pb(II) and Zn(II) in RAB were fitted with the Langmuir and Freundlich isotherm models. Both models fit the experimental data reasonably (see Table 2.5), based on the correlation coefficient (r^2).

Table 2.5 Isotherm parameters estimated from experimental data for raw agave bagasse (RAB).

Metal ion	Langmuir			Freundlich		
	b (L mg^{-1})	q_{max} (mg g^{-1})	r^2	k (mg$^{1-1/n}$L$^{1/n}$ g^{-1})	n	r^2
Cd(II)	0.0627	16.770	0.9878	3.3798	2.764	0.9875
Pb(II)	0.1892	38.4189	0.9838	13.6749	4.055	0.9658
Zn(II)	0.0301	12.1334	0.9908	1.0479	2.032	0.9935

The fit of data by adsorption models would not reflect any sorption mechanism and can hardly have a meaningful physical interpretation due to the complex nature and varied active sites of agave bagasse [82]. However, the Freundlich model (equation 24) was used due to the nature of the biosorbent under study.

$$q_e = K_F C_e^{1/n} \qquad (24)$$

where K_F (mg$^{1-1/n}$L$^{1/n}$ g^{-1}) and n (dimensionless) represent the Freundlich constants related to the sorption capacity and to the strength of the sorption process, respectively. Cd(II), Pb(II) and Zn(II) adsorption isotherms in raw agave bagasse are shown in Figure 2.3, where it can be seen that affinity sequence is Pb>Cd>Zn.
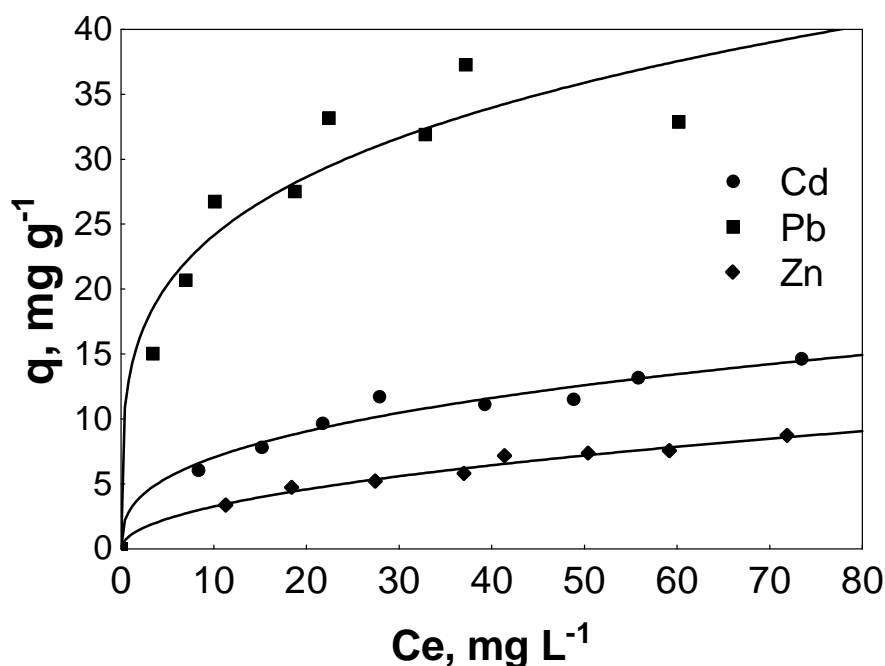
Figure 2.3 Adsorption isotherms of Cd(II), Pb(II) and Zn(II) onto raw agave bagasse (RAB) at 25 °C and pH 5. Continuous lines represent the Freundlich model.

When *Agave salmiana* bagasse was exposed to an equimolar solution of Cd(II), Pb(II) and Zn(II) (1:1:1, 1.544×10^{-5} mol), the metal uptake was 22.64, 4.76 and 3.39 mg g^{-1} for Pb, Cd and Zn ions respectively. Ca, Na and K ions were released during the adsorption process (5.50, 0.64 and 3.19 mg g^{-1} respectively). Those alkaline metal cations are considered micronutrients, and they are found in some of the functional groups contained into the polysaccharides of hemicellulose and soluble compounds of agave bagasse. Their release suggests an ion exchange and/or complexation adsorption mechanism between those functional groups and metal ions, due to the higher electronegativity of heavy metal ions than alkaline (light) metal ions. The affinity of a metal for binding sites depends on its physical and chemical properties. Pb(II) offers a bigger coordination sphere than Cd(II) or Zn(II) since it has a bigger ionic radius (1.21 Å) than Cd (0.97 Å) or Zn (0.74 Å). Hence, Pb ions can bind better with two distant functional groups. Besides, the coordination sphere of Pb(II) embraces a higher number of –OH and –COO$^-$ groups, making Pb-complexes more stable than Cd or Zn-complexes.

In addition, the preference of biosorbents for metals has been related to the metal electronegativity: a more electronegative metal ion will be strongly attracted to the negative surface of a biosorbent [10, 83]; the electronegativity values of Zn(II), Cd(II) and Pb(II) are

1.60, 1.69 and 1.79 respectively. Moreover, the interaction between metal ions and binding sites can be related to the strength of chemical bonds. The higher the covalent index of a metal ion the higher its potential to form covalent bonds with binding sites of biosorbents [83]. The covalent index of Zn(II), Cd(II) and Pb(II) is 4.54, 5.29 and 6.61 respectively. All these parameters are in total agreement with the adsorption capacities reported herein.

It should be mentioned that other adsorbents materials have been tested to remove Pb, Cd and Zn ions from water and the data reported can vary significantly. For instance, the adsorption capacities of the activated carbon Darco [27], orange peel [85] and saltbush flowers [86], at the conditions of our experiments are between 0.38-34.8 mg g^{-1} for Pb, 0.23-25 mg g^{-1} for Cd and 0.31-14 mg g^{-1} for Zn, which is in the same range as the adsorption capacity of agave bagasse.

2.3.4.1. EFFECT OF CHEMICAL MODIFICATION OF AGAVE BAGASSE ON ADSORPTION CAPACITY

Although these results have shown that *Agave salmiana* bagasse is an effective adsorbent for the removal of Cd, Pb and Zn ions in aqueous solutions, a pretreatment with acids or alkali could improve its natural sorption capacity. Strong acids like HCl or HNO$_3$ can protonate unavailable functional groups contained in the structure of biosorbents. Furthermore, HNO$_3$ can also transform functional groups mostly to carboxylic groups by oxidation. On the other hand, formation of carboxylate moieties from esters is carried out by NaOH treatment [41, 42].

Table 2.6 shows adsorption capacities at equilibrium concentration (C_e) of 60 mg L^{-1} for RAB treated with NaOH, HCl and HNO$_3$ solutions at different molar concentrations. Acid treatments with 0.505 M HNO$_3$ increased Pb and Zn sorption capacity but at high concentration of acid this decreased. Comparing with RAB, 1M HCl improved metal uptake about 18.84 and 58.16 % for Pb(II) and Zn(II), respectively. 1M NaOH treatment on RAB increased 38.05, 40.78 and 162% of Cd(II), Pb(II) and Zn(II) uptake respectively at room temperature. It has been demonstrated that lignin contents in lignocellulosic materials appears to have a predominant incidence of metal uptake beyond these treatment conditions [87, 88]. During dilute acids pretreatments in lignocellulosic materials at room temperature it is developed not well-organized cellulose. Because of this, a small portion of lignin is solubilized, condenses and precipitates. Due to this lignin lose, a decrease in metal ion capacity is showed. In the other hand, NaOH swells the cell wall matrix of the lignocellulosic structure by solvation and saponification reactions, which allows a better

diffusion of metal ions and exposes new adsorption sites. Besides, the relative high alkali treatment enhances the chemical modification of functional groups to more carboxylate moieties [38, 70, 87]. Hence, 1 M NaOH worked better than acid treatments at the same conditions.

Table 2.6 Metal sorption capacity (mg g^{-1}) of acid and alkaline modified agave bagasse at pH 5, C_e=60 mg L^{-1} and 25°C.

Metal ion	HN-AB/ mg g^{-1}			HC-AB/ mg g^{-1}			Na-AB/ mg g^{-1}			RAB
	* 0.01	0.505	1	0.01	0.505	1	0.01	0.505	1	
Cd(II)	9.45	13.50	7.58	5.41	7.26	12.50	4.91	10.95	18.32	13.27
Pb(II)	22.50	54.29	32.01	33.10	32.00	42.31	7.51	13.90	50.12	35.60
Zn(II)	4.12	14.43	10.56	6.23	5.34	12.40	3.72	1.57	20.54	7.84

* Molar concentration = mol L^{-1}

Another strategy to enhance the natural binding capacity of RAB was to modify Na-AB, HC-AB and HN-AB with tartaric acid (TNa-AB, THC-AB and THN-AB). Although similar sorption capacities were obtained, the optimal metal uptake occurred when RAB was treated with 0.505 M NaOH, HCl or HNO$_3$ solutions, follow by a modification with 2M tartaric acid at 100°C during 10 min. On the other hand, modified agave bagasse with tartaric acid at 100 °C during 10 min (T-AB) did not improve the natural metal binding capacity of RAB, as shown in Figure 2.4. If cellulose in lignocellulosic materials plays a major role in chemical modification with organic acids [5, 44], then the low content of this fraction in RAB (7.42%) that can be modified and interact with metal ions is reflected in a low adsorption capacity.

Steric effects are much more common when large acids, such as tartaric acid, are used in reactions and can affect the proton exchange from the possible carboxylic acids anchored during the structural re-adjustment when it reacts with metal ions. Modification of RAB with 2M tartaric, citric or oxalic acid at 100 °C during 10 min suggested that although oxalic acid is a relatively strong acid compared to citric or tartaric acid, the stability constants of Pb with oxalic acid (log K_1= 6.54) are higher than those for the other organic acids (log K_1 =3.78, log K_1= 5.2 for tartaric and citric acid respectively). This difference may account for the enhanced sorption affinity of Pb in modified materials with the organic acids, especially with oxalic acid.
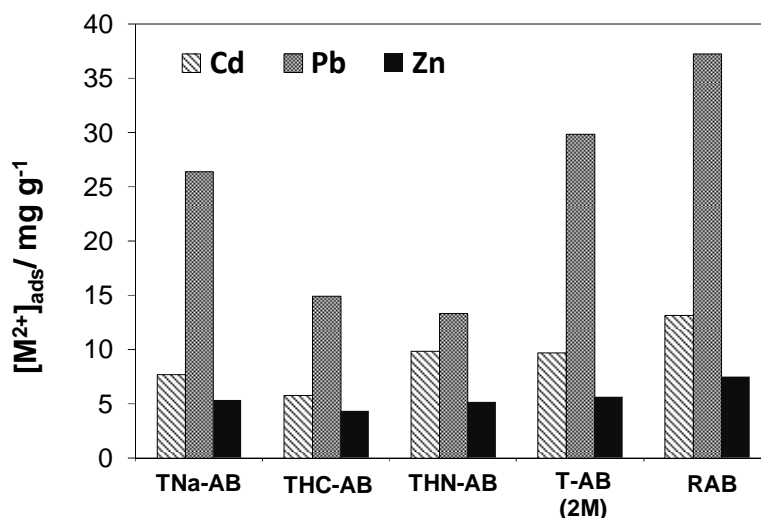
Figure 2.4 Effect of agave bagasse modification on the adsorption capacity of Cd(II), Pb(II) and Zn(II) in aqueous solution at pH 5, C_0= 80 mg L^{-1} and 25 °C.

It is believed that the organic acids were mainly attached on binding sites located on the external surface of the biosorbents, which could restrict the diffusion of metal ions to the interior of the biosorbent. Moreover, the steric effects that are also present reflected the low adsorption capacity compared to non-modified agave bagasse.

The pKa values of citric (pK_1= 3.15, pKa_2= 4.77 and pKa_3= 5.19), oxalic (pKa_1= 1.25 and pKa_2= 4.26) and tartaric (pKa_1= 3.03 and pKa_2= 4.36) acids are lower to the pH of adsorption experiments (pH= 5), thus, they will be in a deprotonated form. This suggests that the negative charge on the modified lignocellulosic matrix surface adsorbs heavy metal ions by electrostatic attractions. However, possible covalent binding between metals and organic acids could "consume" negatively charged groups, and becomes neutral charged groups [33], originating a lower adsorption capacity in the following adsorption binding sites.

From these results (see Table 2.7), it can be concluded that acid or alkali treatments, in agave bagasse, are more efficient to enhance metal sorption capacity than subsequent modifications with tartaric, citric or oxalic acid.

48

Table 2.7 Adsorption capacities of modified agave bagasse with citric, oxalic or tartaric acid. C_0=80 mg L^{-1}, pH=5 and 25°C.

Sorbent	Metal uptake/ mg g^{-1}		
	Cd	Pb	Zn
Cit-AB	10.48	26.01	6.36
Ox-AB	11.99	52.28	6.84
T-AB	9.70	29.89	5.62

2.3.5. REGENERATION OF SATURATED AGAVE BAGASSE

In order to determine the regeneration degree of agave bagasse, metal desorption experiments were carried out with 0.1 N HNO$_3$. This acid was selected aiming at an ion exchange between H$^+$ and the adsorbed metal (COO-M(II)). Figure 2.5 shows Cd(II), Pb(II) and Zn(II) desorption from saturated RAB, Na-AB, HC-AB and HN-AB. If metal ions were adsorbed on carboxyl groups by electrostatic interaction, then acid solutions, such as HNO$_3$, would regenerate the metal-loaded bagasse sorbents. In this case, concentration of H$^+$ increased and the protonation of carboxylic groups occurred, resulting in the following ion exchange as follows:

$$(\equiv R \quad COO) \quad M + H^+ \leftrightarrow M^{2+} + (\equiv R \quad COOH) \quad \text{where} \quad M = Cd, Zn \qquad (25)$$

Figure 2.5b showed that the desorbed metal from agave bagasse sorbents is lower than 25% in all cases, at pH 4. In all cases, Pb desorbed more than Cd and Zn ions with the exception of HN-AB. This could indicate that the possible bridging complexes (found with ATR-FTIR spectra) between carboxylic groups and Pb(II) are little unstable. This complex structure required two Pb molecules and could be the reason of high desorption of Pb ions from agave bagasse sorbents. Besides, K$^+$ released from these sorbents was detected between 0.18-2 mg g^{-1} while Ca^{2+} and Na$^+$ were not detected at this pH. These results suggested that Cd, Pb and Zn ions form more stable sphere coordinated complexes with agave bagasse sorbents.

Conversely, heavy metal ions were desorbed up to 45% at pH 2 from all samples previously saturated with Cd(II), Pb(II) or Zn(II) ions, as can be seen in Figure 2.5a. This result suggests that coordinated complexes between metal ions and carboxylic groups could be of inner-sphere, because these have more stable chemical bonds (e.g. covalent coordinated bonds) that are hard to break even at low pH [89]. Potassium (K, 0.2-2 mg g^{-1}) was the only detected in the desorption experiments at pH 2.

Desorption experiments were also conducted with saturated RAB exposed to an equimolar solution of Cd(II), Pb(II) and Zn(II) (1:1:1, 1.544×10^{-5} mol) at pH 2, see Figure 2.5c. The results showed that Pb display the major desorption quantity, 41.73 %. This result confirmed than complexes between Pb and carboxylic groups (COO-Pb$_2$) were less stable (outer-sphere coordination) than those with Cd and Zn (inner-sphere coordination) since desorption quantity was much lower (3.90 and 1.26 % respectively).
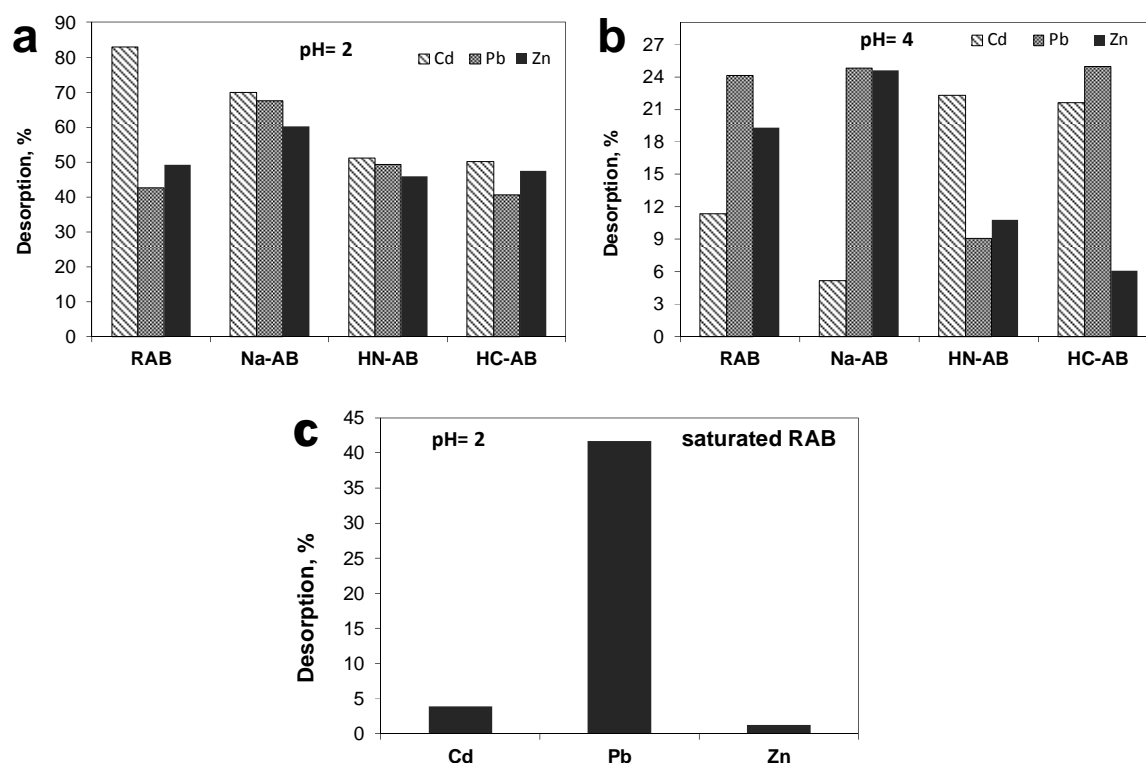
Figure 2.5 Desorption experiments with previously saturated materials with C$_o$= 80 mg L^{-1} of Cd(II), Pb(II) and/or Zn(II) at pH 2 (**a** and **c**) and pH 4 (**b**). Desorption experiments were conducted for 72 h at 25 °C.

Na, K, and Ca were desorbed at 3.47, 0.22 and 4.22 mg g^{-1} respectively (see Figure 2.5c). These results demonstrated that the soluble fraction contained in RAB had alkaline metal ions that were related to an ion-exchange mechanism with Cd(II), Pb(II) and Zn(II) ions, studied in this research. Those alkaline metal ions could balance the uptake of heavy metal ions and protons. Hence, when H$^+$ uptake took place in desorption experiments alkaline metals were released [33].

2.3.6 ADSORPTION MECHANISMS

Titrations, FTIR and desorption results confirmed that oxygen-containing groups (e.g. carboxylic and phenolic) are involved in metal sorption.

Therefore, based on the experimental results, a possible adsorption mechanism for RAB treated with acid (6) and alkali (7) is proposed:

$$(\equiv R - COOH)_n + nM^{z+} \leftrightarrow (\equiv R - COO)_{n-1} M^{(z+)-1} + nH^+ \qquad (26)$$

$$(\equiv R - COO^- Na^+)_n + nM^{z+} \leftrightarrow (\equiv R - COO)_{n-1} M^{(z+)-1} + nNa^+ \qquad (27)$$

where M = Cd, Pb or Zn. A similar mechanism is suggested for cyclic groups, as phenolic and piranose structures, derived from modified cellulose with mineral or organic acids:

$$(C_6H_9O_5 - OH)_n + (R - COOH)_n \xrightarrow{-H_2O} (C_6H_9O_5O - COOH)_n + nM^{(z+)}$$
$$\leftrightarrow (C_6H_5O - COO) - M^{(z+)-1} + nH^+ \qquad (28)$$
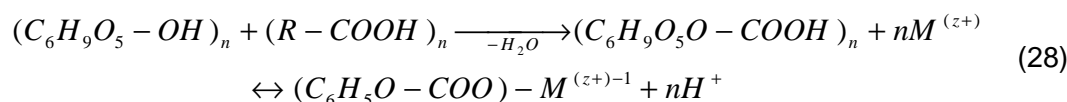
2.4 CONCLUSIONS

Agave bagasse mainly contains carboxyl, hydroxyl, sulfur, and nitrogen containing groups. Furthermore, ATR-FTIR spectra and acid-base titrations results show that carboxylic groups are involved in the uptake of heavy metals. On the other hand, chemical treatments performed to raw agave bagasse with mineral acids or NaOH modified the functional groups implied in the removal of Cd, Pb and Zn ions. Alkali treatment improved the adsorption capacity for Cd(II) and Zn(II) by developing new adsorption sites, as carboxylate moieties, likely inside the swelled lignocellulosic structure. Pb(II) adsorption capacity was improved with HCl treatment due to the protonation of functional groups, specially of those that play a major role (–COOH) in cation biosorption. Chemical modifications with organic acids do not enhance the adsorption capacity due to a possible bulk impediment with the carboxylic and weak functional groups developed during the structural re-adjustment.

Moreover, the suggested sorption mechanisms are ion exchange and complexation, and the saturated bagasse can be regenerated up to 45%. Finally, *Agave salmiana* bagasse is an acceptable biosorbents to remove Cd(II), Pb(II) and Zn(II) ions from aqueous solution, compared to activated carbon and other organic waste materials.

Considering that raw *Agave salmiana* bagasse could be a potential adsorbent for Cd(II), Pb(II) and Zn(II) ions contained in aqueous solutions, it is important to study the chemical behavior of binding sites when those metal ions are adsorbed in the lignocellulosic matrix, and the role that main components (hemicellulose, cellulose and lignin) of agave bagasse play in the adsorption process. This study is presented in the next chapter.

3
CHAPTER

CHEMICAL AND THERMOGRAVIMETRIC ANALYSES OF RAW AND SATURATED AGAVE BAGASSE MAIN FRACTIONS WITH Cd(II), Pb(II) AND Zn(II) IONS: ADSORPTION MECHANISM

ABSTRACT

Agave *salmiana* bagasse, a sub-product from the mescal industry in Mexico, has proved to be a good biosorbent for heavy metal ions in aqueous solution. However, more information about the chemical structure of agave bagasse and the interaction of metal ions with the bagasse main components remain to be understood.

Raw bagasse and its fractions hemicellulose, cellulose and lignin were characterized by acid-base titrations, ATR-FTIR and TGA, before and after they were tested to remove Cd(II), Pb(II) and Zn(II) from aqueous solution. Oxygen, sulfur and nitrogen containing groups were identified in both raw bagasse and in its fractions. On the other hand, thermogravimetric analyses of the exhausted biosorbent demonstrated that Cd(II) and Pb(II) ions shifted the pyrolisis temperature of NDF fraction from 238° C to 247.4 and 252.5^{o} C, respectively, while Zn(II) decreased it to 232.1^{o} C.

Results showed that carboxylic and strong acid groups that contain sulphur or phosphate were main responsible for metal removal and that the sorption affinity of the fractions was Pb>Zn>Cd. Moreover, the soluble fraction was the principal contributor for Cd(II) and Pb(II) uptake, except for Zn(II) where hemicellulose played an important role. Finally, the higher or lower pyrolisis temperature of the exhausted NDF fraction was related to decarboxylation reactions and elimination of hydroxyl groups.

3.1 INTRODUCTION

Agave *salmiana* bagasse, an agro-waste material generated in the production of mescal (an alcoholic beverage), has been studied by our research group due to its great potential as biosorbent of metal ions in aqueous solutions. This lignocellulosic material has shown a high adsorption capacity for Cr(III) compared with sorghum and oat straw. Moreover, it was found that the lignin fraction had major responsibility for chromium uptake [71, 72]. Furthermore, raw and modified agave bagasse have been explored to determine their Cd(II), Pb(II) and Zn(II) adsorption capacity [90].

The low cost and abundance of the biosorbent may contribute to the sustainability of the surrounding environment, and could offer promising benefits in wastewater treatment processes. Previous studies have shown that the adsorption capacities of raw and modified agro-wastes can be related to the main components: cellulose, hemicelluloses and lignin, as well as pectin, proteins, and extractives (sugars, nitrogenous, sulphur and phosphorous compounds, waxes, minerals, lipids) found in the lignocellulosic matrix [91].

Cellulose is the main structural component of these materials and consists of D-glucose subunits linked to each other by β–(1,4)-glycosidic bonds, and hemicellulose, as cellulose, is a polymer constituted of sugar units of pentoses (xylose, ramnoses, and arabinose), hexoses (glucose, mannose, and galactose), and uronic acid (e.g., 4-o.methylglucuronic, D-glucuronic, and D-galactouronic acids). Lignin is a complex and three-dimensional molecule containing cross-linked polymers of phenolic monomers (phenylpropane units) [87].

Regardless of the arrangement of these constituents, their chemical composition includes a variety of functional groups (amino, hydroxyl, carboxylic, carbonyl, nitro, sulphur, phosphorus, among others) that act as binding sites for heavy metal ions. However, not enough information is available about the contribution of biosorbents main components in the removal of metal ions such as Cd, Pb and Zn. Furthermore, the heterogeneous chemical surface of the agave bagasse main components has not been investigated in detail, but this knowledge is essential to understand and to propose the adsorption mechanisms involved in metal ions uptake. Moreover, this information can facilitate the screening of lignocellulosic materials when these are intended to be employed to produce composites, to generate energy or as biosorbents in wastewater treatment.

3.2 MATERIALS AND METHODS

3.2.1. MATERIALS

Agave bagasse (*Agave salmiana*) was collected from a local distillery in San Luis Potosi, Mexico; that followed previous treatments described in section 2.2.1 (Chapter 2). The bagasse was grounded to a particle size of approximately 1 cm and then washed several times with distilled water to remove impurities. Then, it was dried overnight in an oven at 60°C and stored in polyethylene bags. The adsorbent thus obtained was considered as raw agave bagasse (RAB).

3.2.2 FIBER ANALYSIS

A procedure for fiber analysis of raw agave bagasse was applied following the filter bag technique [92] using an ANKOM 200 Fiber Analyzer (Macedon, NY, USA). The neutral detergent fiber (NDF), which contains hemicelluloses, cellulose and lignin, was obtained after solubilizing 0.5 g of raw bagasse during 175 min in a detergent solution consisting in sodium lauryl sulfate, EDTA salt and triethylene glycol (premixed chemical solution from ANKOM Technology) in presence of thermoresistant alpha-amylase. The acid detergent fiber (ADF), which contains cellulose and lignin, was obtained after digesting the NDF fraction during 60 min with cetyltrimethylammonium bromide (CTAB) in 1 N H_2SO_4, while acid detergent lignin (ADL) was obtained by soaking the ADF fraction in a 24 N H_2SO_4 solution during 180 min. These procedures are based on the sequential method proposed by Van Soest [93]. Finally, the samples were calcinated to determine their ash content.

3.2.3 ADSORPTION EQUILIBRIUM EXPERIMENTS

An equimolar solution of 7×10^{-4} mol of Cd(II), Pb(II) and Zn(II) was prepared with deionized water by using $Cd(NO_3)_2 \bullet 4H_2O$ (Fluka Chemika,), $Pb(NO_3)_2$ (Sigma-Aldrich) and $Zn(NO_3)_2 \bullet 6H_2O$ (J.T. Baker). Previous adsorption isotherms showed that agave bagasse is saturated with this concentration of metal ions [90]. Samples of 0.05 g of NDF, ADF or ADL were added to 20 mL of the equimolar solution in conical-bottom polypropylene tubes. The pH of each solution was adjusted daily to 5.0 by 0.1N HNO_3 or NaOH until the equilibrium was achieved. The concentrations of Cd(II), Pb(II) and Zn(II) were determined by inductively coupled plasma-optical emission (ICP-OES), and the amount of adsorbed metal (or adsorption capacity, q_e) for each fraction (mg g^{-1}) was calculated by using equation 21 (see section 2.2.2, Chapter 2).

3.2.4 BIOSORBENT CHARACTERIZATION

Attenuated Total Fourier Transform Infrared spectroscopy and acid-base potentiometric titrations of raw and modified agave bagasse were performed following the methodologies mentioned in sections 2.2.4 and 2.2.5, respectively (Chapter 2). Thermogravimetric analyzes were performed with a Thermo Cahn Versa analyzer (Thermo scientific, USA). 30 to 40 mg of each material was heated from 25 to 800 °C at a rate of 10 °C/min, under N_2 atmosphere. The pore size and surface area of the adsorbents were calculated from N_2 adsorption-desorption isotherms at 77 K (Micrometrics ASAP 2020). Surface area was estimated from the BET isotherms, and the pore size distribution was obtained by using the density functional theory (DFT).

3.3 RESULTS AND DISCUSSION

3.3.1 FIBER ANALYSIS

Table 3.1 shows RAB main components percentage. Cellulose was in major proportion (greater than 40%) compared with hemicellulose and lignin (14.0 and 9.1%, respectively). The percentage of the soluble fraction was around 35.5%, which could be due to the previous cooking of the ripe agave head (also known as "piña") and later milling of it to extract sugars to produce mescal. Sugars, starch, fatty acids and pectin can be the main components of the soluble fraction of RAB. The inorganic fraction contains Ca, Na, K and other metal oxides that are considered micronutrients of agave plant [90, 94].

Table 3.1 Content of main components of *Agave salmiana* bagasse fibers in dry basis.

Fraction fiber	Percentage (%$_{w/w}$)
Soluble	35.60
Hemicellulose	14.00
Cellulose	41.14
Lignin	9.10
Inorganic	0.16

Reported results for sugarcane bagasse showed 28% of lignin and 72% of holocellulose (cellulose + hemicelluloses) in dry and extractive-free basis [87]. Both agave and sugarcane bagasse, agrowastes, are defined as lignocellulosic materials by their holocellulose and lignin content greater than their corresponding soluble fraction.

3.3.2 PHYSICAL PROPERTIES AND FUNCTIONAL GROUPS OF AGAVE BAGASSE FIBER AND FRACTIONS.

In order to understand the role of the main components of *Agave salmiana* bagasse in the adsorption process of Cd(II), Pb(II) and Z(II) ions, the fractions obtained in the fiber analysis of the previous section were used to describe such metal ion uptake. It is important to consider that the fractions studied, that contain cellulose, hemicellulose and/or lignin, are not exactly the same to the originally found in the natural fiber. This is due to the strong digestion procedure that followed the raw fiber to obtain the fraction main components, which could propitiate a structural rearrangement of the lignocellulosic matrix.

Table 3.2 shows that NDF fraction (composed only by hemicellulose, cellulose and lignin) posses 36% less surface area than raw agave bagasse (RAB). In other hand, ADF fraction lost around 76% of its surface area with respect of NDF, and was due to the removal of hemicellulose. The lignin fraction represented 29% of the total surface area of the lignocellulosic bagasse. RAB and its fractions are considered as non-porous materials due to their low porosity and extremely low surface area. Besides, it was found that the sequential extraction procedure reduced around 50% of meso and macropore volume. Micropore volume was not detected. These results demonstrated that the extraction procedure to obtain each main component of the lignocellulosic material eliminated 71% of its total surface area and porosity.

Table 3.2 Physicochemical characterization of raw and main fractions of agave bagasse.

| Sample | BET (m^2 g^{-1}) | Pore volume (cm^3 g^{-1}) | | | pH_{PZC} |
		Micropore (<2 nm)	Mesopore (2-50 nm)	Macropore (>50 nm)	
RAB	0.52	0	0.0010	0.0018	8.33
NDF	0.33	0	0.0004	0.0005	7.09
ADF	0.25	0	0.0006	0.0007	7.54
Lignin	0.15	0	0.0006	0.0009	9.26

ATR-FTIR spectra are shown in Figure 3.1. The absorption bands in RAB indicated the presence of C=O stretching vibration from carboxylic groups or ester groups at about 1722 and 1614 cm^{-1}, as well as alkyl chains (CH_3 and CH_2) and –OH groups at 2911, 2861

and 3338 cm^{-1}, respectively. Bands between 1455 and 1037 cm^{-1} confirmed the presence of coupled C-O and O-H vibrations of aliphatic and phenolic structures, respectively (Figure 3.1a) [76]. Broader and intense peaks were observed after RAB was treated to obtain the NDF fraction. This is attributed to the chemical and thermal process applied to RAB to remove its soluble compounds, which makes oxygen, sulphur, phosphorous and nitrogen containing groups more freely vibrate, and hence well defined signals of these functional groups obtained. A weak overlap band situated in 3342 cm^{-1} in NDF fraction can be related to O-H stretching and H-bonded in dimerized acids moieties. The presence of carbonyl groups was confirmed from bands situated in 1600-1800 cm^{-1}. Furthermore, defined overtone or combination bands can be found between 2300 and 1890 cm^{-1}, indicating aromatic groups. Weak absorption bands about 771 and 640 cm^{-1} suggest the presence of aromatic NH$_2$ and sulphur containing compounds (-SO$_4^{2-}$, -SH, -S=0) in RAB and NDF samples, and can be related to C-N and C-S stretching vibrations.

The presence of phosphorous containing groups such as -P=O in RAB can be related to a sharp and strong absorption band in 1317 cm^{-1}, while in the NDF fraction was not confirmed due to the overlap of bands and weak signals. Nevertheless, the presence of sulphur, nitrogen or phosphorous containing groups in the NDF sample may suggest that some reagent residue remained in the lignocellulosic matrix, since sodium lauryl sulfate (NaC$_{12}$H$_{25}$SO$_4$), EDTA salt (C$_{10}$H$_{16}$N$_2$O$_8$) and sodium phosphate (Na$_3$PO$_4$) were present in the detergent solution. Hemicellulose, cellulose and lignin contained in the NDF residue possess a wide content of heterogeneous compounds with a complex structure.

Once RAB was treated to get the NDF fraction, some functional groups were developed or increased in amount, and were attributed to the hydrolysis of soluble organic elements (carbohydrates, lipids, among others), or to the loss of minerals during the extraction procedure.

The infrared of a pectin standard showed a similar composition to RAB, as illustrated in Figure 3.1b, with bands attributed to C=O carboxylic groups or ester groups at about 1731 and 1608 cm^{-1}, as well as to free –OH and aromatics groups (3378 and 1091 cm^{-1}, respectively). These values indicated that pectin is one of the soluble compounds. NDF showed an analogous similitude to the cellulose standard, with –OH, C=O, CH$_3$ and CH$_2$ vibrations in 3411, 1581, 2942 and 2832 cm^{-1}, respectively, and overtone or combinations of characteristic bands situated between 2400 and 1800 cm^{-1} for aromatic and cyclic compounds (piranose, phenolic, among others).
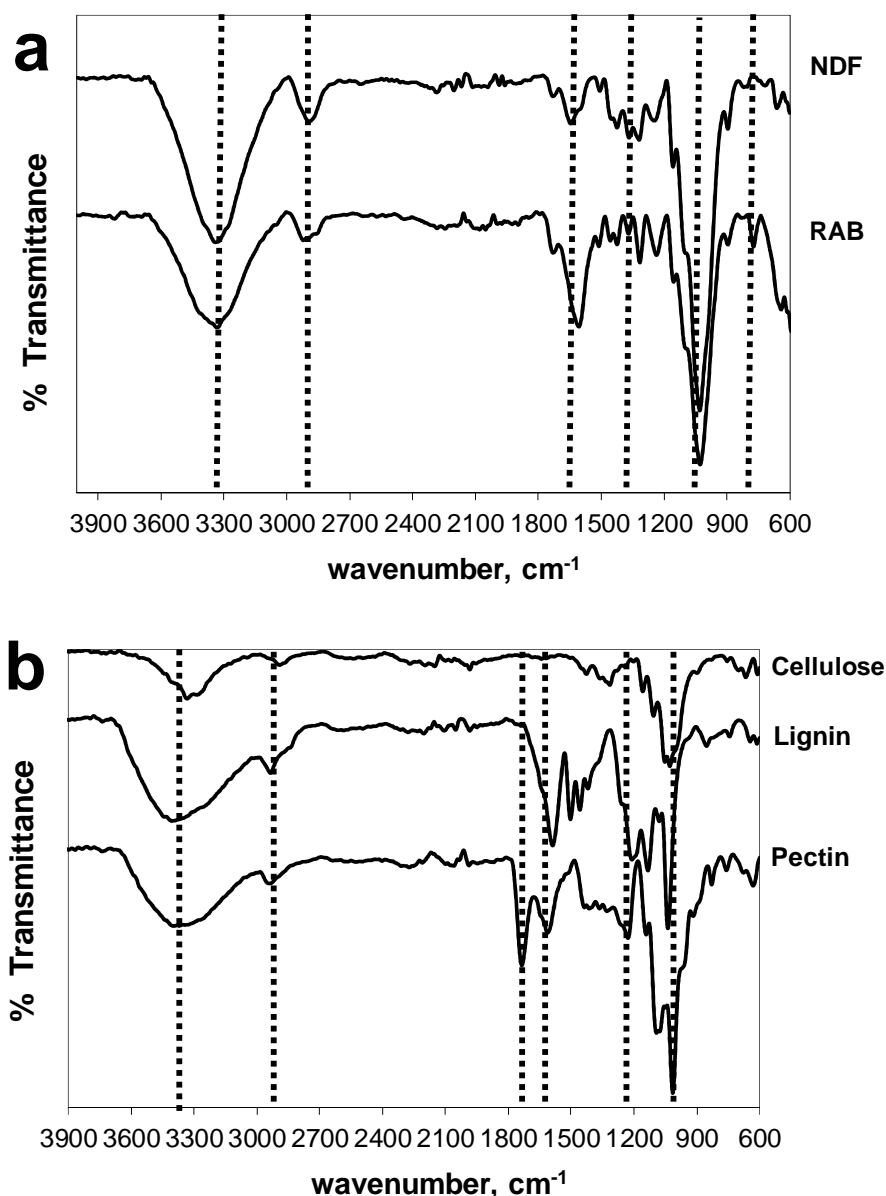
Figure 3.1 ATR-FTIR spectra of: a) NDF and, b) commercial standards.

3.3.3 ADSORPTION CAPACITY OF RAB AND DETERGENT FIBERS

Taking into account that the NDF fraction has a heterogeneous chemical surface due to its cellulose, hemicellulose and lignin content, we decided to compare the adsorption capacities of ADF and ADL fractions in order to understand the role of each of these constituent on the removal of Cd, Pb and Zn. It is important to remark that those fractions are used to give an approximate idea of the adsorption process, as was described in previous section.

59

Both Langmuir and Freundlich models isotherms fitted well the experimental data (see Table 3.3). However, these models hardly predict a sorption mechanism and have a meaningful interpretation due to the complex nature and varied active sites of agave bagasse constituents. Nevertheless, the Freundlich model (equation 24, section 2.3.4 from Chapter 2) was used to fit the experimental data due to the heterogeneous nature of the fractions under study.

Table 3.3 Isotherm parameters estimated from experimental data of Cd(II), Pb(II) and Zn(II) adsorption on NDF, ADF and ADL residues of Agave bagasse at pH=5 and 25°C.

Residue	Metal	Langmuir			Freundlich		
		q_{max} (mg g^{-1})	b (L mg^{-1})	r^2	K_F (L$^{1/n}$ mg/mg^{1-1n} g^{-1})	n	r^2
NDF	Cd(II)	4.67	0.57	0.978	2.10	4.799	0.910
	Pb(II)	14.40	0.17	0.957	4.61	3.694	0.979
	Zn(II)	14.53	0.03	0.979	0.94	1.697	0.991
ADF	Cd(II)	8.95	0.03	0.984	0.67	1.839	0.980
	Pb(II)	17.33	0.04	0.983	1.68	2.002	0.985
	Zn(II)	202.87	0.001	0.993	0.26	1.057	0.993
ADL	Cd(II)	4.90	0.59	0.992	1.93	4.363	0.987
	Pb(II)	10.67	17.34	0.969	6.87	6.084	0.960
	Zn(II)	6.20	0.14	0.940	1.44	2.779	0.985

Figure 3.2 shows the metal isotherms onto the residues of agave bagasse fibers where the adsorption affinity was established as Pb>Zn>Cd (the adsorption mechanism is reported in section 3.3.5, Figure 3.4). The metal uptake by ADL at equilibrium concentration (C_e) of 20 mg L^{-1} was 3.22, 11.75 and 3.52 mg g^{-1} for Cd(II), Pb(II) and Zn(II), respectively.

NDF (cellulose, hemicelluloses and lignin) and ADF (cellulose and lignin) presented a comparable adsorption capacity than ADL, as can be observed in Figure 3.2. NDF had an adsorption capacity of 4.46, 11.30 and 4.01 mg g^{-1}, while ADF presented 4.42, 8.04 and 3.89 mg g^{-1} for Cd(II), Pb(II) and Zn(II) respectively, at C_e of 20 mg L^{-1}. It can be seen from the adsorption isotherms that soluble compounds play around 60% of the total adsorption capacity of agave bagasse.
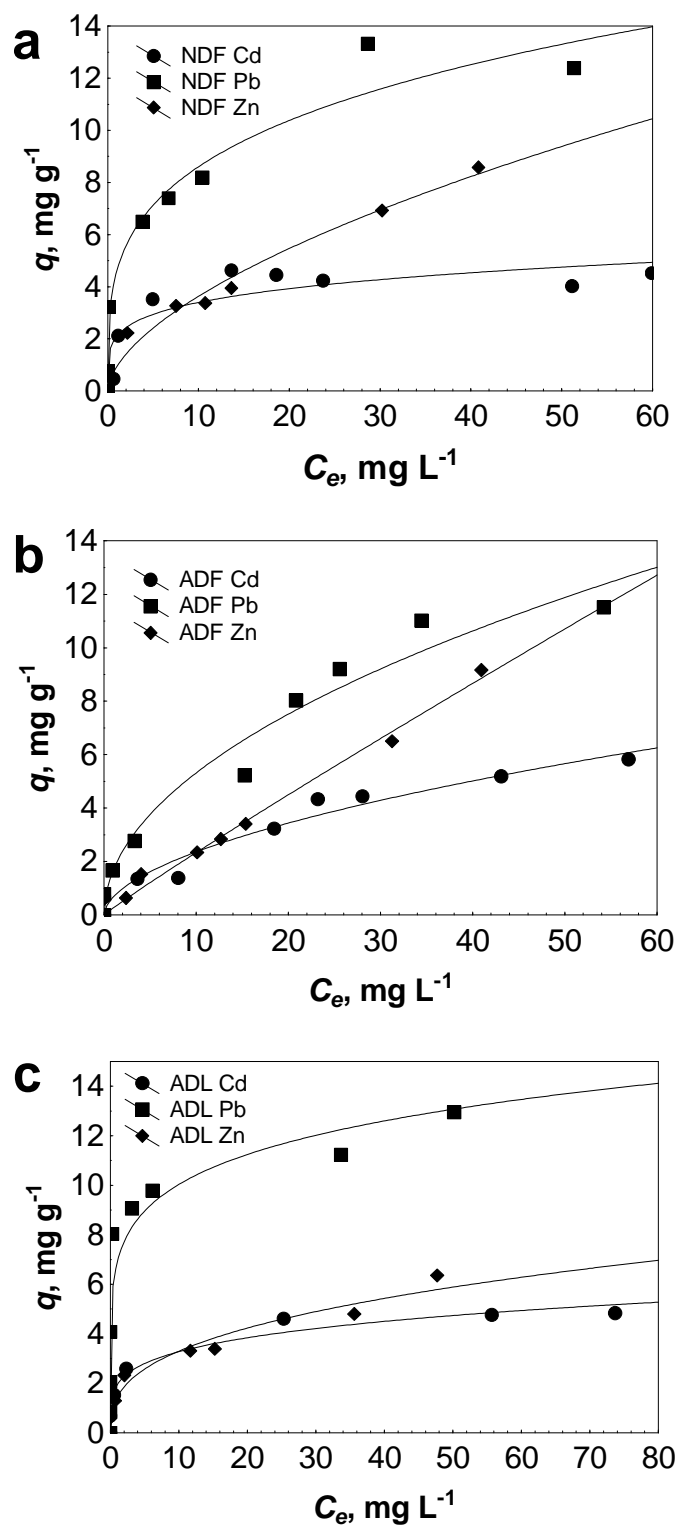
Figure 3.2 Contribution of a) NDF, b) ADF and c) ADL fractions of agave bagasse exposed to Cd(II), Pb(II) or Zn(II) ions in aqueous solution at pH=5 and 25°C. Continuous lines represent the Freundlich model.

This can be due to the soluble fraction, which was described in section 3.3.1, that possesses heteropolysaccharides (like pectine, see Figure 3.3) rich in galacturonic acids and some proteins. These type of macromolecules contain in their chemical structure mainly –COOH, as well as -SH and -NH$_2$ groups (corroborated by FTIR analyses in section 3.3.2) that play an important role in heavy metals adsorption due to their high affinity. It is for this reason that all these organic groups contained in the soluble fraction confer to the raw agave bagasse a remarkable natural adsorption capacity compared to cellulose, hemicellulose and lignin. ADL fraction showed the lowest adsorption capacity for Cd and Zn ions, and could be related to the extraction procedure were a portion of lignin was solubilized, condensated and/or precipitated, decreasing the content of this fraction [38]. Pb(II) is highly adsorbed by lignin, compared to NDF fraction, that could be due to the higher affinity by –OH groups (mainly content in this fraction) than Cd(II) or Zn(II) ions.
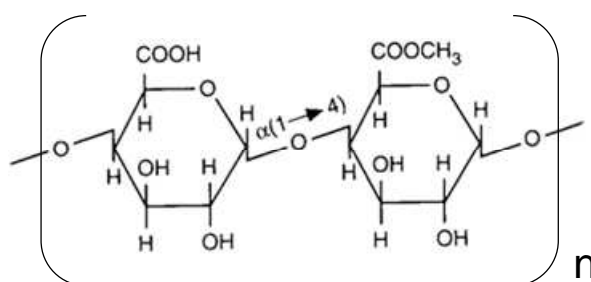
Figure 3.3 Chemical structure of pectin.

The increase of Zn(II) uptake in the NDF fraction could suggest that the extraction procedure to obtain this fiber swollen the lignocellulosic matrix of bagasse fibers, allowing Zn^{2+} (0.74 Å) to diffuse into the bagasse matrix and hence be adsorbed in a greater extend. The physicochemical properties of metal ions on study will be discussed later in section 3.3.4. In order to determine the possible adsorption mechanism of Cd, Pb and Zn on hemicellulose, cellulose and lignin of *Agave salmiana* bagasse, potentiometric titrations and TGA analyses of RAB fractions and of unsaturated and saturated RAB were performed.

3.3.4 POTENTIOMETRIC TITRATIONS FOR RAB AND NDF

RAB and the NDF fraction have a diversity of functional groups that can be quantified by acid-base titration. This procedure can also help to estimate the cationic exchange capacities of these samples, and to identify the possible binding sites that could

participate in metal uptake. Table 3.4 shows the acidic functional groups determined by potentiometric titrations when using 0.1N NaOH as titrant.

Table 3.4 Quantity of acidic groups determined by potentiometric titration with 0.1N NaOH at 25°C. Total acidity was obtained at pH=10.04.

Material	Quantity of acidic groups (mmeq g^{-1})			
	Strong	Weak		*Total
		Very weak	-COOH	
RAB	0.0045	0.060	0.007	0.072
NDF	0.0095	0.109	0.033	0.152
NDF-Cd	0.0085	0.082	a	0.090
NDF-Pb	0.0045	0.339	a	0.343
NDF-Zn	0.0065	0.138	a	0.144

[a]Functional group not observed.

The concentration of acidic groups in the materials under study and their pK$_a$ values were determined by identifying the inflection points of the first derivative of the titration curves and the zero values of the second derivative [79]. The amount of strong acidic groups (sulphur or phosphorous containing groups) at pH<4 was determined from the first peak, while the total number of acidic groups was determined from the final peak. The number of weak acidic groups (-COOH, C=O, some proteic groups) at 4<pH<7, and very weak groups attributed to phenolic and amines (including the ionization of amino groups of proteins) at pH>7, were calculated by difference [80, 81].

Strong acidic groups were detected in all samples, which was confirmed by FTIR. The increase of these acidic groups in NDF fraction may corroborate our hypothesis that sulphur or phosphorous containing groups can be attached to the lignocellulosic matrix. Weak acidic groups were also enhanced, and could be related to a possible chemical modification of the original functional groups contained in RAB and to the loss of soluble compounds that over express hide organic groups in the fiber structure. The determination of these and other chemical groups, to the best of our knowledge, has not been conducted for the NDF fraction of lignocellulosic materials. This information is valuable to understand the adsorption mechanism of metal ions.

When the NDF fraction was previously exposed to Cd(II), Pb(II) or Zn(II) ions, carboxylic groups were not detected since *pK$_a$* values in this range (4<pH<7) were not

found (Table 3.4). This suggests that –COOH groups are the main responsible for metal uptake. The strong acidic content of NDF residue decreased when loaded with metal ions, being more notorious for NDF-Pb. This can be related to the properties of Pb(II), for instance, this offers a bigger coordination sphere than Cd(II) or Zn(II) since this has a bigger ionic radius (1.21 than 0.97 or 0.74 Å, respectively) [10], therefore this can bind better with distant functional groups. Besides, the affinity for strong acidic groups is more evident for Pb(II) than Cd(II) or Zn(II) ions.

It is important to point out that the content of very weak functional groups is higher for NDF loaded with Pb(II) or Zn(II) ions. This may be related to hydroxyl or amine groups that are considerably weaker than carboxylic groups, and therefore might only interact with cations at pH>10. Thus, the increase of very weak functional groups could be related to a higher density of oxygen (mostly in the phenolic and piranose configuration confirmed by FTIR) developed after carboxylic and strong acid binding sites were first occupied by the metal ions. Cd(II) uptake by the NDF fraction showed a slight decrease in strong and very weak groups content, compared with the NDF fraction. This indicates that Cd(II) may strongly interact with very weak acidic compounds than Pb(II) or Zn(II) ions, even when these groups were expected to interact at basic conditions due to their pk_a value (pH>10). The interaction of Cd ions with strong acidic groups of NDF was less evident than with Pb(II) or Zn(II) ions.

On the other hand, a shift in the point of zero charge (pH_{PZC}) from 8.33 to 7.09 was appreciated when soluble compounds were removed from RAB to give the NDF fraction. Subsequently, ADF and lignin presented a pH_{PZC} of 7.54 and 9.26, respectively (see Table 3.2). Those results demonstrated that cellulose and hemicellulose provide certain acidity to RAB fractions that made decrease the pH_{PZC}; otherwise, lignin could be considered as a basic component due to its high point of zero charge.

3.3.5 THERMOGRAVIMETRIC ANALYSIS OF RAB AND NDF FRACTION

The analysis of weight loss derivative, where the peaks represent the weight lost as a result of the thermal decomposition, provides information of the trend in the chemical changes of the lignocellulosic matrix. Cellulose, hemicelluloses and lignin exhibit different thermal decomposition. Hemicellulose is the most unstable of these components and decomposes first (around 160-250° C) followed by lignin (110-282°C) and cellulose (higher than 250°C) [89, 95, 96].

TGA curves reported in Figure 3.4 show that RAB presented a broad peak at 69.5°C that can be attributed to the loss of alcohol organic compounds like methanol or ethyl acetate (an ester of ethanol and acetic acid), see Figure 3.4a. This result is in agreement with that reported by Chavez-Guerrero and Hinojosa [97], and corroborated that bagasse fibers are impregnated with alcohols and moisture of organic compounds due to their previous thermal and mechanical treatment. The cooking step of agave could develop methanol and ethyl acetate. In addition, a weak peak located at 103°C is attributed to the loss of residual water (dehydration). A third stage occurred at 232°C, due to the decarboxylation of hemicellulose (releasing CO, CO_2 and some hydrocarbons). This peak showed a weak shoulder around 190°C that could be due to a possible overlapping of the decomposition of fats, waxes, sugars, starch, fatty acids, pectin, among others, contained in RAB when hemicelluloses decomposed. The lost mass in this stage corresponds to 13.09 mg (60.5%) of the total content of mass sample. This signal confirms that the thermal degradation of fiber bagasse starts at low temperature due to the transformation of the fiber structure into a more labile arrangement, reported first by Nieto-Delgado *et al* [98]. Two final peaks were situated at 364 and 560°C, related to the decomposition of lignin and cellulose by disintegration of monomeric phenols, aromatic rings and piranose structures contained in those fractions [95, 98]. The final residue from RAB pyrolisis was 21.57% (4.66 mg) of the initial mass. This value indicates that the inorganic fraction left after the thermal decomposition of RAB is 21.27%, which may consist of stable micronutrients that could be found in the ripe Agave *salmiana* head like Al, Si and Fe oxides as well as elements like Na, K and Ca that are stable at higher temperatures. Comparing the thermal profile of RAB with the NDF fraction (see Figure 3.4a), the first thermal decomposition stage of NDF occurred at 69.5°C. Nevertheless, this value could not be attributed to alcohol or moisture elimination, found it in RAB, due to its previous removal by the detergent solution. However, this peak could be attributed to residual sodium phosphate, which decomposes at 73.3-76.7°C and that is a reagent used to obtain the NDF.

It is also possible that this signal could be related to an unstable hemicellulosic fraction contained in the NDF fraction. A second peak occurred at 238°C, and represents the decomposition of hemicellulose. The loss of mass corresponding to this stage was 19.61 mg (56.93%). A combination of cellulose and lignin disintegration may occur after hemicellulose decomposition, however, a possible overlapping of those stages made it

difficult to identify them in the thermogravimetric curves. The final residue of the NDF fraction was 21.04% (7.24 mg).
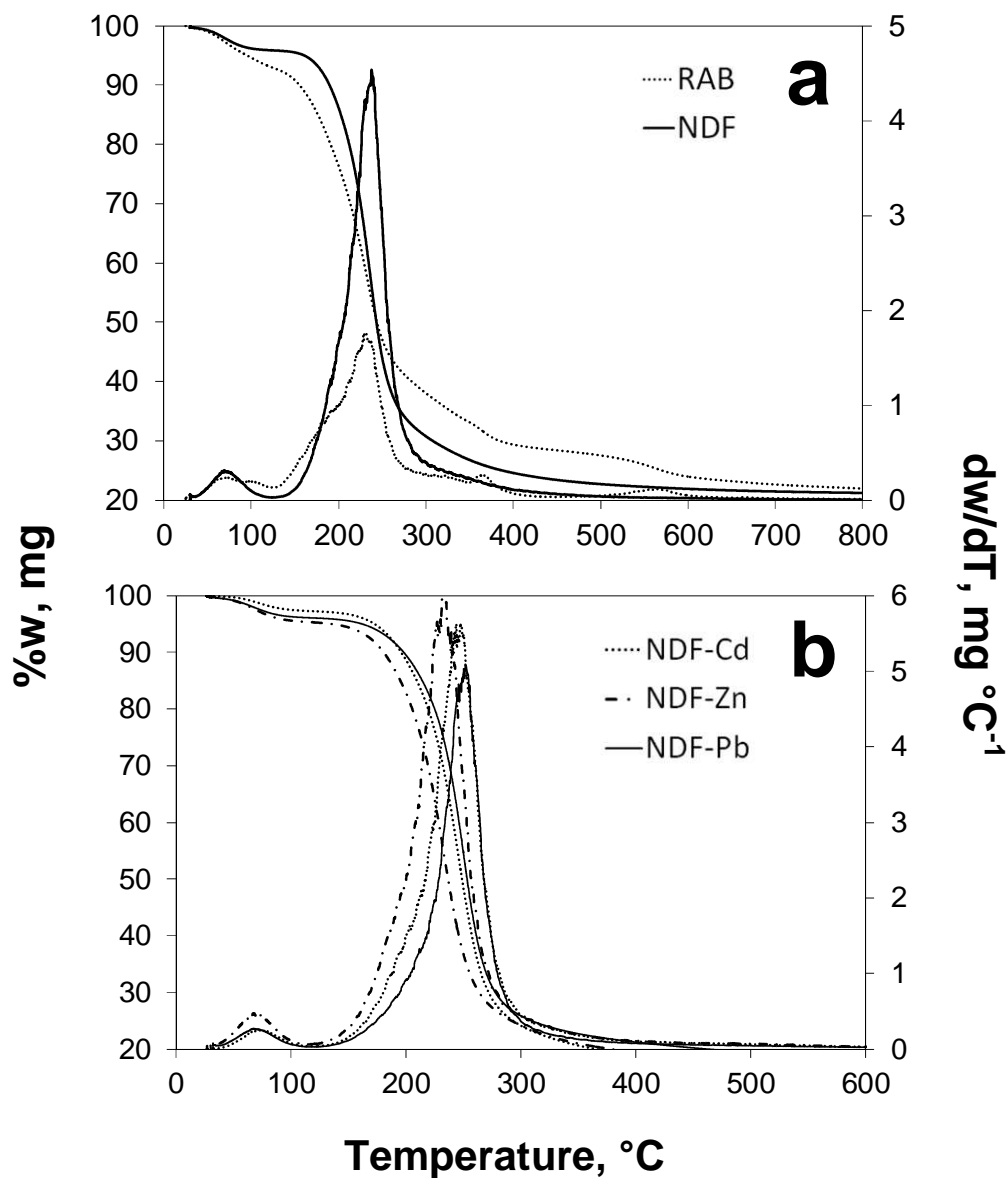
Figure 3.4 Thermogravimetric and derivative thermogravimetric profiles of a) RAB and NDF fraction, and b) NDF loaded with Cd(II), Pb(II) or Zn(II) ions (Co= 80 mg L^{-1}, pH=5 and 25°C), heated in nitrogen atmosphere at 10°C/min.

The thermal decomposition of the NDF fraction changed when this was loaded with Cd(II), Pb(II) or Zn(II). The first stage about 70°C, previously assigned to a possible reagent or unstable hemicellulose, did not show any change between the three NDF-metal

samples (Figure 3.4b). A second stage was observed at 247.4, 252.5 and 232.1°C for NDF loaded with Cd(II), Pb(II) and Zn(II), respectively (see Figure 3.4b), where the decomposition of the hemicellulose and lignin degradation takes part. The peak of this second stage was shifted 9.4 and 14.5 °C for NDF loaded with Cd and Pb ions, respectively, suggesting that these metal ions increased the temperature of decomposition of NDF. Zn ions presented the opposite effect and decreased the decomposition temperature of NDF fraction in about 5.9°C. This can be because Zn(II) can acts as a dehydrating agent, catalyzing the cleavage of hydroxyl groups present in lignocellulosic materials and giving rise to the formation of double bonds inside the biopolymer chain of the lignocellulosic matrix [96], making easy the gasification process.

On the other hand, previous studies have shown Pb prefers to bind oxygen compounds and to fit with more than two distant groups, making Pb-complexes more stables than Cd or Zn-complexes [84,99], due to its high electronegativity and bigger ionic radius (1.79 and 1.21 Å, respectively). Hence Pb increases the decomposition temperature of the NDF faction. The final residue of NDF loaded with Cd(II), Pb(II) or Zn(II) was 14.6% (5.56 mg), 15.74% (4.98 mg) and 15.44% (6.63 mg), respectively. Comparing these results with the pyrolysis of NDF (21.04 % loss), it is clear that the metals ions used in this study promoted dehydration and decarboxylation reactions.

Although thermal decomposition of the NDF fraction is a complex pathway of reactions where the overlay of decomposition stages makes difficult its characterization, a sorption mechanisms can be proposed considering two important factors: 1) agave bagasse fibers contain mostly cellulose (41.14%), which has oxygen-containing compounds such as hydroxyl groups where metal ions adsorb, and 2) the primary decomposition product of cellulose by combustion is levoglucosan (1,6-anhydro-β-D-glucopyranose), as can be seen in Figure 3.5.

The conversion of cellulose-to-levoglucosan decreased when metal ions were added to biomass, meaning that the effect of metal ions tend to stabilize a proportion of the lignocellulosic matrix [98, 100]. The metal ion can promote the bond cleavage or eliminate the hydroxyl groups from cellulose, due to its catalytic activity. Nevertheless, the formation of aromatic structures and molecular rearrangements in the polymer can lead to a more condensed structures and enhanced lignocellulosic char yield by forming crosslinks.
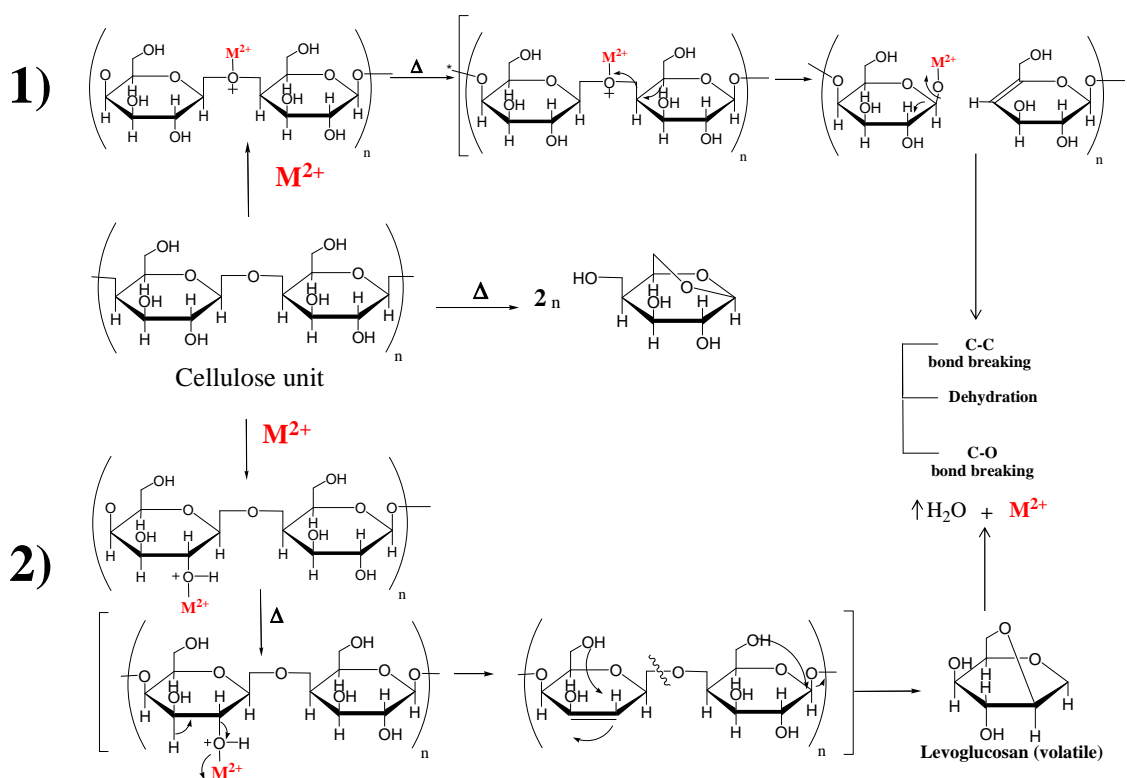
Figure 3.5 Sorption mechanism proposed when metal ions are loaded in agave bagasse cellulose, and its possible thermal decomposition. M^{2+}= Cd(II), Pb(II) or Zn(II).

3.4 CONCLUSIONS

ATR-FTIR spectra demonstrate that the possible binding sites of raw bagasse and NDF (hemicellulose, cellulose and lignin) fraction include oxygen, sulphur, phosphorous and nitrogen-containing groups.

NDF fraction has a higher adsorption capacity due to the presence of hemicellulose for Cd(II), Pb(II) and Z(II) ions than ADF or ADL fractions. Moreover, the soluble compounds account for about 60% of the total adsorption capacity. In all cases, the metal affinity was establish as Pb>Cd>Zn.

Acid-base titration results shown that weak and strong acidic groups are involved in metals uptake, and the extraction procedure to obtain the NDF fraction affected the original functional groups contained in raw bagasse fibers.

Thermogravimetric analyses established that Cd(II) and Pb(II) ions shift to higher temperature the thermal decomposition of NDF fraction, while Zn(II) present the opposite effect. This is because Zn(II) acts as a dehydrating agent, catalyzing the cleavage of

hydroxyl groups present in lignocellulosic materials, making easy the gasification of NDF fraction, whereas Pb(II) and Cd(II) form stable metal complexes with functional groups of this fraction, delaying the pyrolysis process.

Other priority pollutants that can be present in aqueous streams are anions, like fluoride (F$^-$). A promising adsorbent developed to bring down hazardous concentration levels of this anion found in drinking water and water supplies is discussed in the next chapter.

4

CHAPTER

ZIRCONIUM-CARBON HYBRID SORBENT FOR REMOVAL OF FLUORIDE FROM WATER: OXALIC ACID MEDIATED Zr(IV) ASSEMBLY AND ADSORPTION MECHANISM

ABSTRACT

When activated carbon (AC) is modified with zirconium(IV) by impregnation or precipitation, the fluoride adsorption capacity is typically improved. There is significant potential to improve this hybrid sorbent by controlling the impregnation conditions, which determine the assembly and dispersion of the Zr phases on carbon surfaces.

Here, commercial activated carbon was modified with Zr(IV) together with oxalic acid (OA) used to maximize the zirconium dispersion and enhance fluoride adsorption. Adsorption experiments were carried out at pH 7 and 25 °C with a fluoride concentration of 40 mg L^{-1}. The OA/Zr ratio was varied to determine the optimal conditions for subsequent fluoride adsorption. The data was analyzed using the Langmuir and Freundlich isotherm models. FTIR, XPS and the surface charge distribution were performed to elucidate the adsorption mechanism. Potentiometric titrations showed that the modified activated carbon (ZrOx-AC) possesses positive charge at pH lower than 7, and FTIR analysis demonstrated that zirconium ions interact mainly with carboxylic groups on the activated carbon surfaces. Moreover, XPS analysis demonstrated that Zr(IV) interacts with oxalate ions, and the fluoride adsorption mechanism is likely to involve –OH$^-$ exchange from zirconyl oxalate complexes.

4.1 INTRODUCTION

Fluoride can be present in drinking water and it is considered beneficial at levels about 0.7 mg L^{-1}, but hazardous if it exceeds 1.5 mg L^{-1}, which is the limit recommended by the World Health Organization (WHO) [15]. Exposure to high fluoride concentrations often occurs through drinking groundwater, one of the main sources of potable water, and can result in fluorosis (dental and skeletal abnormalities) or neurological damage in severe cases [2]. Fluoride concentrations, up to 30 mg L^{-1} can be found in ground water in many parts of the globe, and it is present at least in 25 countries [15, 16, 101].

A number of papers have focused on engineered adsorbents for fluoride removal from aqueous solutions, and the sorbents include activated and impregnated alumina [102, 103], clays, minerals and plants [104-106], activated carbon and nanotubes [107, 108], rare oxides [109], polymeric materials and resins [110, 111]. It is also know that the incorporation of some metal oxides like iron(III), manganese(II, IV), lanthanum(III), aluminum(III), zirconium(IV) or titanium(IV) into sorbent surfaces can significantly increase fluoride adsorption capacity [58, 102, 112-115]. Activated carbon, with native (unmodified) surfaces, is a poor sorbent for fluoride from water, but can provides a stable support for achieving high dispersion of metal phases that are powerful fluoride sorbents, and can also inhibit sintering or bulk precipitation of those active metal particles. When this carbonaceous material is impregnated with Zr(IV) and its metal complexes, the adsorption capacity has been reported to improve by a factor of 3-5 [116]. The control over carbon surface area and the size distribution of the loaded metal phases are key factors to increase the fluoride adsorption capacity.

Some research has been focused in loading Zr(IV) into several adsorbents by impregnation or precipitation using base-initiated particle nucleation of metal salt solution [112, 117-121]. While this synthesis is simple to carry out, it is difficult to understand and optimize due to the effects of pH, ionic strength, the presence of complexing agents, or others that are known to affect the aggregation and reorganization of Zr(IV) particles. In many cases, the sorbent specific area drops due to pore blockage by Zr-containing particles whose average sizes range from nanometers to micrometers, and are uncontrolled in the conventional synthesis. We believe the intentional use of complexing (or chelating) ligands that can bind to particle surfaces or nuclei during the synthesis, could be potentially useful to control the growth and final particle size distribution of the dispersed metal. Organic acids have demonstrated a positive effect on reduction of oxide nanoparticle size during the nucleation and aggregation stage [122, 123]. This approach

has not been systematically used to load Zr-containing nanoparticles onto carbonaceous surfaces such activated carbons, and thus, take advantage of the high mechanical strength, excellent permeability in flow-through systems and high surface of activated carbon for future use in defluoridation processes for drinking water systems.

The aim of this research was to improve the fluoride adsorption capacity of granular activated carbon by controlling the particle size of Zr(IV)-containing particles with oxalic acid as complexing ligand during the impregnation process, and to propose the possible fluoride adsorption mechanisms.

4.2 MATERIALS AND METHODS

4.2.1 ADSORBENTS

Zirconium impregnated activated carbon was prepared according to an experimental design that considered the ratio Zr(IV)/organic capping agent (Zr/OA) to determine the conditions that produced an adsorbent with the highest fluoride adsorption capacity. 0.1 g of commercial activated carbon (AC, F400) was added to 10 mL of $ZrOClO_2 \cdot 8H_2O$ solutions from 0.01 to 15% of Zr^{4+} during two days. Subsequently, the impregnated carbon was mixed with 10 mL of 0.01-12.2% oxalic acid solution during 1 day, and then it was filtered, rinsed, and dried at 60°C during 12 h. The impregnated adsorbent thus obtained was designated as ZrOx-AC. An analogous procedure was followed adding F400 to $ZrOClO_2 \cdot 8H_2O$ solution, and the resultant material was denoted as Zr-AC. All the impregnation processes were performed at 25°C.

4.2.2 BATCH ADSORPTION EXPERIMENTS

A fluoride ion stock solution (100 mg L^{-1}) of NaF was prepared in deionized water, and the test solutions were made by subsequent dilution of the fluoride solution. Samples of 0.1 g of modified or non-modified activated carbon were added to 30 mL of fluoride solution (0.1 to 60 mg L^{-1}) to conical-bottom polypropylene tubes. The solution's pH was adjusted daily to 7.0±0.25 using 0.1 N HCl or NaOH, and all the experiments were monitored until equilibrium was achieved, this took about 7 days. Each adsorption point was performed by duplicated, and the standard deviation was less than 5%. The fluoride concentration was measured by an Orion potentiometer coupled with a fluoride ion selective electrode. 10 mL of a Total Ionic Strength Adjustment buffer (TISAB II) were added to 10 mL of water sample (withdrawn from each experiment) and standards. All the

experiments were carried out at 25°C, and the adsorption capacity (q_e, mg g^{-1}) was calculated with equation 21 (see section 2.2.2, Chapter 2). The experimental adsorption data was fitted by Freundlich (equation 24) and Langmuir isotherm models, expressed as:

$$q_e = \frac{q_{max}bC_e}{1+bC_e} \qquad (29)$$

where q_{max} is the maximum adsorption capacity (mg g^{-1}) and b (L mg^{-1}) the Langmuir constant related to the adsorption energy or "affinity".

4.2.3 ADSORPTION KINETICS AND EFFECT OF CO-EXISTING ANIONS

A 1000 mg L^{-1} of fluoride stock was prepared from NaF in deionized water, and dilutions were made from this solution. For kinetic experiments, 0.63 g of the adsorbent were placed in a rotating basket that was positioned in a 1 L reactor filled with 0.75 L of deionized water, at pH 7. The reactor was then placed in a water bath at 25°C, and the basket impeller that was connected to a motor was set a 470 min^{-1}. Once a certain stock volume was added to the reactor to set the initial fluoride concentration at 20 mg L^{-1}, the experiment began.

The effect of 1, 10 and 50 mg L^{-1} of a co-existing anion mixture (chloride, sulphate, nitrate, carbonate and phosphate, prepared from sodium reagents) was performed in batch reactors during fluoride adsorption at 25°C, with a fixed adsorbent dose of 3.33 g L^{-1} and an initial fluoride concentration of 20 mg L^{-1}. The solution pH was adjusted daily at pH 7 until equilibrium was achieved (this took about 7 days). Then, water samples were withdrawn to measure the residual concentration, as already described.

4.2.4 MATERIALS CHARACTERIZATION

Potentiometric titrations, as well as pore size and surface area of Zr-oxalate modified activated carbon were obtained as was described in section 2.2.5 and 3.2.4 (Chapter 2 and 3, respectively). FTIR analyses were performed with a Nicolet iS10 FT-IR spectrophotometer, using KBr pellets and following the spectra parameters defined in section 2.2.4 (Chapter 2). XPS measurements were made in a SPECS spectrometer with a Phoibos 100 hemispherical analyzer. The base pressure in the UHV chamber was below 10^{-7} kPa. The X-ray radiation source was monochromatic Al K (1486.74 eV) at 100 W X-ray power and anode voltage of 14.00 kV. The photo-excited electrons were analyzed in constant pass energy mode, using pass energy of 50 eV for the survey spectra and 10 eV for the high-resolution core level spectra. For comparative purposes, all spectra are

referenced to 284.5 eV corresponding to C 1s region. Casa XPS software was used for data processing. Core level curve fitting in different components was performed using a Shirley background and a standard least squares algorithm.

The zirconium content in 40 mg of each adsorbent was determined by acid digestion with 20 mL of HNO_3:H_2SO_4 (5:1) solution, then, the mixture was digested by 1 h at 150°C in a microwave advanced digestion system (Milestone, Ethos 1), where the remaining solution was diluted until 50 mL with deionized water and then analyzed by inductively coupled plasma-optical emission spectroscopy (ICP-OES). The particle size and morphology of the anchored Zr(IV) particles were determined by scanning electron microscopy (SEM, FEI XL 30SFEG). The crystalline structure of Zr(IV) particles were determine by X-ray diffraction (XRD) patterns obtained with a step time of 10 s and 2θ of 0.02° with a XRD D8 Advanced-Bruker Axs (Cu Kα radiation λ=1.546Å). The modified Zr-carbon materials were crushed before SEM and XRD analysis.

4.3 RESULTS AND DISCUSSION

4.3.1 STUDY OF OXALIC ACID AS COMPLEXING AGENT TO CONTROL THE PARTICLE SIZE OF Zr(IV)

It has been reported that the most suitable way to load transition metals onto activated carbon surfaces would be as a metal oxide, for being the most thermodynamically stable form. Zirconium oxide of nanometric sizes (<100 nm), known as zirconia (ZrO_2), and its (hydro)oxide forms have been synthesized by precipitation methodologies using NaOH or ammonia. However, the precipitation of zirconium has not been explored under acidic conditions by using organic acids such as oxalic acid that is a precursor for the synthesis of zirconia (ZrO_2) nanoparticles. This complexing agent controls the hydrolysis of zirconium oxychloride which forms $ZrOOH^+$ or $[ZrO(OH)_2 \cdot 4H_2O]_4^{8+}$) species in aqueous solution, and avoids its polymerization generating nanoparticles [116, 121]. This methodology could be used to load zirconium oxalate into the activated carbon without blocking pores.

The effect of NaOH and oxalic acid on the size of Zr(IV) particles can be shown in Figure 4.1. It is possible to see that oxalic acid stabilized the hydro(oxo) zirconia particles (<800 nm) from pH 2-11 due to the reduction of surface energy of the transition metal that contributes in the aggregation and nucleation process, while NaOH formed bulky flocks (>1000 nm) when the media tends to be more basic. This study demonstrated that the size

of Zr aggregates formed with oxalic acid (about 500 nm) can be 7 times smaller than those synthesized with NaOH (up to 5000 nm) at a pH between 2 and 11.
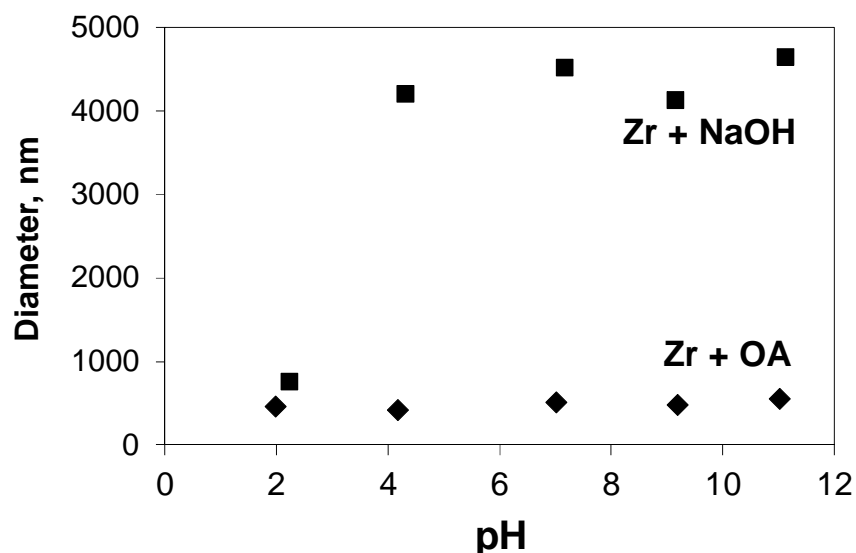
Figure 4.1 Effect of oxalic acid and NaOH in Zr(IV) particle size as a function of pH.

4.3.2 EFFECT OF Zr/OXALIC ACID RATIO ON ADSORPTION CAPACITY

The measured adsorption capacity (q, mg g^{-1}) as a function of the Zr/OA ratio showed that the maximum q was obtained with Zr/OA= 1.05 (7% of each Zr(IV) and OA), as observed in Figure 4.2a and Table 4.1. When oxalic acid was added at high concentration (14.3%, Zr/OA= 0.52) the adsorption capacity decreased about 94%, whereas an increase in q was noticed a lower percentages (2<Zr/OA<3.5) with Zr/OA 6.11 and 2.10, respectively. The adsorption capacity was 0.75 and 2.04 mg g^{-1} when Zr and OA were in equal concentrations of 2 and 12%, respectively, but the organic acid by itself did not improve the adsorption capacity when Zr(IV) was at 0.01% (Zr/OA 0.001). When F400 was impregnated only with Zr(IV), the adsorption capacity was 62 % lower compared to the optimal ratio. The Pareto plot (Figure 4.2b) demonstrated the effect of the production variables established in the modification methodology, where the bars represent the influence of the factor in the impregnation process. The concentration of oxalic acid (OA) and Zr(IV) was more significant ($p<0.05$) over the adsorption capacity when forming the Zr-oxalate complex in one step (LR): L denotes the interaction between OA and Zr, and R the opposite relation.
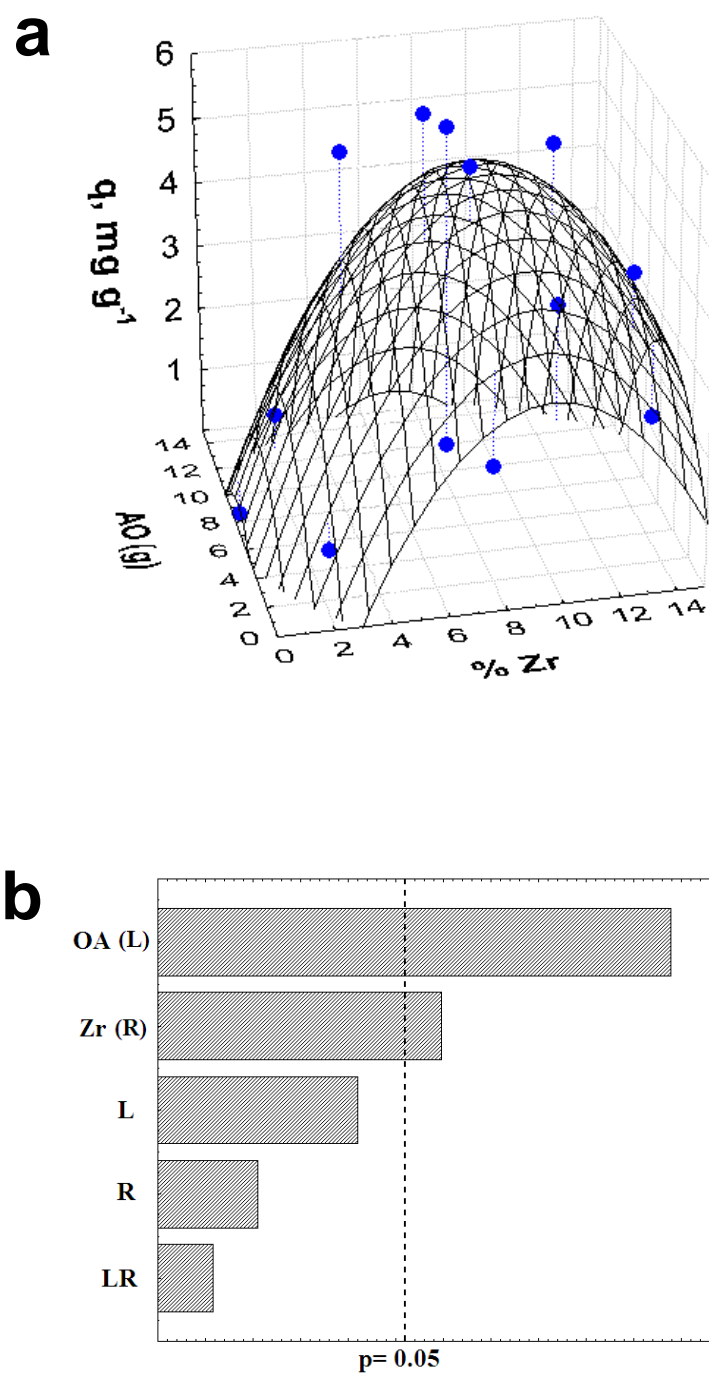
Figure 4.2 a) Response surface of fluoride adsorption capacity as function of percentage of Zr(IV) and OA solution, at pH 7 and 25°C. b) Pareto chart for ZrOx-AC experimental design.

Table 4.1 Surface response experimental data of single points for fluoride removal at pH 7, 25°C and Co= 40 mg L^{-1}.

Point	% Zr(IV)	% OA	q, mg g^{-1}
1	7.50	0	2.25
2	2.20	12.20	0.72
3	12.80	12.20	2.04
4	12.80	2.09	4.47
5	7.50	7.15	5.94
6	7.50	14.3	0.38
7	0.01	7.15	0.33
8	15	7.15	1.16
9	2.20	2.09	0.75
10	3.75	7.15	5.72
11	11.25	7.15	5.54
12	7.5	3.57	5.80
13	7.5	10.72	5.51

4.3.3 ADSORPTION ISOTHERMS

Fluoride adsorption isotherms of the optimum modified and non-modified F400 (Zr/OA= 1.05) are presented in Figure 4.3. The experimental data were reasonably fitted by both Langmuir and Freundlich models, based on the correlation coefficient (r^2), see Table 4.2. The low values for parameter b (<1) and n (<2) indicated a high fluoride affinity for the adsorbent. Aside from the Langmuir q_{max} parameter, that can be interpreted as monolayer coverage, these models were used only to quantitatively describe the data and to compare the sorbent performance.

From the adsorption isotherms, it was shown that q_{max} was 17.70 mg g^{-1} when OA was used as complexing agent. This could be due to a possible enhancement of the positive charge of Zr(IV) that was formed when the zirconyl oxalate complexes with the OA. The unpaired electrons, located in the oxygen atoms of Zr-oxalate containing molecules, can attract the electronegativity of the metallic ion to make it more positive, which allow a better attraction for F$^-$. By contrast, q_{max} for Zr-AC was lower than that of

F400, indicating that in absence of OA the complexation of Zr(IV) complexes could be occurring in agreement with a previous work from our research group for TiO_2-AC [124].
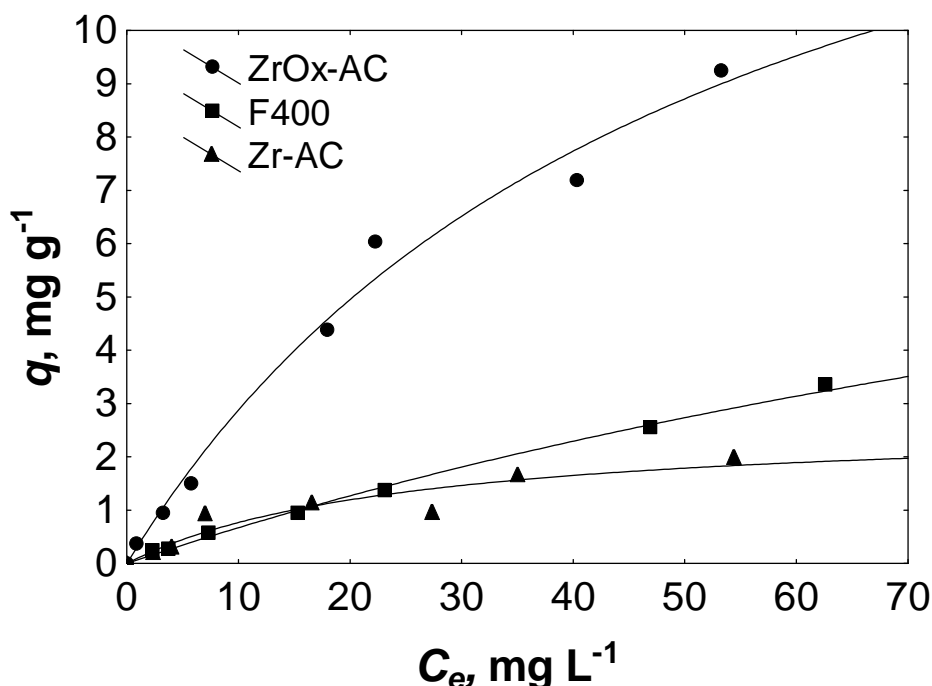
Figure 4.3. Fluoride adsorption isotherms of modified and non-modified F400, at pH 7 and 25°C. The solid lines indicate the Langmuir model.

Without the presence of OA, the adsorption capacity of Zr-AC, at C_e= 40 mg L^{-1}, was 68% lower than ZrOx-AC. The maximum adsorption capacity for ZrOx-AC was 3 times higher than Zr-impregnated coconut shell carbon (1.75 mg g^{-1}), iron-impregnated granular ceramic (2 mg g^{-1}), Ca-impregnated nutshell carbons (2.3 mg g^{-1}) and aligned carbon nanotubes [108,115,126,127]; but still lower in comparing with TiO_2 (12.1 mg g^{-1}) pellets and surface functionalized foam (7.8 mg g^{-1}) [111,113]. It can be seen from Table 4.2 that both ZrOx-AC and Zr-AC showed higher values of the parameter b. This is an indication that in presence of Zr(IV) the modified carbonaceous material has a higher trend to adsorbed fluoride from aqueous phase [125]. Besides, F400 does not contain zirconium, but Zr-AC and ZrOx-AC have 0.16 and 0.77% of the metal, respectively. It was found that the oxalic acid carried out more Zr(IV) ions from the solution to form oxalate complexes [128], and this behavior could indicated that in the presence of OA an enhancement in Zr(IV) ions content makes more favorable the fluoride affinity in the adsorbent. This result

agreed with the increase of fluoride adsorption capacity of ZrOx-AC compared to Zr-Ac that does not contain the complexing agent (OA).

Table 4.2. Isotherms parameters from the experimental data of fluoride adsorption on F400 modified or non-modified with Zr(IV) and oxalic acid, at pH 7, 25°C.

Sample	Langmuir			Freundlich		
	q_{max}, $mg\ g^{-1}$	b, $L\ mg^{-1}$	r^2	K, $(mg^{1-1/n}L^{1/n}\ g^{-1})$	n	r^2
F400	11.90	0.006	0.998	0.110	1.228	0.998
ZrOx-AC	17.70	0.019	0.994	0.577	1.431	0.990
Zr-AC	2.67	0.041	0.947	0.17	1.10	0.962

4.3.4 KINETIC STUDIES AND EFFECT OF CO-EXISTING IONS

Adsorption kinetics were performed in order to evaluate the fluoride adsorption rate in ZrOx-AC, and the results are shown in Figure 4.4a. The Zr-impregnated activated carbon removed 71% of the fluoride initial concentration in the first 15 min. The adsorption rate was considered fast [129, 130], because the initial fluoride concentration decreased around 90% in 1 h and the equilibrium was reached in 50 min. During the fluoride uptake the initial pH decreased during the first 40 min of analysis until pH 6.84, then, this kept constant up to 80 min of staring the experiment. It is important to point out that the surface of Zr-containing particles anchored on AC may not be very high, and some patches of unmodified activated carbon could participate during the fluoride sorption as well. In the course of the fluoride adsorption process, some reactions could be achieved at the same time between the non-modified and Zr-oxalate complexes of ZrOX-AC surface. This comparison can be appreciated with the pH change of F400 during fluoride uptake (Figure 4.4b) that behaves in similar way to ZrOx-AC. This behavior suggests a possible H^+ exchange from oxygenated F400 groups and/or from the Zr-oxalate complexes with the fluoride anions when the adsorption process was performed. Afterwards, the pH increased up to 6.93, which can be attributed to –OH released from the Zr-oxalate complexes.
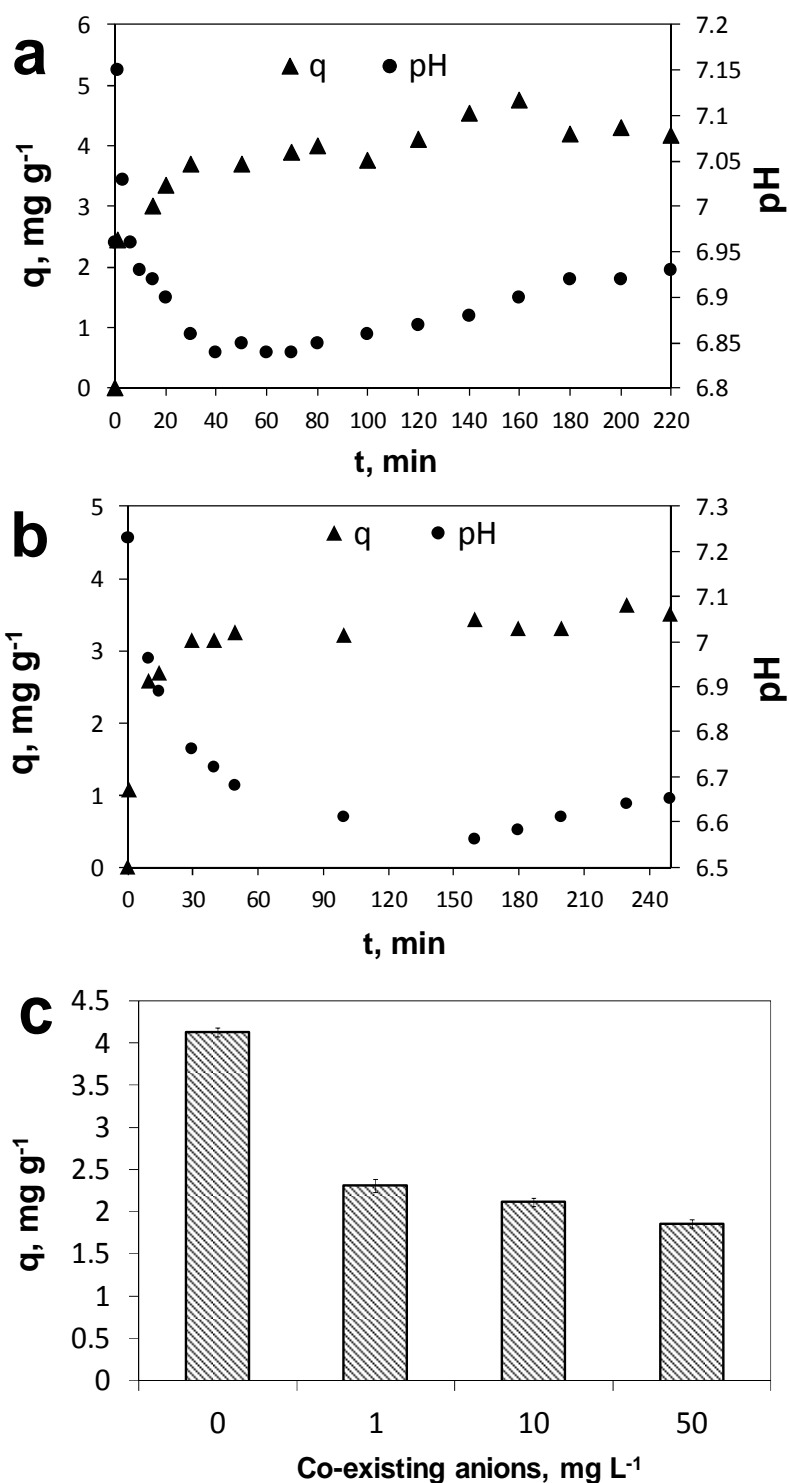
Figure 4.4 Fluoride adsorption rate on a) ZrOx-AC and b) F400. c) Effect of competing Cl^-, SO_4^{2-}, NO_3^-, PO_4^{3-} and CO_3^{2-} at 0, 1, 10 and 50 mg L^{-1} of each anion in presence of 20 mg L^{-1} of F^- at pH 7 and 25°C. Adsorbent dose of 0.84 g L^{-1}.

The effect of co-existing anions such chloride, sulphate, nitrate, phosphate and carbonate, usually found in water, on ZrOx–AC fluoride adsorption capacity is shown in Figure 4.4c. Results showed a decreased of 44, 49 and 55% on the adsorption capacity when competing anions were presented in a mixture of 1, 10 or 50 mg L^{-1} of each anion, corresponding to 0.11, 1.08, 5.40 the molar concentrations of fluoride, respectively. Although the fluoride adsorption capacity notably decreased, it can be observed that Zr-oxalate complexes have affinity for fluoride ions even at very high concentration (>10 mg L^{-1}) of co-existing anions.

4.3.5 MATERIAL CHARACTERIZATION
4.3.5.1 PHYSICAL PROPERTIES

Table 4.3 shows that the surface area of F400 (926.83 m^{2}g^{-1}) decreased 6.5% when contains Zr-oxalate complexes, but without the presences of oxalic acid (Zr-AC) the surface area falls about 50%. The increase of macropore volume in ZrOx-AC and Zr-AC can be attributed to big clusters (>50 nm) that partially blocked the macropore range, creating more cavities between aggregates and adding more pore volume in this region. In other hand, when oxalic acid (the capping agent) is added the development of aggregates is inhibited. Moreover, a reduction of 16 and 60% of micro- and mesopore volume, respectively, was also observed in ZrOx-AC. This suggests that some of Zr-oxalate particles are less than 2 nm in size.

Table 4.3 Physicochemical characterization of modified and non-modified activated carbon F400.

Sample	BET (m^2 g^{-1})	Pore volume (cm^3 g^{-1})			pH$_{PZC}$	Zr%	q*, mg g^{-1}
		Micropore (<2 nm)	Mesopore (2-50 nm)	Macropore (>50 nm)			
F400	927	0.330	0.074	0.003	9.97	ND	2.25
Zr-AC	546	0.174	0.030	0.004	3.28	0.16	1.85
ZrOx-AC	867	0.278	0.029	0.025	11.18	0.77	7.40

ND= non determined.
*Adsorption capacity at C_e= 40 mg L^{-1}, pH 7 and 25°C.

4.3.5.2 MICROSCOPY STUDIES

The surface morphology of ZrOx-AC is shown in Figure 4.5a. The bright correspond to the Zr-containing particles, confirmed later by EDS analyses (see Figure 4.5b and 4.5d); and from the microscopy scale it can be seen that the size of those particles loaded on the F400 surface was less than 10 nm when OA was added. On the other hand, the Zr(IV) particle size on Zr-AC was up to 100 nm (see Figure 4.5c). The presence of residual chloride was noticed in the Zr-containing particles due to the ZrOCl$_2$ used as a source of zirconium ions. Furthermore, Al (0.62%) and Si (0.13%) were found in the modified activated carbon due to the main components of the activated carbon, besides of C (76.3%) and O (6.4%) elements.
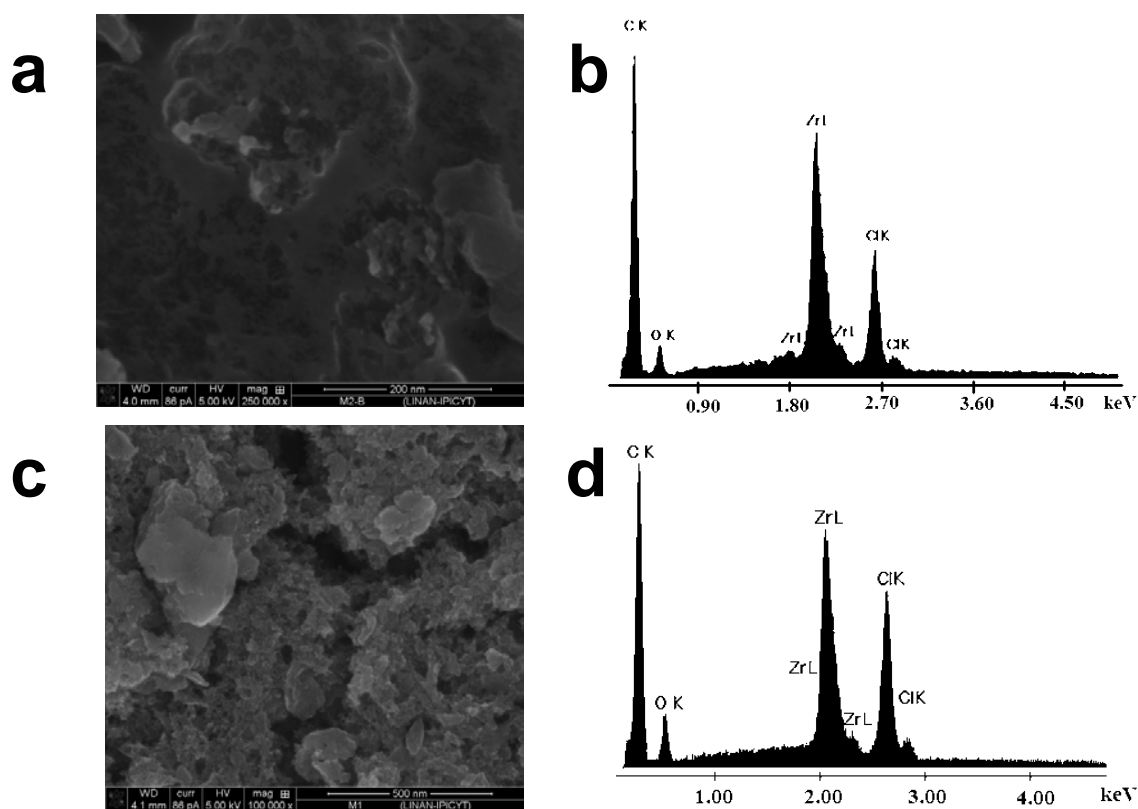
Figure 4.5 FTIR spectra of: a) oxalic acid (OA), b): F400, C: Zr-AC, D: ZrOx-AC, and e) ZrOx-AC saturated with fluoride ions (ZrOx-AC + F).

4.3.5.3. SPECTROSCOPY EVIDENCE

Changes in the vibrational frequencies of Zr(IV) bonds with functional groups of F400 surface were studied in order to elucidate the interaction of the metal ion with the carbonaceous surface and the complexing agent.

The FTIR spectra of OA and those of ZrOx-AC before and after the adsorption of fluoride are shown in Figure 4.6. The spectra of F400 (Figure 4.6b) showed fewer peaks of weaker intensity around 1510 and 1164-968 cm^{-1} that indicate the vibration of C=O, C-O and –OH from carbonyl, lactones and phenolic groups, respectively. A band in 3423 cm^{-1} was associated with silanol groups (Si-OH) and adsorbed water. When F400 was impregnated with Zr(IV) the FTIR spectra showed 2 absorption bands in the region of 600-700 cm^{-1} that were attributed for Zr-O bond in coordinated complexes [78]. A weak vibration band in 1084 cm^{-1} was related to Z=O from zirconyl groups [131, 132]. Furthermore, a broad band centered in 1495 cm^{-1} may be attributed to bidentate carbonates formed from the interaction between atmospheric CO_2 and O_2^- Zr^{4+} pairs, as well a weak broad band in 471 cm^{-1} indicated that Zr(IV) can be found in a monoclinic and tetragonal phase of ZrO_2 [131].

ZrOx-AC showed a broad and sharper band of great intensity in 467 cm^{-1} that was associated with Zr-O (related to ZrO_2) and Zr=O. The broad peaks centered at 992 and 1506 cm^{-1} were assigned to Zr-O and Zr-OH bonds, respectively, while peaks around 880 and 1108 cm^{-1} were related to C-O-C and –OH bonds from the OA and Zr-oxalate complex, respectively. Bands at 1308 and 1348 cm^{-1} denoted a combination of Zr-O and Zr-OH vibration bonds [133, 134]. The peak at 3400 cm^{-1} was due to the stretching and bending modes of coordinated water and –OH bond from Zr-OH and the organic acid. A narrow band of big intensity at 1680 cm^{-1} indicated the presence of C=O groups. It is important to point out the presence of atmospheric CO_2 that ZrOx-AC could have adsorbed, and it is related at 2328 and 2349 cm^{-1}.
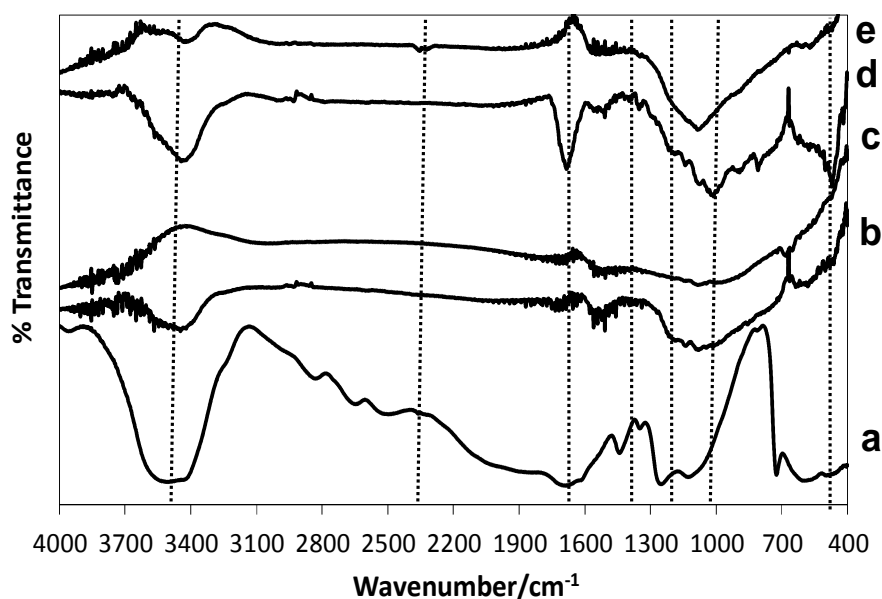
Figure 4.6 FTIR spectra of a) oxalic acid (OA), b) F400, c) Zr-AC, d) ZrOx-AC and e) ZrOx-AC saturated with fluoride ions (ZrOx-AC + F).

The IR spectrum of OA (Figure 4.6a) showed peaks at 563, 715, 1010, 1364, 1668 and 3452 cm^{-1} that are attributed to normal vibration modes of the oxalic acid. The broad of these peaks may be due to absorbed water in the sample. There were similarities and shifts in absorption bands of OA and ZrOx-AC spectrums. The most important differences related to carboxylic groups ($\Delta = \Delta_{C=O} - \Delta_{C-OH}$) are due to the symmetry of the carbon-oxygen bonds, and reflect Zr(IV) interaction with the organic complexing agent. The band shift between ZrOx-AC and OA were 12 and 98 cm^{-1}, respectively. These results indicated that Zr(IV) ions have more involvement with the acidic –OH than with the carboxylate group (COO$^-$) from OA to form Zr-oxalate complexes.

When fluoride was adsorbed (ZrOx-AC+F, spectra e), the peak related to –OH groups (3400 cm^{-1}) had a sharper form and low intensity than ZrOx-AC (spectra d). These imply that hydroxyl groups are involved in fluoride adsorption process. Furthermore, vibrational changes occurred between 400-500 cm^{-1} when F$^-$ was adsorbed and could be due to the formation of fluoride complexes with Zr-O groups. A broad and intense band at 1046 cm^{-1} could be an overlapping of vibration of Zr-O, C-O and Zr-OH bonds due to the interaction with fluoride ions. It is important to notice an "inverse" peak around 1680cm^{-1} that could be due to the C=O stretching vibrations found in this range. Those vibrations are

more intense in the s-polarized than in the p-polarized scans, and a p:s ratio was used to present the FTIR spectra [135].

4.3.5.4. X-RAY DIFFRACTION STUDIES

Powder X-ray diffraction was carried out in order to identified the polymorphic phases of ZrO_2 found in FTIR analysis when F400 was modified with Zr(IV) and OA. Figure 4.7 shows the XRD patterns for ZrOx-AC, where two peaks at 2θ angles of 26.58 and 43.1° correspond to monoclinic and 35-36.5° to tetragonal zirconia structures, respectively [136]. ZrO_2 has three polymorphic phases at ambient temperature: monoclinic, tetragonal and cubic. The monoclinic phase is described as a distorted fluorite structure with the Zr atoms in seven-fold coordination sites, while the cubic structure is an 8-coordinated zirconium ions face-centered cubic lattice where each oxygen ion is located in a 4-coordinated zirconium tetrahedron. The tetragonal structure can be derived by stretching the cubic one [137].
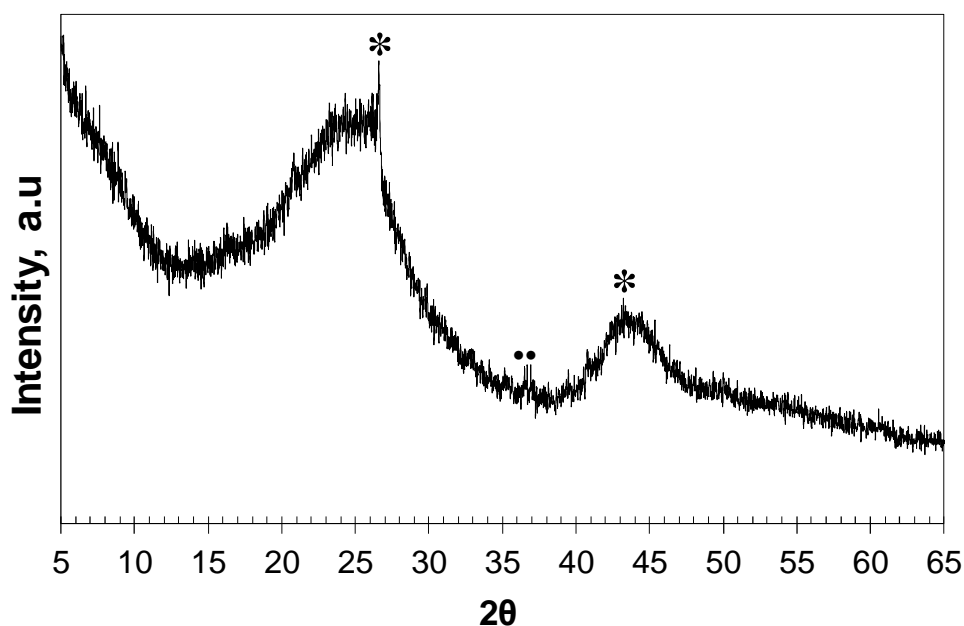
Figure 4.7 XRD diffraction pattern for ZrOx-AC. The symbols indicate the ZrO_2 structure in *monoclinic and ● tetragonal phases.

4.3.5.5. SURFACE CHARGE AND pK_a DISTRIBUTION

Proton binding curves obtained from potentiometric titrations in Figure 4.8 demonstrated that Zr(IV) shifted the point of zero charge (pH$_{PZC}$) of F400 from 9.97 to

3.28, however, when the adsorbent contained OA to form the Zr-oxalate complexes, the pH$_{PZC}$ increased to 11.18 (see Table 4.3). Activated carbon has high affinity for Zr(IV) ions, and when they are adsorbed on carbon surfaces, zirconium-based Lewis acid sites are generated [126, 128]. The adsorption sites become basic with the addition of OA to form Zr-oxalate complexes, due to the unpaired electrons and the π-bond system of the oxygen atoms of the oxalate ligand. ZrOx-AC thus possesses positive charge at the pH of adsorption experiments (pH 7). These conditions are favorable for fluoride adsorption due to electrostatic attraction between the positively charged adsorbent and the anionic F$^-$. At pH greater than the pH$_{PZC}$, the adsorbent is negatively charged and disfavor the adsorption process.
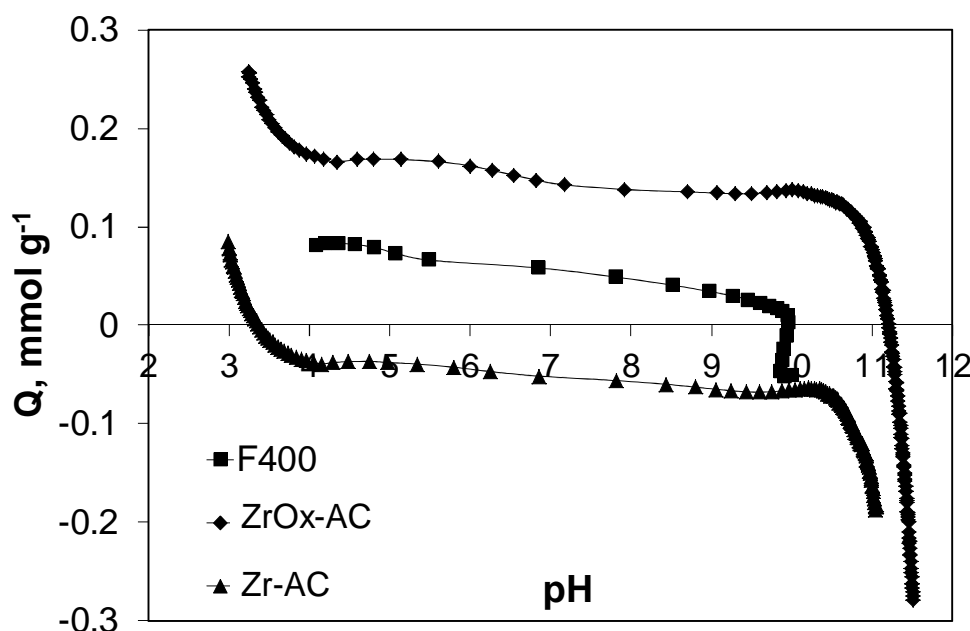
Figure 4.8 Surface charge distribution of F400, Zr-AC and ZrOx-AC in 0.1M NaCl.

The pK_a intensity and distribution of modified and non-modified F400 is presented in Figure 4.9a. It can be seen an increase of weak acidic groups in pKa~11 when Zr(IV) was anchored on the F400 surface. A reduction of carboxylic groups (4<pK_a<7) was noticed when Zr and its oxalate complexes were loaded on the carbon surfaces, while an increase of phenolic and C=O groups (9<pK_a<11) was appreciated. The results demonstrated that –COOH groups played an important role in zirconium ion anchoring.

Because Zr(IV) is considered a strongly acidic cation with pK_a values between -4 and 1 (in aqueous solution) [138], an increased in the surface acidity of F400 was noticed

when Zr(IV) is loaded in the carbonaceous surface. This was confirmed by pK_a 2.66 and 2.92 in Zr-AC and ZrOx-AC, respectively, where the shift in the pK_a value could be due to the interaction between the metal ion and some of the oxygenated groups contained in the F400 surface. The pK_a positions and amount of groups are listed in Table 4.4.

Table 4.4 pK_a positions and amount of groups of F400, Zr-AC and ZrOx-AC, determined by potentiometric titration.

Sample	meq/g	pK_a
F400	0.0357	4.81
	0.0190	7.66
	0.0626	9.94
Zr-AC	0.4324	2.66
	0.0171	6.16
	0.0143	8.58
	0.3435	10.95
ZrOx-AC	0.3256	2.92
	0.0329	6.58
	0.0004	7.99
	0.9577	11.60
ZrOx-AC + F	0.004	4.50
	0.021	6.42
	0.0051	8.35

When fluoride ions were adsorbed on ZrOx-AC (see Figure 4.9b), the distribution and intensity of pK_a peaks changed due to the interaction of zirconyl complexes with F^-. A pK_a shift of 0.16 was observed in pK_a ~6 related to carboxylic groups (4<pK_a<7) when F^- was presented in ZrOx-AC+F, as well as a decreased in intensity and amount of the functional group (see Table 4.4). Moreover, a new peak can be noticed around pK_a 4.50 that could suggest a structural arrangement in the Zr-oxalate complex where a carboxylic group (from the OA) may arise again when fluoride was linked to the metal complex.

The identification of fluoride in the Zr-oxalate complexes may be related to a pK_a peak around 8.35. The fluoride ions increase the basicity of the metal complex, due to the basic adsorption sites developed of the interaction between Zr(IV) and OA, with the addition of a strong Lewis base such F^-. It is important to notice the low intensities of pK_a peaks when fluoride was adsorbed, where concentrations of less than 0.004 meq g^{-1} were detected.
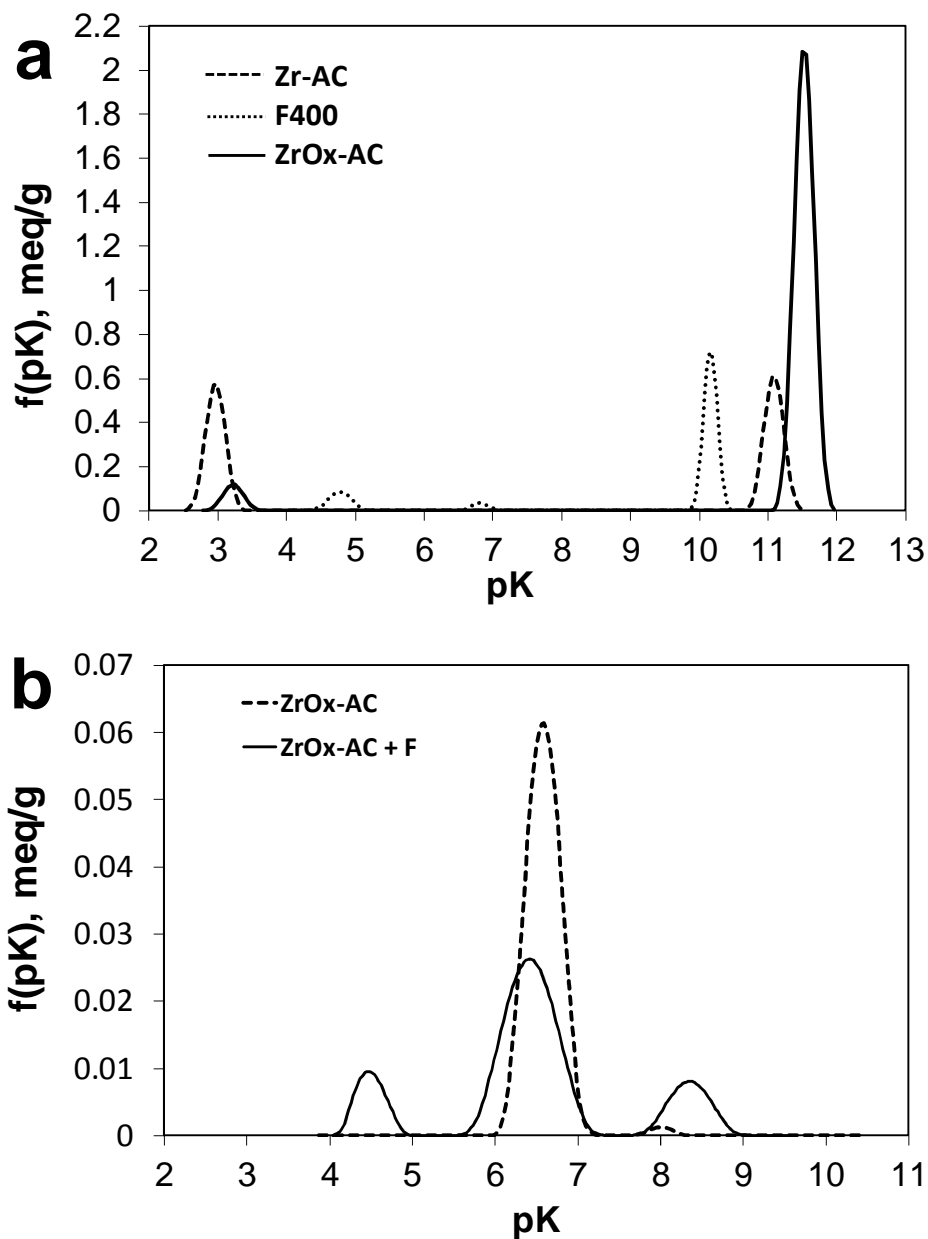
Figure 4.9 pK_a distribution for: a) modified and non-modified F400, and b) ZrOx-AC loaded with fluoride ions at pH 7 and 25°C (ZrOx-AC + F).

4.3.5.6. XPS ANALYSES

XPS analyses were performed to find out the possible Zr(IV)/oxalic acid structure formed during the impregnation process and the way that fluoride interacts with the metallic complex. Figure 4.10 shows the XPS full spectra referenced to C 1s level at 284.5

eV. It can be seen that the binding energy of Zr 3d region corresponding to Zr-AC and ZrOx-AC was 182.5 eV in good agreement with 182.3 eV for Zr^{+4} in ZrO_2 [139]. An important increase can be noticed in the binding energy up to 183.3 eV for zirconium in ZrOx-AC. This is in agreement with 183.6 eV in the $3d^{5/2}$ region for $Zr(OH)_4$.

In addition, the binding energy of O 1s region showed an increase in the ZrOx-AC up to 532.5 eV compared to 531.5 eV for Zr-AC and ZrOx-AC+F samples. F 1s region was not detected in Figure 4.10 for ZrOx-AC+F.

By contrast, Cl 2p is present in all samples with binding energies in the Cl 2p region of 198.5, 201 and 200 eV for Zr-AC, ZrOx-AC and ZrOx-AC+F, respectively. The binding energy in Cl $2p^{3/2}$ region of chloride salts has been reported at 198.6 eV [140], which is in agreement with Zr-AC. Binding energies in Cl $2p^{3/2}$ region clearly increased in ZrOx-AC and ZrOx-AC+F. These results suggest that OA plays an important role in the capture and surface interaction between C at Zr atoms.

Figure 4.11 shows the XPS spectra in the C 1s region referenced at 284.5 eV. It can be seen from deconvoluted peaks that Zr-AC (Figure 4.10a) and ZrOx-AC+F (Figure 4.11a) showed similar functional groups. Besides C=C peak at 284.4 eV that corresponded to sp^2 carbon bonding, all samples showed carbonyl (C=O) and carboxylic groups (COOH) at very similar binding energies at 286.2 and 289.5-290.0 eV, respectively. However, ZrOx-AC (Figure 4.11b) developed an additional peak at high binding energy, about 293.3 eV. Okpalugo et al. [141] attributed this peak to π→π* transitions. It can also be attributed to C=C-O surface group formed by OA surface functionalization [142-144].

Figure 4.12 shows the XPS spectra in the Zr 3d region. Zr-AC and ZrOx-AC+F spectra showed similar binding energy of 182.5 eV in the Zr 3d5/2 region in agreement with the formation of ZrO_2 [145]. In presence of OA, ZrOx-AC showed an enhancement in the binding energy up to 183.3 eV. This indicates a more positive surface charge around Zr atoms, probably by the interaction of hydroxyl groups from activated carbon surface and Zr(IV) ions to form $Zr(OH)_2Cl_2$.

The high value of 183.3 eV for the binging energy in Zr 3d5/2 region is in agreement with that reported by Barr [139] for $Zr(OH)_4$. Also, a small peak about 180.6 eV was detected and attributed to the formation of Zr-Cl bonding in agreement with that reported for Zr-Br at 179.3 eV [146].
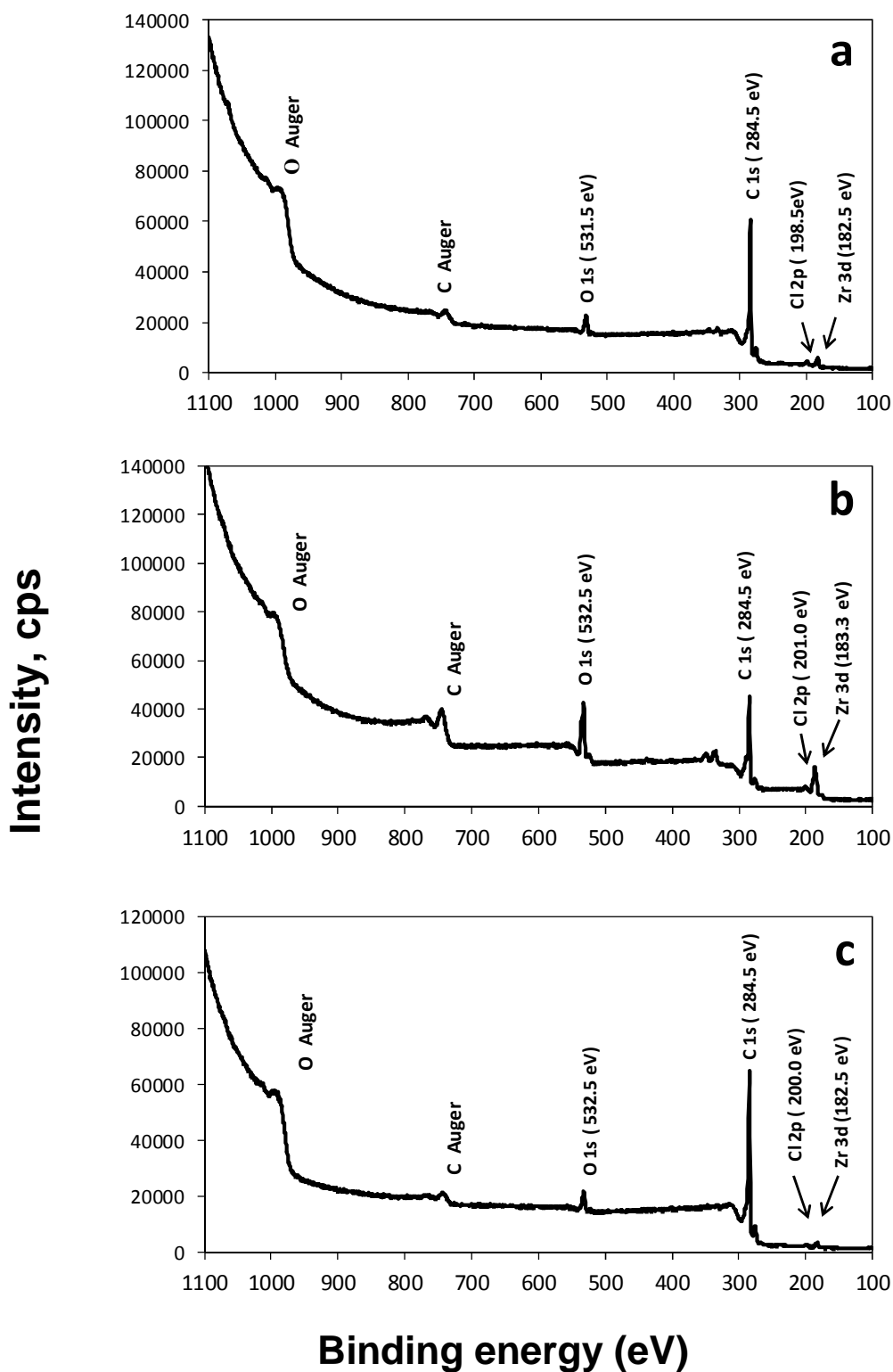
Figure 4.10 XPS full spectra referenced to C 1s level at 284.5 eV for: a) Zr-AC, b) ZrOx-AC, and c) ZrOx-AC+F.
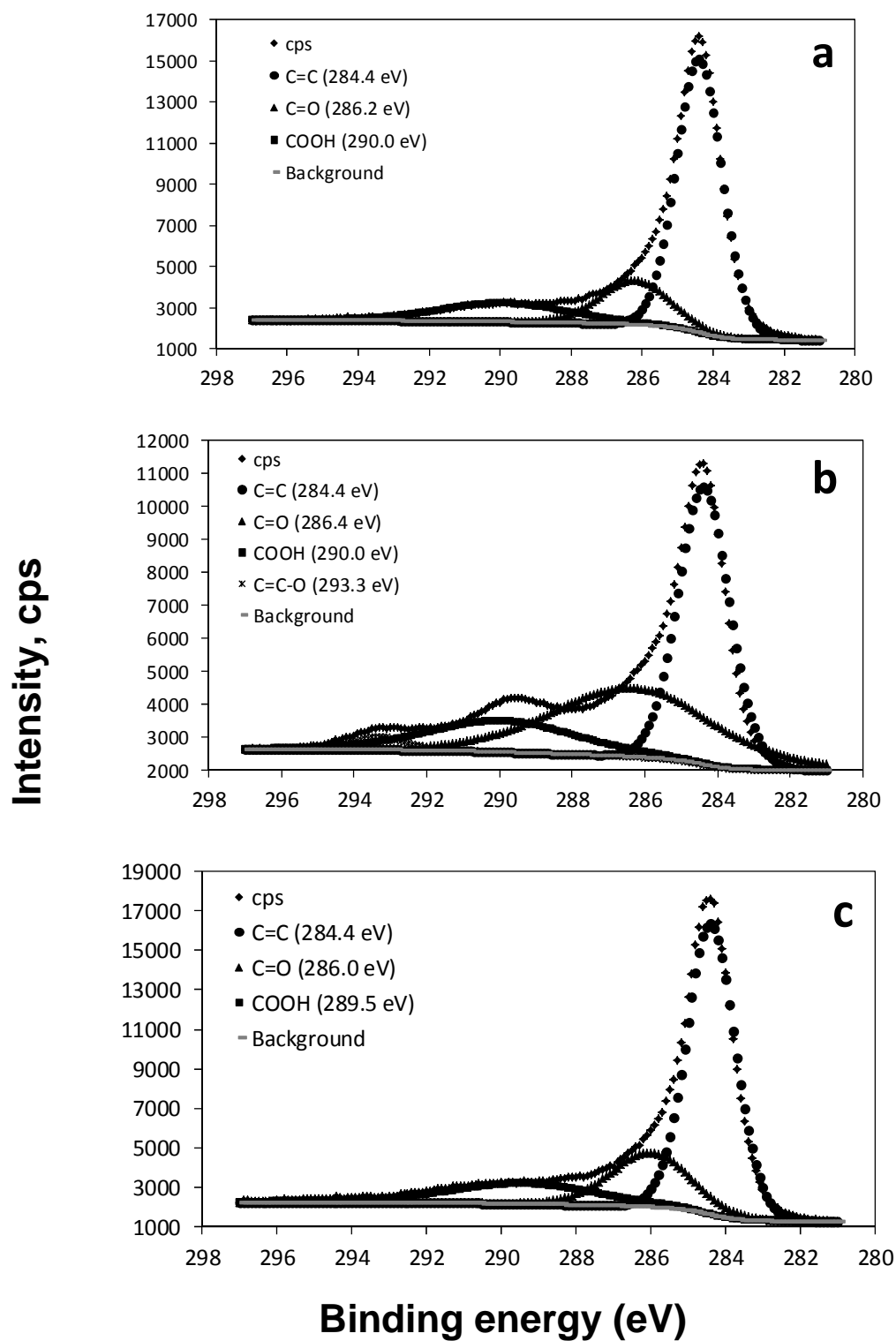
Figure 4.11 XPS spectra in the C 1s region referenced at 284.5 eV for: a) Zr-AC, b) ZrOx-AC, and c) ZrOx-AC+F.
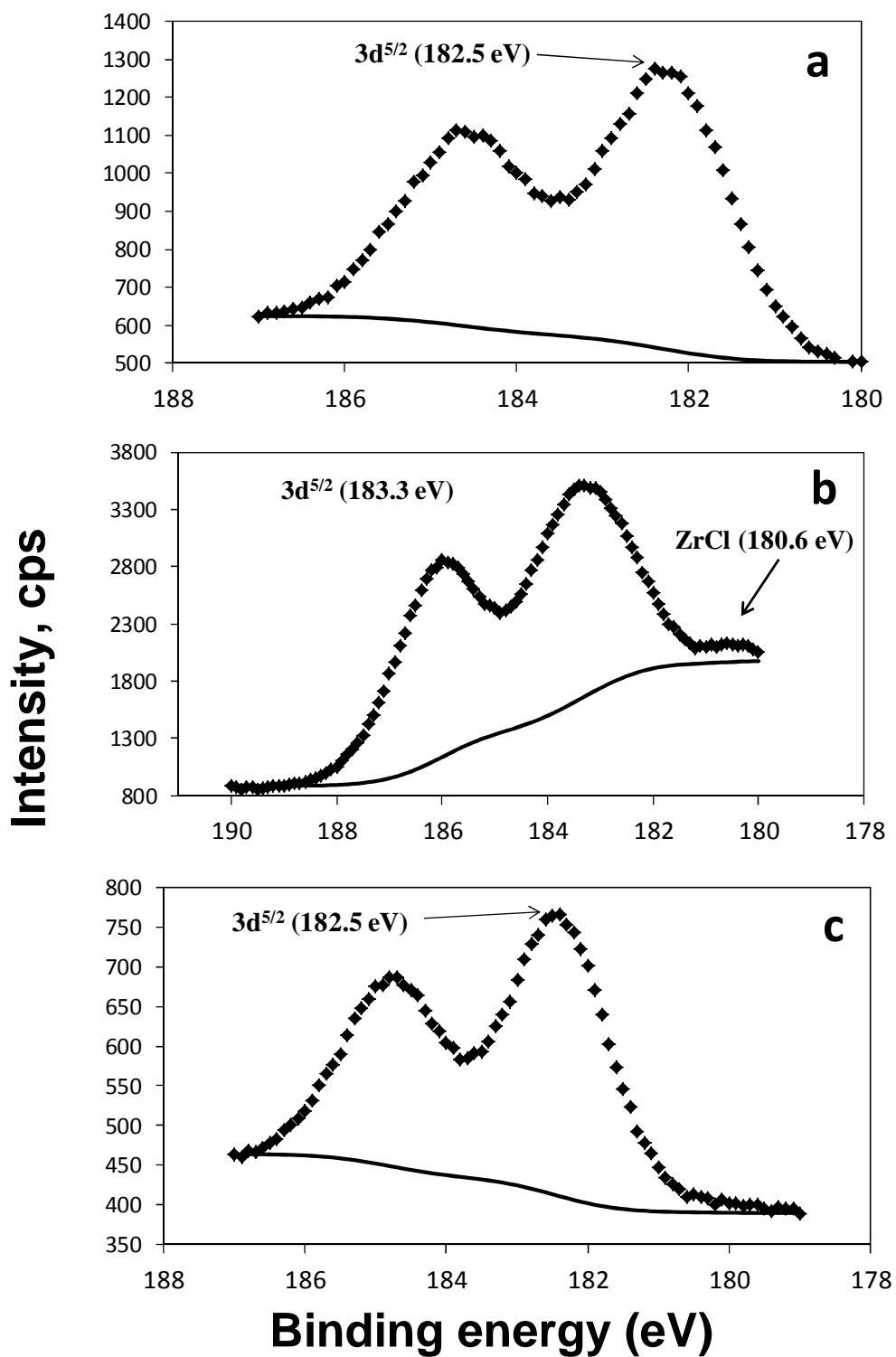
Figure 4.12 XPS spectra in the Zr 3d region corrected to C 1s level at 284.5 eV in a) Zr-AC, b) ZrOx-AC, and c) ZrOx-AC+F.

The shift to higher binding energies for Zr-Cl in comparison to Zr-Br is due to Cl having more electronegative than Br, and therefore, the binding energy corresponding to Zr-Cl must be higher than that of Zr-Br bond. The presences of chloride in the Zr-oxalate particles were corroborated by EDS analyses, as discussed in Section 4.3.5.2.

XPS spectra suggest that OA clearly influences the formation of different Zr-based groups on carbon surface in agreement with the different oxygenated functional groups detected from the deconvoluted peaks of C 1s region showed in Figure 4.11. This inference was confirmed from the changes in the atomic surface composition (At wt.), compiled in Table 4.5.

Table 4.5 Summary of XPS analysis referenced at C 1s level at 284.5 eV.

Sample	Element	Region	Position (eV)	At (%)	At-C/At-i [a]
Zr-AC	C	1s	284.5	90.313	1.0
	O	1s	531.5	7.189	12.6
	Zr	3d	182.5	1.052	85.8
	Cl	2p	198.5	1.446	62.5
ZrOx-AC	C	1s	284.5	79.197	1.0
	O	1s	532.5	13.840	5.7
	Zr	3d	183.3	3.115	25.4
	Cl	2p	201.0	3.848	20.6
ZrOx-AC+F	C	1s	284.5	91.631	1.0
	O	1s	532.5	6.858	13.4
	Zr	3d	182.5	0.669	137.0
	Cl	2p	200.0	0.862	106.3

Carbon surface composition are higher in Zr-AC and ZrOx-AC+F samples than in ZrOx-AC. Oxygen surface composition in ZrOx-AC showed a remarkable increase from about 7 to 14% in comparison of Zr-AC and ZrOx-AC+F. This was due to the high degree of functionalization promoted by OA. Concomitantly, the atomic ratios At-C/At-Zr and At-C/At-Cl in ZrOx-AC showed a remarkably decrease in comparison of ratios estimated for Zr-AC. This result indicated a remaining of Zr and Cl in ZrOx-AC by a stronger interaction

with OA, probably due to a specific oxygenated surface groups such C=C-O, indicated in Figure 4.10.

4.3.6 FLUORIDE ADSORPTION MECHANISM

The multiple spectroscopic techniques used here together with potentiometric titrations provided valuable information regarding the fluoride adsorption process in Zr-oxalic acid impregnated activated carbon (ZrOx-AC). The spectroscopy analyses identified the main functional groups involved in both the anchoring of Zr(IV) ions on the commercial activated carbon (F400) and in the fluoride uptake. Moreover, these analyses helped to identify the zirconyl fluoride species on the carbon surface.

Hence, with all the evidence shown in this study, a possible fluoride adsorption mechanism can be postulated (Figure 4.13). First, Zr(IV) species from the hydrolysis of $ZrOCl_2$ ($ZrOOH^+$ or $[Zr(OH)_{2+x} \bullet (4-x)H_2O]_4^{(8-4x)+}$) [121] adsorb on AC by –COOH groups through electrostatic interactions to form C-O-Zr bonds. It is important to consider that Zr(IV) can form tetrahedric and octahedric polymeric structures [118, 147]. Therefore, it is possible to propose a first interaction between the oxygen functionalities of activated carbon surface, see Figure 4.13a.

A second reaction occurred when oxalic agent was added to form the zirconyl oxalate complex, where Zr(IV) interacts with –OH from the oxalic acid. It is possible to form six Zr-oxalate structures and several other configurations like dodecahedric arrangements [146,148]. ZrO_2 forms as well and could produce a 7-coordinated polyhedral species [132]. To simplify such configurations, an interaction between Zr(IV) and OA can be suggested in Figure 4.13b.

The hydrolysis of $ZrOCl_2$ in aqueous solution produces structures of four Zr atoms in each tetramer complex that is arranged in a square, and each zirconium atom is coordinated by four bridging OH groups and H_2O molecules that tend to polymerize. The concentration of the polymeric species can reach a supersaturation level and crystal nuclei of hydrous zirconia are generated, forming then primary particles [147]. The last step occurs when the aggregation of the primary particles takes place, see Figure 4.14, and it is apparently controlled by the formation of the primary particles.
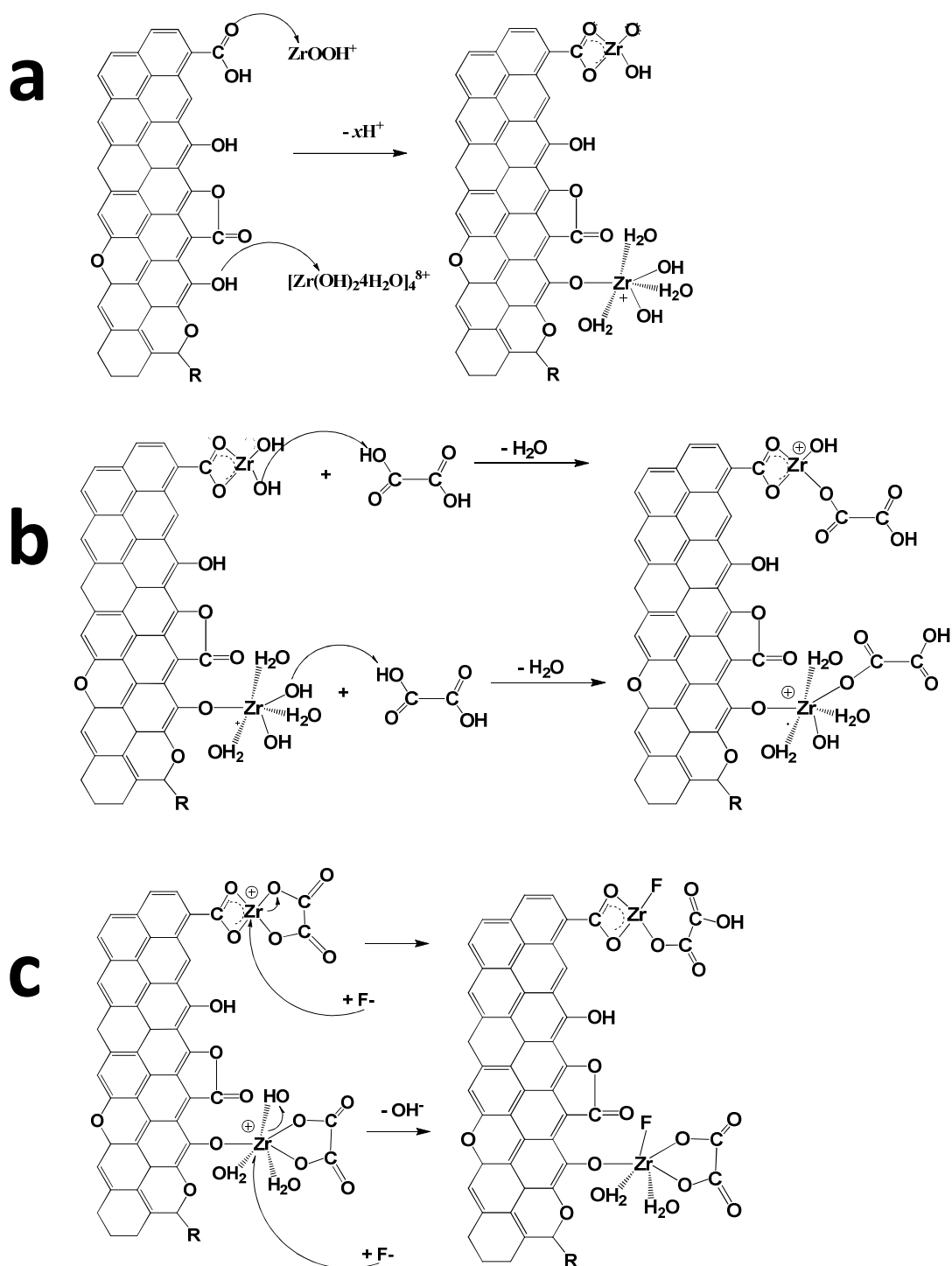
Figure 4.13 Possible fluoride adsorption mechanism.

The presence of oxalic acid in this step can avoid the aggregate growth due to steric effects and electrostatic repulsion between particles, which is in agreement with the particle size of Zr-complexes reported by microscopy studies. The particle surface of the small Zr-oxalate particles bonded on AC and polymeric or based Zr-oxalate complexes physical or locally attached in the carbonaceous surface contribute to the increase of fluoride adsorption capacity.

Finally, fluoride attack Zr(IV) ions in the metal complexes and its adsorption occur in the ZrOx-AC surface with –OH displacement from the Zr-oxalate complexes. A chemical rearrangement could be carried out to form –COOH groups in the OA and/or to form Zr-oxyfluoride species (ZrOF$_x$), see Figure 4.13c. It is important to point out that ZrO$_2$ can develop di-, tri-, tetra-, and pentafluoro zirconium species without the presence of a complexing agent such as oxalic acid [132].
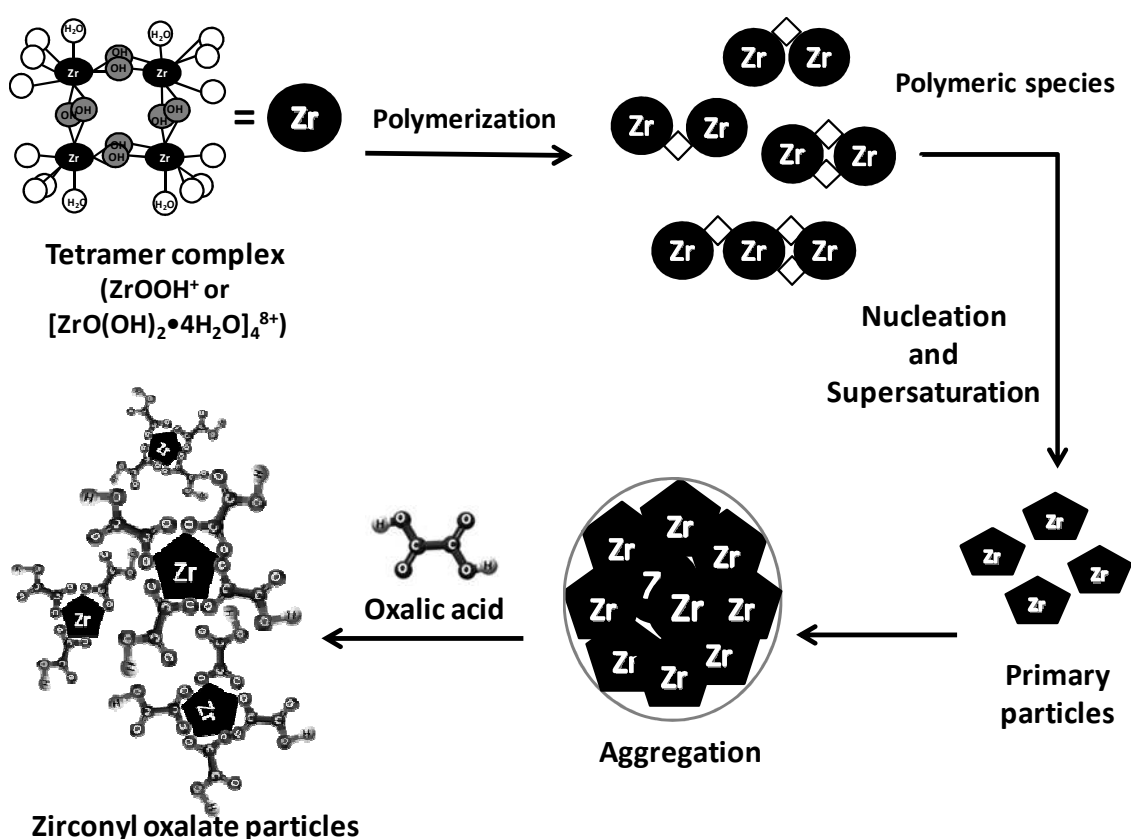
Figure 4.14 Scheme of hydrous zirconia formation by hydrolysis of ZrOCl$_2$ solution, its polymerization and the interaction of Zr with oxalic acid to form Zr-oxalate complexes. ◊ represents –ol bridge. Adapted from [132].

4.4 CONCLUSIONS

It was shown that addition of oxalic acid during the Zr-doping of activated carbon increased the fluoride adsorption capacity by a factor of 3 over simple Zr-doped AC at an optimum Zr/OA ratio of 1.05. Our work suggests that the enhancement mechanism involves OA complexation with Zr ions, which controls the nucleation and limits the growth of ZrO_2 particles that reduce Zr dispersion in the conventional method. Suppressing particle growth increases the zirconium active surface area and leaves some highly active Zr in the form of OA molecular complexes associated with carbon surface sites. Finally, the proposed fluoride adsorption mechanisms were a hydroxyl exchange from the Zr-oxalate surface sites and fluoride interaction with the positive charge of zirconium ions in Zr=O groups.

5
CHAPTER

FINAL REMARKS

The use of several materials to remove pollutants from aqueous is still in progress. Due to the recent developments in generic sorbents for water purification, adsorption has become a key factor for separation processes in aqueous streams. Adsorption can be compared with other separation methods like chemical precipitation or reverse osmosis, but it is advantageous due to the availability of new and better adsorbents.

Several agrowaste materials have been employed for heavy metals removal from aqueous solutions, as well as modified activated carbons for water defluoridation. Moreover, research has been mainly focused in determining adsorption capacities, but the adsorbents chemical composition and the adsorption mechanisms need to be studied in detail, in order to synthesize better adsorbent materials.

Agave salmiana bagasse is an agro-waste lignocellulosic material generated in the mezcal industry, in hundreds of tons every year, and its disposal produces ecological impacts. Faced with this problematic, agave bagasse has been tested for heavy metal ions removal from aqueous, and it is considered a better biosorbent than oat and sorghum wastes. This material could be used to reduce the industrial pollutants concentrations in wastewater at low-cost water treatment.

On the other hand, high fluoride concentrations in groundwater, for example up to more than 4 mg L^{-1} in San Luis Potosi [150], are due to the natural pollution by deep groundwater flow that is pumped by public supply boreholes. This problem could be solved by using Zr-modified activated carbon. Zr(IV) confers to the carbonaceous material high selectivity to fluoride ions by forming stable Zr-F complexes.

During this research, it was demonstrated that *Agave salmiana* bagasse and Zr-modified activated carbon were feasible adsorbents for metal ions and fluoride removal, respectively. The results obtained generated valuable information that support the viability of using these adsorbents in water treatment processes.

Cd(II), Pb(II) or Zn(II) ions can be removed from aqueous solutions by raw agave bagasse (RAB). To increase the natural adsorption capacity of this lignocellulosic material, HCl, HNO_3, NaOH and tartaric acid were selected due to their easy manipulation and low cost. When RAB was modified with the acid or alkali solutions, new functional groups (mainly carboxylic and phenolic groups) were developed on its surface, as can been seen in the IR spectra of Figure 2.1. Furthermore, band shifts indicated more involvement of carboxylate groups forming complexes with Pb(II) and Cd(II) ions when RAB was modified with NaOH and with tartaric acid. Analytical techniques such as potentiometric titrations corroborated that -COOH plays the major role in metal ions biosorption, which was able to detect minimum acidic concentrations in the order of 6.62×10^{-5} meq g^{-1} (Table 2.3).

In addition, elemental analyses showed that the chemical modifications performed on RAB increased the concentration of oxygenated groups (as carboxyl groups), and reduced the ash content due to the loss of the soluble and inorganic fraction contained in the lignocellulosic sorbent. It is important to take into account that although carboxylic groups are mainly responsible for metal complexing, there are –OH or strong acidic groups like sulfur that may also interact with cations too, among others.

Agave bagasse showed an affinity to adsorb Pb>Cd>Zn, as can be seen from the adsorption isotherms of Figure 2.3. The physical and chemical properties of the metal ions under study could define the preference during the adsorption process, where the ionic radius, the electronegativity and covalent index of Cd(II), Pb(II) and Zn(II) were key factors to understand their behavior during metals uptake by agave bagasse. All these parameters were in complete agreement with the adsorption capacities reported herein. Additionally to the adsorption process, Ca, Na and K ions were released during the metal uptake, and suggested an ion exchange and/or complexation adsorption mechanism. Regarding this issue, homopolygalacturonic fragments (present in pectin and hemicellulose) contains carboxyl groups linked by calcium bridges, but once the calcium is released to the solution, the carboxyl groups act as active adsorption sites for the metal ions.

When RAB was modified with acids or alkali solutions at room temperature, it was noticed that 0.5 M HNO_3 and 1 M HCl increased the Pb(II) and Zn(II) sorption capacity in about 152 and 84%, 18.8 and 58.2%, respectively (see Table 2.5). 1 M NaOH treatment increased 38.0, 40.8 and 162% of Cd(II), Pb(II) and Zn(II) uptake respectively. Therefore, NaOH seems to work better than the acid treatments under the same conditions. When we modified these adsorbents with tartaric acid at 100°C, similar sorption capacities were obtained (see Figure 2.4). Nevertheless, the optimum metal uptake was reached with 2 M

tartaric acid at 100°C during 10 min. On the other hand, modified agave bagasse just with 2 M tartaric, citric or oxalic acid at 100 °C during 10 min (T-AB, Cit-AB and Ox-AB) did not improve the natural metal binding capacity of RAB, as shown in Table 2.6. At this point, steric effects played an important factor when large acids such as citric and tartaric acids were used during chemical modifications to increase metal ions removal. In order to regenerate raw and modified agave bagasse that was saturated with Cd(II), Pb(II) or Zn(II) ions; HNO_3 was selected to promote an ion exchange between H^+ from the mineral acid and the adsorbed metal (COO-M(II)). At pH 2, up to 45% of metal ions were desorbed from agave bagasse (see Figure 2.5a), whereas at pH 4 only less than 25% of metal ions were desorbed, as can be seen in Figure 2.5b. Pb desorbed more than Cd and Zn ions when they were adsorbed at the same time, as demonstrated in Figure 2.5c. This results confirmed that complexes between Pb and carboxylic groups (COO-Pb_x) were less stable (outer-sphere coordination) than those with Cd and Zn (inner-sphere coordination). Besides, the presence of Na, K, and Ca ions desorbed with the release of the metal ions suggest that an important mineral fraction remains after the adsorption process and could be related to ion-exchange.

Taking into account that agave bagasse is considered a lignocellulosic material composed by cellulose, hemicellulose and lignin, it is important to study the influence of such components during Cd(II), Pb(II) and Zn(II) uptake. Such information can facilitate the screening of lignocellulosic materials when these are intended to be employed like biosorbents in wastewater treatments.

Cellulose was in major proportion (greater than 40%) compared with hemicellulose and lignin (14.0 and 9.1%, respectively). The soluble fraction was around 35.5% and the ash content (interpreted as inorganic fraction) 0.16%. Sugars, starch, fatty acids and pectin are possibly the main components of the soluble fraction of agave bagasse, while the inorganic fraction may content Ca, Na, K, among others. Besides, the cooking of the ripe agave head (also known as "piña") and later milling of it to extract sugars to produce mezcal could originated the proportion of cellulose, hemicellulose and lignin. Once RAB was treated to separate the main fractions (NDF, ADF and ADL), the original functional groups were affected during the extraction procedure, as well as the structural arrangement of the lignocellulosic matrix components. This could be attributed to the hydrolysis of soluble organic elements (carbohydrates, lipids, among others), a swelling of the lignocellulosic matrix and/or to the loss of minerals during the fiber extraction. It is well known that hemicellulose, cellulose and lignin possess a wide content of heterogeneous

compounds with a complex structure. The functional groups identified in RAB and in its fractions include hydroxyl, carboxyl, sulfur, nitrogen and phosphorous compounds, as was demonstrated by the FTIR spectra of Figure 3.1a. Furthermore, the infrared spectrum of a pectin standard showed a similar composition to RAB (see Figure 3.1b).

The adsorption capacity of main fractions was showed in Figure 3.2, where the adsorption affinity was established as Pb>Cd>Zn. NDF (cellulose, hemicelluloses and lignin) and ADF (cellulose and lignin) presented a comparable adsorption capacity than ADL. Nevertheless, the ADL fraction showed the lowest adsorption capacity for Cd and Zn ions, which may be related to the extraction procedure were a portion of lignin was solubilized, condensated and/or precipitated, decreasing the content of ADL fraction. Potentiometric titrations were used to estimate the ion exchange capacity of main components, and to identify the possible binding sites that could participate in metal uptake. The results indicated an increase in -COOH and very weak groups attributed to phenolic and amines after the NDF extraction procedure applied to RAB (see Table 3.3). Moreover, in presences of Cd(II), Pb(II) or Zn(II) ions, carboxylic groups were no detected, and suggests that –COOH groups are the main responsible for metal uptake. This behavior was corroborated by FTIR analyses. In despite of the increase of very weak functional groups, the higher density of oxygen developed after carboxylic and strong acid binding sites made this active sites the first occupied by the metal ions. At the other site, Cd(II) uptake by NDF fraction showed a slight decrease in strong and very weak groups content, and could indicate that Cd(II) may strongly interact with very weak acidic compounds. Thermogravimetric analyses were used to provide information of the trend in the chemical changes of the lignocellulosic matrix when the metal ions under study were loaded in the agave bagasse. This knowledge is usually not explored in biosorbents research when they are used to remove metal ions and could be valuable to understanding the adsorption mechanism of metal ions. The results indicated that Zn(II) shifted to lower temperatures the thermal decomposition of NDF due to its dehydrating power over lignocellulosic matrix, while Cd(II) and Pb(II) presented the opposite effect (see Figure 3.3b). In the other hand, Pb(II) prefers to bind oxygen compounds and to fit with more than two distant groups, making Pb-complexes more stables than Cd or Zn-complexes. This statement can be supported by the behavior of Pb^{2+} in terms of its high electronegativity and bigger ionic radius than the other metal ions. Once again, the physical and chemical properties of metal ions play an important role during the adsorption

process, and may establish the affinity of metal uptake by agave bagasse and other biosorbents, as was previously seen in Chapter 2 (section 2.3.4).

Exploring other kind of adsorbents as in the second part of this research, it was found that when a commercial activated carbon was modified with Zr(IV), the fluoride adsorption capacity improved. The optimal Zr/OA ratio was 1.05, and from the adsorption isotherms (Figure 4.3) it was determined an improvement of 68% (3 times higher) in comparison with Zr-modified activated carbon without the presence of oxalic acid (Zr-AC). Besides, in the presence of oxalic acid (ZrOx-AC) more zirconium was found in the activated carbon (see Table 4.3) that was associated to its higher adsorption capacity. This behavior was related to the unpaired electrons of the oxygen atoms, found in the structure of the organic acid, that may enhance the positive charge of the Zr ions to allow a better attraction for F^-, and that carried out more Zr ions from the solution to form zirconyl-oxalate complexes. Although Zr content on the activated carbon is less than 0.77% in the optimal adsorbent, it is still possible to detect X-ray diffraction patterns of the polymorphic phases of zirconium. Our results demonstrated that we produced ZrO_2 particles during the modification process with oxalic acid. Finally, this adsorbent has Zr-oxalate complexes which give a basic character (pH_{PZC} 11.18) in aqueous solutions. These conditions were favorable for fluoride adsorption due to electrostatic attraction between the positively charged adsorbent and the anionic F^- at pH 7. In contrast, Zr(IV) shifted the point of zero charge (pH_{PZC}) of F400 from 9.97 to 3.28. Besides, proton binding curves from those results demonstrated that –COOH groups played an important role when Zr(IV) was anchored on the activated carbon surface during the first step of the impregnation process. Another important factor is the interaction of Zr(IV)-oxalic acid during the second step of the modification. This process occurred through the acid –OH from the carboxylate group, as was shown in the spectra of Figure 4.6. Moreover, when fluoride was adsorbed the peak related to –OH groups changed in vibrational mode, form and intensity, as well in the pK_a distribution; implying that hydroxyl groups were involved during fluoride adsorption process. Those result showed that potentiometric titrations, FTIR and XPS analyses can be a powerful analytical techniques to detect Zr(IV) interactions with the organic complexing agent, and to establish a possible fluoride adsorption mechanism with pK_a and band shifts.

Zr-impregnated activated carbon removed 71% of the initial fluoride concentration in the first 15 min, and this was considered a fast adsorption process. In this point, the external mass transfer resistance could play an important role during the fluoride uptake

since the Zr-modified activated carbon has high porosity and surface area. Although fluoride ions are found in presence of other anions such Cl^-, SO_4^{2-}, NO_3^-, PO_4^{3-} and/or CO_3^{2-} in potable water, the performance of ZrOx-AC was evaluated in those conditions. The results revealed a decreased of up to 50% on the fluoride adsorption capacity, as was shown in Figure 4.4c. It is important to mention that Zr-modified activated carbon had a great affinity for fluoride, even at concentrations up to 10 mg L^{-1} of co-existing anions.

Although Zr-impregnated activated carbon regeneration was not explored in this study, several researches have established NaOH solution as eluent to desorb fluoride ions from the modified carbonaceous material by ion exchange. This basic solution provides hydroxyl ions ($-OH^-$) that will be exchange by F^- adsorbed in the material, and thus, regenerate the adsorbent. In other hand, Zr-impregnated activated carbon saturated with fluoride could be treated as not hazardous material, due to zirconium low toxicity and its unknown biological role in the human body. The final disposal of this saturated adsorbent could be carry out under a proper confinement.

Although the adsorption capacities of the adsorbents studied through this research were comparable with several materials tested for the removal of the same priority pollutants contained in aqueous solutions, more research is needed in order to design an adsorbent that may accomplish the standards and settings on water treatment processes in Mexico and around the world.

6

CHAPTER

6.1 GENERAL CONCLUSIONS

Water pollution can be an important factor in limiting available potable water sources in arid and semi-arid regions around the world, like in San Luis Potosi (Mexico). This is due to industrial and acid mine drainage that release toxic metal ions, as well as high fluoride concentrations in groundwater (the major source of potable water). In this thesis was proved that raw and modified *Agave salmiana* bagasse, as well as Zr-modified activated carbon can provide adequate water quality for humans and environmental needs.

Although agave bagasse mainly contains carboxyl, hydroxyl, sulfur, and nitrogen containing groups, carboxylic groups are involved in the uptake of Cd(II), Pb(II) and Zn(II) ions. NaOH treated agave bagasse improves the adsorption capacity for Cd(II) and Zn(II) by developing new adsorption sites inside the swelled lignocellulosic structure. On the other hand, Pb(II) adsorption capacity is improved with HCl due to the protonation of functional groups, specially of those that play a major role (–COOH) in cation biosorption. Chemical modifications with organic acids such as tartaric, citric or oxalic acid do not enhance the adsorption capacity due to a possible steric impediment. The saturated bagasse can be regenerated up to 45%, and the possible sorption mechanisms are ion exchange and complexation.

When the lignocellulosic material losses its soluble fraction: sugars, starch, fatty acids and pectin, to get in its main components (NDF: cellulose, hemicellulose and lignin), a higher adsorption capacity for Cd(II), Pb(II) and Zn(II) ions is achieved. Nevertheless, the soluble compounds account for about 60% of the total metal adsorption capacity. Although the extraction procedure to obtain the NDF fraction affects the original functional groups contained in raw bagasse fibers, it is possible to demonstrate that weak and strong acidic groups were involved in metals uptake. This is due to the sequential extractive methods that are not selective and affect the structural composition of the lignocellulosic matrix.

When Cd(II) and Pb(II) ions are loaded in the NDF fraction, its thermal decomposition shifts to higher temperature while Zn(II) presents the opposite effect. These findings support the idea that Zn(II) acts as a dehydrating agent, catalyzing the cleavage of hydroxyl groups present in lignocellulosic materials to make easy the gasification of NDF fraction, whereas Pb(II) and Cd(II) form stable metal complexes which are hard to break.

On other hand, activated carbon modified with Zr(IV)/oxalic acid shows 3 times higher fluoride adsorption capacity than iron-impregnated granular ceramics and Ca-impregnated nut shell carbons. This behavior can be related to its high pH_{PZC} that makes the fluoride adsorption favorable onto the adsorbent. It was possible to form Zr-oxalate particles of less than 2 nm, where the oxalic acid played an important role to control the polymerization of Zr(IV). Besides, it was possible to form ZrO_2. The distribution and intensity of pK peaks changed due to the interaction of zirconyl surface complexes with the anionic F^- contaminant, while the adsorption mechanism was due to both a hydroxyl exchange (from the Zr-oxalate surface sites) and to fluoride interaction with the positive charge of zirconium ions in Zr=O groups. The adsorption mechanism may involve the formation of $ZrOF_x$, due to a reduction of Zr atoms in the ZrOx-AC surface composition.

6.2 FUTURE WORK AND PERSPECTIVES

The presence of heavy metals and fluoride in drinking water and water supplies have been more strongly regulated since an intimate relationship with the increase on illnesses and diseases over global population has been demonstrated. For this case, efforts to reduce these pollutants from water to acceptable limits are essential, and needs to be researched vigorously all over the world.

Agave salmiana bagasse was used in this research to remove Cd(II), Pb(II) and Zn(II) ions from aqueous solutions, and proved to be a good adsorbent. Nevertheless, more research needs to be done for a better understanding on the use of this biosorbents for metal ions uptake, as well for the screening of biosorbents for a future application in wastewater treatment.

First, we reported that heavy metals removal using agave bagasse was performed through an ion exchange and complexation with Ca, Na, K, and H^+ from –COOH groups at pH 5. Nevertheless, the release of others components like sugars, fats, starch, etc. (found in the soluble fraction of agave bagasse) during the adsorption process needs to be

determine. This knowledge will help to determine a possible use of this bioadsorbent in wastewater treatment, or even to support the adsorption mechanism for heavy metal removal in aqueous solution.

Also, it will be important to explore other pH variations according to wastewater treatment and water purification guidelines, to evaluate the adsorption capacity of the material in order to establish the optimal conditions for its future use. Another important point to study is the effect of As, Al, Hg and/or Sn during Cd(II), Pb(II) and Zn(II) uptake; because those elements are considered important to being removed due to their great toxic effect over the human health and their presence in wastewater and water supplies.

It was found that desorption of Cd(II), Pb(II) and Zn(II) previously adsorbed in agave bagasse was achieved at pH 2, and using a HNO_3 solution (see Chapter 2). However, adsorption-desorption cycles are needed in order to determine the adsorption capacity loss of the bioadsorbent between each regeneration step.

The role of agave bagasse main components was studied in Chapter 3, and the results showed that carboxylic and strong acid groups were the main responsible for metal removal. Even though the same active sites were detected when agave bagasse was chemical modified with HCl, HNO_3 or NaOH, there is no information about the elemental composition of each bagasse fraction and if this could have any kind of effect on the process in terms of adsorption capacity. The performance of elemental analyses to figure out which chemical treatment on main components produced higher adsorption capacity will help to understand the adsorption mechanism of metal ions. Furthermore, thermogravimetry coupled to FTIR analyses may help to understand the implications of a chemical modification on the bioadsorbent, and the way that metal ions affect the functional groups contained in the hemicellulose, cellulose and lignin fractions.

Thermogravimetric kinetics can be also performed in order to determine the heat transfer and reactions rates of agave bagasse pyrolisis. This is because the agave bagasse represents a suitable sustainable source for production of conventional and new chemicals and fuels.

Finally, the disposal of agave or its fractions (main components) still containing metal ions could be unfavorable in environmental managing terms. However, we can propose the development of metal nanoparticles from the conversion of the metal ions attached to the surface of the lignocellulosic matrix. This solution may offers the opportunity to remove metal ions from aqueous effluents using bioadsorbents, and then, converting the saturated biomass in a commercial product like nanomaterial with a

possible use in the industrial and research fields. This pathway has been employed by Chefetz *et al.*, to produce silver, lead or ruthenium nanoparticules from Ag^+, Pb^{2+} or Ru^{3+} ions adsorbed by *Azolla filiculoides* (an aquatic plant) with a microwave procedure [148].

On other hand, the results in Chapter 4 demonstrated that Zr-modified activated carbon was useful to remove fluoride, and could be a good adsorbent for a future use in defluoridation of drinking water or other water supplies. However, it is necessary to explore the performance of this adsorbent in real adsorption processes like fixed-bed columns, and using groundwater to evaluate the effect of organic matter over the adsorption capacity. Besides, pH variations could help to corroborate the fluoride adsorption mechanism, taking into account the natural pH range of natural waters (6.8<pH<8). Adsorption kinetics need to be corroborated under different rotating-basket conditions and temperature used in this research (470 min^{-1} and 25°C, respectively), in order to establish if the gradient concentration affects or does not affect the external mass transfer and kinetics parameters.

Although Zr(IV) was chosen to develop a new selective site for fluoride removal, it would be important to test the presence of other metal ions like Fe(III), Ti(IV) or La(III) to increase the fluoride adsorption capacity by forming bimetallic oxides loaded on the activated carbon surface.

The impregnation methodology used to modify the commercial activated carbon was chosen for its simplicity and low cost, however, it is worth the possibility to explore new methodologies like microwave assisted techniques in order to produce ZrO_2 nanoparticles in less time and with high reproducibility. With this procedure, we expect to modify homogeneously the carbonaceous surface and to make more efficient the modification process.

6.3 LIST OF PUBLICATIONS

1.   Velazquez-Jimenez Litza Halla, Rangel-Mendez Jose Rene.; Chemical characterization of raw and treated agave bagasse and its potential as adsorbent of metal cations from water, Industrial Crops and Products 43 (2013) 200-206.

2.   Velazquez-Jimenez Litza Halla, Hurt H. Robert, Matos Juan, Rangel-Mendez Jose Rene; Zirconium-carbon hybrid sorbent for removal of fluoride from water: oxalic acid

mediated Zr(IV) assembly and adsorption mechanism, Environ. Sci. Technol. 48 (2014) 1166-1174.

3.   Velazquez-Jimenez Litza Halla, Rangel-Mendez Jose Rene.; Chemical and thermogravimetric analyses of raw and saturated agave bagasse main fractions with Cd(II), Pb(II) and Zn(II) ions: adsorption mechanisms, Submitted to Industrial and Engineering Chemistry Research.

4.   Velazquez-Jimenez Litza Halla, Vences-Alvarez Esmeralda, Flores-Arciniega Jose Luis, Rangel-Mendez Jose Rene; Metal oxides/hydroxides/oxyhydroxides, and mixed metal oxides for water defluoridation. In preparation.

6.4 ATTENDANT TO CONFERENCES

•   2o. Congreso Interdisciplinario de Posgrados, IPICYT. "Carbón activado modificado con Zr(IV): una alternativa para remover fluoruro del agua potable". October 3-4, 2013, San Luis Potosí, S.L.P., Mexico.

•   Annual World Conference on Carbon. "Adsorption mechanism of fluoride in zirconium-impregnated activated carbon". July 14-19, 2013, Rio de Janeiro, Brazil.

•   International Water Association, Young Water Professionals, IWA-Mexico 2013. "Fluoride removal by using zirconium impregnated activated carbon". April 24-26, 2013, San Luis Potosí, S.L.P., México.

•   International Annual World Conference on Carbon, con el cartel: "Zirconium modified activated carbon materials for water defluoridation". June 17-22, 2012, Krakow, Poland.

•   1er. Congreso Interdisciplinario de Posgrados, IPICYT." Estudio de la modificación química del bagazo de Agave salmiana en la captación de Cd(II), Pb(II) y Zn(II) en soluciones acuosas". November 18, 2011, San Luis Potosí, S.L.P., México.

- 1st International Symposium on Agave and 29th International Specialized Symposium on yeast. "Effect of chemical modification of agave bagasse on heavy metal biosorption". August 29-September 2, 2011, Guadalajara, Jalisco, México.

REFERENCES

1. WHO, Guidelines for drinking water quality, 4rd ed. World Health Organization, Geneva, 2011.

2. Hawkes S.J.; What is a heavy metal? J. Chem. Educ. 74 (1997) 1374-1377.

3. Ochiai E.; Toxicity of heavy metals and biological defense, J. Chem. Edu. 72 (1995) 479-484

4. Jarüp L.; Hazards of heavy metal contamination, British Med. Bull. 68 (2003) 167-182.

5. O'Connell D.W., Birkinshaw C., O'Dwyer T.F.; Heavy metals adsorbents prepared from the modification of cellulose: a review, Biores. Technol. 99 (2008) 6709-6724.

6. SEMARNAT, NOM-001-ECOL-1996.

7. SEMARNAT, NOM-002-SEMARNAT-1996.

8. SSA, NOM-127-SSA1-1994.

9. EPA, National Primary Water Regulations in EPA 40 CFR Parts 141-143. Environmetal Protection Agency, USA, 1991.

10. Prasher S.O., Beaugeard M., Hawari J., Bera P., Patel R.M., Kim S.H.; Biosorption of heavy metals by red algae (Palmaria palmate), Environ. Technol. 25 (2004) 1097-1106.

11. Gosh A., Mukherjee K., Gosh S.K., Saha B.; Sources and toxicity of fluoride in the environment, Res. Chem. Intermed. 39 (2013) 2881-2915.

12. Doull J., Boekelheide K., Farishian B.G., Isaacson R.L. , Klotz J.B., Kumar J.V.; Fluoride in drinking water: a scientific review of EPA's standards, Committee on Fluoride in Drinking Water, Board on Environmental Studies and Toxicology, Division on Earth and Life Sciences, National Research Council of the National Academies, National Academies Press, Washington, D.C. 2006.

13. Ozsvath D. L.; Fluoride and environmental health: a review, Rev. Environ. Sci. Technol. 8 (2009) 59-79.

14. Dey S., Goswami S., Gosh U.C.; Hydrous ferrix oxide (HFO)-A scavenger for fluoride from contaminated water, Water Air Soil Poll. 158 (2004) 311-323.

15. UNICEF; WaterFront, Fluoride in water: an overview, Programme Division, 13 (1999) 11-14.

16. Mohapatra M., Anand S., Misha B.K., Giles D.E., Singh P.; Review of fluoride removal from drinking water, J. Environ. Man. 91 (2009) 67-77.

17. Ayoob, S., Gupta A.K., Bhat V.T.; A conceptual overview on sustainable technologies for the defluoridation of drinking water, Critical Rev. Environ. Sci. Technol. 38 (2008) 401-470.

18. Yang R.T.; Adsorbents: fundamentals and applications, ed. Wiley, USA, 2003.

19. Gardea-Torresday, J.L., Tiemann K.J., Armendariz V., Bess-Oberto L., Chianelli R.R., Rios J., Parson J.G., Gamez G.; Characterization of chromium (VI) binding reduction to chromium (III) by the agricultural byproduct of Avena monida (oat) biomass, J. Haz. Mat. B 80 (2000) 175-188.

20. Montanher S.F., Oliveira E.A., Rollemberg M.C.; Removal of metal ions from aqueous solutions by sorption onto rice bran, J. Haz. Mat. B 117 (2005) 207-211.

21. Murugan M., Subramanian E.; Studies on defluoridation of water by Tamarind seed, an unconventional biosorbents, J. Water Health 4 (2006) 453-461.

22. Asgaria G., Roshanib B., Ghanizadeh G.; The investigation of kinetic and isotherm of fluoride adsorption onto functionalized pumice stone, J. Haz. Mat. 217 (2012) 12-132.

23. Zouboulis A.I., Kydros K.A.; Use of red mud for toxic metals removal: the case of nickel, J. Chem. Technol. Biotechnol. 58 (1993) 95-101.

24. Tor A., Danaoglu N., Arslan G., Cengeloglu Y.; Removal of fluoride from water by using granular red mud: batch and column studies, J. Haz Mat. 164 (2009) 271-278.

25. Dimitrova S.V.; Metal sorption on blast furnace slag, Water Res. 30 (1996) 228-232.

26. Moges G., Zewge F., Socher M.; Preliminary investigation on the defluoridation of water using fires clay chips, J. African Earth Sci. 22 (1996) 479-482.

27. Wilson W., Yang H., seo C.W., Marshhall W.E.; Select metal adsorption by activated carbon made from peanut shells, Biores. Technol. 97 (2006) 2266-2270.

28. Ramos R.L., Ovalle-Turrubiartes J., Sanchez-Castillo M.A.; Adsorption of fluoride from aqueous solution on aluminium-impregnated carbon, Carbon 37 (1999) 609-617.

29. Puka L.R.; Fluoride adsorption modeling and the characterization of clays for defluoridation of natural waters, MSc dissertation, Faculty of Science, Rand Afrikaans University.
http://etd.rau.ac.za/theses/available/etd-08172004120118/restricted/Abstract.pdf.

30. Vengris T., Binkiene R., Sveikauskaite A.; Nickel, copper and zinc removal from wastewater by a modified clay sorbent, Appl. Clay Sci. 18 (2000) 183-190.

31. Miretzky P., Cirelli Fernandez A.; Fluoride removal from water by chitosan derivatives and composites: a review, J. Fluorine Chem. 132 (2011) 231-240.

32. Rorrer G.L., Hsien T.Y., Way J.D.; Synthesis of porous-magnetic chitosan beds for removal of cadmium ions from wastewater. Ind. Eng. Chem. Res. 32 (1993) 2170-2178.

33. Volesky B.; Potential of biosorption, Sorption and Biosorption, BV Sorbex Inc., Montreal-St. Lambert, Que., Canada, 2003.

34. Cochrane E.L., Lu S., Gibb S.W., Villaescusa I.; A comparison of low-cost biosorbents and comercial sorbents for the removal of copper of aqueous media, J. Haz. Mat. B137 (2006) 198-206.

35. Bailey, S.E, Olin T.J., Bricka M.,Adrian D.D.; A review of potentially low-cost sorbents for heavy metals, Wat. Res. 33 (1999) 2469-2479.

36. Sud D., Mahajan G., Kaur M.P.; Agricultural waste material as potential adsorbent for sequestering heavy metal ions from aqueous solutions- A review, Biores. Technol. 99 (2008) 6017-6027.

37. Figure modified from http://www.smartplanet.com/blog/intelligent-energy/could-cow-guts-help-expand-the-biofuel-industry/. Accessed on November 19, 2013.

38. Hendriks A.T.W.M., Zeeman G.; Pretreatments to enhance the digestibility of lignocellulosic biomass, Biores. Technol. 100 (2009) 10-18.

39. Kumar P., Barret D.M., Delwiche M.J., Stroeve P.; Methods for pretreatment of lignocellulosic biomass for efficient hydrolysis and biofuel production, Ind. Eng. Chem. Res. 48 (2009) 3713-3729.

40. Perez J., Dorado J.M., Rubia T.D., Martinez J.; Biodergadation and biological treatment of cellulose, hemicellulose and lignin: an overview, Int. Microbiol. 5 (2002) 53-63.

41. Krishnani K.K., Ayyappan S.; Heavy metals remediation of water using plants and lignocellulosic agrowastes, Rev. Environ. Contam. Toxicol. 188 (2006) 59-84.

42. Ngah W.S.W., Hanafiah M.A.K.M.; Removl of heavy metal ions from wastewater by chemically modified plant wastes as adsorbents: a review, Biores. Technol. 99 (2008) 3935-3948.

43. Gardea-Torresday J.L., de la Rosa G., Peralta-Vide J.R.; Use of phytofiltration technologies in the removal of heavy metals: review, Pure Appl. Chem. 76 (2004) 801-813.

44. Rowell R.M.; Chemical modification of agricultural fibers for property enhanced composites, in Olesen et al. eds. Research in industrial application of non food drops,

I: plant fibers: Proceedings of a seminar; Denmark Academy of Technical Sciences, May 1995, 49-70.

45. Gadd G.M.; Biosorption: critical review of scientific rationale, environmental importance and significance for pollution treatment, J. chem. Technol. Biotechnol. 84 (2009) 13-28.

46. Igwe J.C.; Abia A.A.; A bioseparation process for removing heavy metals from waste water using biosorbents, African J., biotechnol. 5 (2006) 1167-1179.

47. Bansal R.C., Goyal M.; Activated carbon adsorption, Francis&Taylor, USA, 2005.

48. Mohan D., Pittman C.R. Jr.; Activated carbons and low cost adsorbents for remediation of tri-and hexavalent chromium from water, J. Haz. Mat. B137 (2006) 762-811.

49. Dias J.M., Alvim-Ferraz M.C.M., Almeida M.F., Rivera-Utrilla J, Sáchez-Polo M.; Waste materials for activated carbon preparation and its use in aqueous-phase treatment: a review, J. Environ. Man. 85 (2007) 833-846.

50. Marsh H., Rodrigues-Reinoso F.; Activated carbon, Elsevier Science&Tecnology Books, 2006.

51. Bandosz T.J., Activated Carbon surfaces in environmental remediation, Elsevier, New York, USA, 2006.

52. Montes-Moran M.A., Súarez D., Menéndez J.A., Fuente E.; On the nature of basic sites on carbon surfaces: an overview, Carbon 42 (2004) 1219-1225.

53. Yin C.Y., Aroua M.K., Daud W.M.A.W.; Review of modifications of activated carbon for enhancing contaminant uptakes from aqueous solutions.

54. Puttamraju P. SenGupta AK. Evidence of tunable on-off sorption behaviours of metal oxide nanoparticles: role of ion exchange support. Ind. Eng. Chem. Res. 45 (2007) 7737-7742.

55. Jolivet, J.P., Henry M., Livage J.; Metal oxide chemistry and synthesis: from solution to solid state. New York, John Wiley, 2000.

56. Adhoum N., Monser L.; Removal of cyanide from aqueous solution using impregnated activated carbon, Chem. Eng. Process. 41 (2002) 17–21.

57. Huang C.P., Vane L.M.; Enhancing As^{5+} removal by a Fe^{2+}—treated activated carbon, J. Water Pollut. Contam. Fed. 61 (1989) 1596–1603.

58. Leyva Ramos R., Ovalle-Turrubiartes J., Sanchez-Castillo M.A.; Adsorption of fluoride from aqueous solution on aluminium-impregnated carbon, Carbon 37 (1999) 609–617.

59. Sverjensky D.A., Fukushi K.; Anion adsorption on oxide surface: inclusion of water dipole in modeling the electrostatic of ligands Exchange. Environ. Sci. Technol. 40 (2006) 263-271.

60. Lagergren S.; About the theory of so-called adsorption of soluble substances, Kungl. Sven. Veterskopskada Handl. 24 (1898) 1-39.

61. Ho Y.S., Ng D.H.L.; Kinetic models for the sorption of dye from aqueous solution by wood. Process Saf. Environ. Prot. 76 (1998) 183-191.

62. Weber W.J., Morris J.C.; Kinetic of adsorption on carbon from solution, J. Sanit. Eng. Div. Am. Soc. Civ. Eng. 89 (1963) 31-59.

63. Chakrapani C.H., Babu C.H. S., Vani K.N.K., Rao K.S.; Adsorption kinetics of the removal of fluoride form aqueous solution by activated carbon adsorbents derived from the peel of selected citrus fruits, E-J. Chem. 7 (2010) S419-S472.

64. Sawalha M.F., Peralta-Videa J.R., Saupe G.B., Dokken K.D., Gardea-Toresday, J.L.; Using FTIR to corroborate the identity of functional groups involved in the binding of Cd and Cr to saltbush (Atriplex canescens) biomass, Chemosphere 66 (2007) 1424-1430.

65. Sanchez-Silva L., López-Gonsález D., Villaseñor J., Sánchez P., Valverde J.L.; Thermogravimetric-mass spectrometric analysis of lignocellulosic and marine biomass pyrolisis, Biores. Technol. 109 (2012) 163-172.

66. Martínez-Gutierrez G.A., Iñiguez-Covarrubias G., Ortiz-Hernandez Y.D., López-Cruz J.Y., Bautista-Cruz M.A.; Tiempos de apilado del bagazo del maguey mezcalero y su efecto en las propiedades del compost para sustrato de tomate, Rev. Int. Contam. Ambie. 29 (2013) 209-216.

67. Devaprasath P.M., Solomon J.S., Thomas B.V.; Removal of Cr(VI) from aqueous solution using natural plant material. J. Appl. Sci. Environ. Sanitation 2, (2007) 77-83.

68. Garg U., Kaur M.P., Jawa G.K., Sud D., Garg V.K., 2008. Removal of cadmium(II) from aqueous solutions by adsorption on agricultural waste biomass. J. Haz. Mat. 154 (2008) 1149-1157.

69. Lee B.G., Rowell R.M.; Removal of heavy metal ions from aqueous solutions using lignocellulosic fibers. J. Nat. Fibers 1 (2004) 97-108.

70. Miretsky P., Fernandez Cirelli A.; Cr(VI) and Cr(III) removal from aqueous solution by raw and modified lignocellulosic materials: A review, J. Haz. Mat.180 (2010) 1-19.

71. Zhu B., Fan T., Zhang D.; Adsorption of copper ions from aqueous solution by citric acid modified soybean straw, J. Haz. Mat. 153 (2008) 300-308.

72. Garcia-Reyes R.B., Rangel-Méndez J.R., Alfaro-De la Torre M.C.; Chromium (III) uptake by agro-waste bisorbents: chemical characterization, sorption-desorption studies, and mechanism, J. Haz. Mat. 170 (2009) 845-854.

73. Garcia-Reyes R.B., Rangel-Méndez J.R.; Contribution of agro-waste material main components (hemicelluloses, cellulose and lignin) to the removal of chromium (III) from aqueous solution, J. Chem. Technol. Biotechnol. 84 (2009) 1533-1538.

74. Fourest E., Volesky B.; Contribution of sultanate groups and alguinate to heavy metal biosorption by the dry biomass of Sargassum fruitans. Environ. Sci. Technol. 30 (1996) 277-282.

75. Wong K.K., Lee C.K., Low K.S., Haron M.J.; Removal of Cu and Pb by tartaric acid modified rice husk from aqueous solutions. Chemosphere 50 (2003) 23-28.

76. Silverstein R.M., Webster F.X., Kiemle D.J., 2005. Spectrometric identification of organic compounds. Fifth ed. John Wiley & Sons, New York.

77. Chen J.P., Yang L.; Study of a heavy metal biosorption onto raw and chemically modified Sargassum sp. via spectroscopic and modeling analysis. Langmuir 22 (2006) 8906-8914.

78. Socrates G.; Infrared and Raman characteristics group frequencies. Tables and Charts, third ed. John Wiley & Sons, United Kingdom, 2004.

79. Skoog D.A., West D.M. Holler F.J., Crouch, S.R.; Química analítica, seventh ed. McGraw Hill, Mexico, 2001.

80. Murphy V., Hughes H., McLoughlin P.; Cu(II) binding by dried biomass of red, green and brown macroalgae. Water Res. 41(2007) 731-740.

81. Naja G., Mustin C., Volesky B., Berthelin J.A.; A high-resolution titrator: a new approach to studying binding sites of microbial biosorbents. Water Res. 39 (2005) 579-588.

82. Liu Y., Wang J.; Fundamentals and applications of biosorption isotherms, kinetics and thermodynamics. Nova Science, New York, 2009.

83. Texeira Tarley C.R., Zezzi Arruda M.A.; Biosorption of heavy metals using rice milling by-products. Characterisation and application for removal of metals from aqueous effluents. Chemosphere 54 (2001) 987-995.

84. Niober E., McBryde W.A.E.; Free-energy relationships in coordination chemistry. III. A comprehensive index to complex stability. Can. J. Chem. 51 (1973) 2512-2524.

85. Li X., Tang Y., Cao X., Lu D., Luo F., Shao W.; Preparation and evaluation of orange peel cellulose adsorbent for effective removal of cadmium, zinc, cobalt and nickel. Colloids Surf. A. 317 (2008) 512-521.

86. Sawalha M., Peralta-Videa J.R., Duarte-Gardea M., Gardea-Torresday J.L.; Removal of cooper, lead and zinc from contaminated water by saltbush biomass: analysis of the optimum binding, stripping, and binding mechanism. Biores. Technol. 99 (2008) 4438-4444.

87. Basso M.C., Cerrella E.G., Cukierman A.L.; Lignocellulosic materials as potential biosorbents of trace toxic metals from wastewater, Ind. Eng. Chem. Res. 41 (2002) 3580-3585.

88. Krishnani K.K., Meng X., Dupont L.; Metal binding onto lignocellulosic biosorbent. J. Envrion. Sci. Health A. 44 (2009) 688-699.

89. Smith M.B., March, J.; March's Advanced Organic Chemistry, sixth ed. John Wiley & Sons, New Jersey, 2007.

90. Velazquez-Jimenez L.H., Pavlick A., Rangel-Mendez J.R.; Chemical characterization of raw and treated agave bagasse and its potential as adsorbent of metal cations from water, Ind. Crops Prod. 43 (2013) 200-206.

91. Hubbe M.A., Hasan S.H., Ducoste J.J.; Cellulosic substrate for removal of pollutants from aqueous systems: a review. 1. Metals, Bioresources 6 (2011) 2161-2287.

92. Komarek A.R.; An improved filtering technique for the analysis of neutral detergent fiber and acid detergent fiber utilizing the filter bag technique, J. Anim. Sci. 71 (2003) 824-829.

93. Van Soest P.J.; Use of detergents in the analysis of fibrous feeds. II. A rapid method for the determination of fiber and lignin, J. Assoc. Off. Agric. Chem. 46 (1963) 829-285.

94. Gentry H.S.; Agaves of Continental North America, The University of Arizona Press, USA, 2003.

95. Chen Y., Sun, L., Negulescu, I.I., Moore, M.A., Collier B.J.; Evaluating efficiency of alkaline treatment for waste bagasse, J. Macromolec. Sci. 44 (2005) 397-411.

96. Raveendran K., Ganesh, A., Khilar, K.C.; Pyrolysis characteristics of biomass and biomass components, Fuel 75 (1996) 987-988.

97. Chavez-Guerrero L., Hinojosa M.; Bagasse from mezcal industry as an alternative renewable energy produced in arid lands, Fuel 89 (2010) 4049-4052.

98. Nieto-Delgado C., Terrones M., Rangel-Mendez J.R.; Development of highly micoporous activated carbon from the alcoholic beverage industry organic by-products, Biomass and Bioenergy 35 (2011) 103-112.

99. Wörmeyer K., Ingram, T., Saake, B., Brunner, G., Smirnova, I.; Comparison of different pretreatment methods for lignocellulosic materials. Part II: influence of pretreatment on the properties of rye straw lignin, Biores. Technol. 102 (2011) 4157-4164.

100. Mayer Z., Apfelbacher, A., Hornung, A.; A comparative study on the pyrolisis of metal- ans ash-enriched wood and the combustion properties of the gained char, J. Anal. Appl. Pyrol. 96 (2012) 196-202.

101. Ozsvath, D.L. Fluoride and environmental health: a review. Rev. Environ. Sci. Technol. 8 (2009) 59-79.

102. Tripathy S.S., Raichur A.M.; Abatement of fluoride from water using manganese dioxide-coated activated alumina. J. Haz. Mat. 153 (2008) 1043-1051.

103. Ku Y., Chiou H.M.; The adsorption of fluoride ion from aqueous solution by activated alumina. Water Air Soil Pollut. 133 (2002) 349-360.

104. Srimurali M., Pragathi A., Karthikeyan J.; A study on removal of fluorides from drinking water by adsorption on to low-cost materials. Environ. Pollut. 99 (1998) 285-289.

105. Gopal K., Srivastava S.B., Shukla S., Bersillon J.L.; Contaminants in drinking water and its mitigation using suitable adsorbents: an overview. J. Environ. Biol. 2 (2004) 1-10.

106. Bower C.A., Hatcher J.T.; Adsorption of fluoride from aqueous solution by soils and minerals. J. Soil Sci. 3 (1967) 151-154.

107. Abe I., Iwasaki S., Tokimoto T., Kawasaki N., Nakamura T., Tanada S.; Adsorption of fluoride ion onto carbonaceous materials. J. Colloid Interface Sci. 275 (2004) 35-39.

108. Li Y.H., Wang S., Zhang X., Wei J., Xu C., Luan Z., Wu D.; Adsorption of fluoride from water by aligned carbon nanotubes. Mat. Res. Bull. 38 (2003) 469-476.

109. Raichuir A.M., Basu M.J.; Adsorption of fluoride onto mixed rare earth oxides. Sep. Purif. Technol. 124 (2001) 121-127.

110. Mahmood S.J., Taj F., Parveen F., Usmani T.H., Azmat R., Uddin F.; Arsenic, fluoride and nitrate in drinking water: the problem and its possible solution. Res. J. Eviron. Sci. 1 (2007) 179-184.

111. Krupadam R.J., Khan M.S., Das S.; Adsorption of fluoride from water by surface-functionalized polyurethane foam. Water Sci. Technol. IWA 2010, 62.4, 759-765.

112. Liao X.P., Shi B.; Adsorption of fluoride on zirconium(IV)-impregnated collagen fiber. Environ. Sci. Technol. 39 (2005) 4628-4632.

113. Li Z., Deng S., Zhang X., Zhou W., Huang J., Yu G.; Removal of fluoride from water using titanium-based adsorbents. Front. Environ. Sci. Eng. China 4 (2010) 414-420.

114. Fang L., Ghimiere K.N., Kuriyanna M., Inoue K., Makino K.; Removal of fluoride using some lanthanum (III)-loaded adsorbents with different functional groups and polymer matrices. J. Chem. Technol. Biotechnol. 78 (2003) 1038-1047.

115. Chen N., Zhang Z., Feng C., Li M., Zhu D., Sugiura N.; Studies on fluoride adsorption of iron-impregnated granular ceramics from aqueous solutions. Mat. Chem. Phys. 125 (2011) 293-298.

116. Janardhana C., Rao N.G., Sathish R.S., Lakshman V.S.; Study on the defluoridation of drinking water by impregnation of metal ions in activated charcoal. Indian J. Chem. Technol. 13 (2006) 414-416.

117. Schmidt G.T., Vlasova N., Zuzaan D., Kersten M., Daus B.; Adsorption mechanism of arsenate by zirconyl-functionalized activated carbon. J. Coll. Inter. Sci. 317 (2008) 228-234.

118. Biswas B.K., Inoue J., Inoue K., Ghimire K.N., Harada H., Ohto K., Kawakita H.; Adsorptive removal of As(V) and As(III) from water by a Zr(IV)-loaded orange waste gel. J. Haz. Mat. 154 (2008) 1066-1074.

119. Zheng Y.M., Lim S.F., Chen J.P.; Preparation and characterization of zirconium-based magnetic sorbent for arsenate removal. J. Coll. Interf. Sci. 338 (2009) 22-29.

120. Sandoval R., Cooper A.M., Aymar K., Jain A., Hristovsi K.; Removal of arsenic and methylene blue from water by granular activated carbon media impregnated with zirconium dioxide nanoparticles. J. Haz. Mat. 193 (2001) 296-303.

121. Sathish R.S., Raju N.S.R., Raju G.S., Rao N., Kumar K.A., Janardhana C.; Equilibrium and kinetic studies for fluoride adsorption from water on Zirconium impregnated coconut shell carbon. Sep. Sci. Technol. 42 (2007) 769-788.

122. Pettibone J.M., Cwiertny D.M., Sherer M., Grassian V.H.; Adsorption of organic acids on TiO_2 nanoparticles: effects of pH, nanoparticle size, and particle aggregation. Langmuir 24 (2008) 6659-6667.

123. Ketabi S.A., Kazemi A.S., Bagheri-Mohagheghi M.M.; The effect of complexing agent on the crystallization of ZnO nanoparticles. J. Phys. 77 (2011) 679-688.

124. Cordero T., Chovelon J.M., Duchamp C., Ferronato C., Matos J.; Surface nano-aggregation and photocatalytic activity of TiO_2 on H-type activated carbons. Appl. Catal. B: Environ. 73 (2007) 227-235.

125. Matos J., Hofman M., Pietzrak R.; Synergy effect in the photocatalytic degragation of methylene blue on a suspended mixture of TiO_2 and N-contianing carbons. Carbon, 54 (2013) 460-471.

126. Sathish R.S., Sairam S., Raja V.G., Rao G.N., Janardhana C.; Defluoridation of water using zirconium impregnated coconut fiber carbon. Sep. Sci. Technol. 43 (2008) 3676-3694.

127. Hernández-Montoya V., Ramirez-Montoya L.A., Bonilla-Petriciolet A., Móntes-Morán M.A.; Optimizing the removal of fluoride from water using new carbons obtained by modification of nut shell wit calcium solution from egg shell. Biochem. Eng. J. 62 (2012) 1-7

128. Venable F.P.; Zirconium and its compounds, American Chemical Society, The chemical catalog company Ed. New York: USA, 1922.

129. Vitela-Rodriguez A.V., Rangel-Mendez J.R.; Arsenic removal by modified activated carbon with iron hydro(oxide) nanoparticles. J. Environ. Manag. 114 (2013) 225-231.

130. Swain S.K., Patnaik T., Singh V.K., Jha U., Patel R.K., Dey R.K.; Kinetics, equilibrium and thermodynamic aspects of removal of fluoride from drinking water using meso-structured zirconium phosphate. Chem. Eng. J. 171 (2011) 1218-1226.

131. Guo G.Y., Chen Y.L.; New Zirconium Hydroxide. J. Mater. Sci. 39 (2004) 4039-4043.

132. Chitrakar R., Tezuka S., Sooda A., Sakane K., Ooi K., Hirotsu T.; Selective adsorption of phosphate from seawater and wastewater by amorphous zirconium hydroxide. J. Coll. Inter. Sci. 97 (2006) 426-433.

133. Duo X., Mohan D., Pittman C.U., Yang S.; Remediating fluoride form water using zirconium oxide. Chem. Eng. J. 198 (2012) 236-245.

134. Jere G.V., Santhamma M.T.; IR and laser Raman Studies on peroxo fluoro species of zirconium. Inorg. Chim. Acta 24 (1977) 57-61.

135. Hansen D.M., Albaugh C.E., Moran P.D., Kuech T.F.; Chemical investigations of Ga As wafer bonded interfaces. J. Appl. Phys. 90 (2001) 5991-5999.

136. Hristovsi K.D., Westerhoff P.K., Crittenden J.C., Olson L.W.; Arsenate removal by nanostructured ZrO_2 spheres. Environ. Sci. Technol. 42 (2008) 3786-3790.

137. Qunbo F., Fuchi W., Huiling Z., Feng Z.; Study of ZrO_2 phase structure and electronic properties, Molecular Simulation. 34 (2008) 1099-1103.

138. Wulfsberg G.; Inorganic Chemistry, University Science Books, U.S.A, 2000.

139. Barr T.L.; An ESCA study of termination of the passivation of elemental metals. J. Phys. Chem. 82 (1978) 1801-1810.

140. Dillard J.D., Taylor L.T., Seals R.D., Alexander R.; Core electron binding energy study of Group IIb-VIIa compounds. Inor. Chem. 12 (1973) 2485-2487.

141. Okpalugo T.I.T., Papakonstantinou P., Murphy H., McLaughlin J., Brown N.M.D.; High resolution XPS characterization of chemical functionalized MWCNTs and SWCNTs. Carbon 43 (2005) 153-161.

142. Balazs D.J., Triandafillu K., Chevolot Y., Aronsson B.O., Harms H., Descouts P., Mathieu H.J.; Surface Modification of PVC endotracheal tubes by oxygen discharge to reduce bacterial adhesion. Surf. Inter. Anal. 35 (2003) 301-309.

143. Lee W.H., Kim S.J., Lee W.J., Lee J.G., Haddon R.C., Reucroft P.J.; X-ray photoelectron spectroscopy studies of surface modified single-walled carbon nanotube materials. Appl. Surf. Sci. 181 (2001) 121-7.

144. Martinez M.T., Callejas M.A., Benito A.M., Cochet M., Seeger S., Anson A. Schreiber J.; Sensitivity of single wall carbon nanotubes to oxidative processing: structural modification, intercalation and functionalization. Carbon 41 (2003) 2247-2256.

145. Liu B., Hu J., Ford J.S.; Electrochemical deposition of zirconia films on diamond electrodes. Electrochem. Solid-State Lett. 14 (2011) D20-D22.

146. Ebert H., Knecht M., Muhler M., Helmer O., Bensch W.; Experimental and theoretical band structure of the layer compound ZrSiTe. J. Phys. Chem. 99 (1995) 3326-3330.

147. Koji M., Ohgai M.; Formation mechanism of hydrous zirconia particles produced by the hydrolysis of $ZrOCl_2$ solutions: III, kinetics study for the nucleation and crystal-growth processes of primary particles. J. Am Ceram. Soc. 84 (2001) 2303-2312.

148. Cotton F.A., Wilkinson G.; Advanced Inorganic Chemistry, 5th, ed.; Wiley: USA, 1998.

149. Chefetz B., Moninski L., Pinchas M., Ginsburg T., Elmachli S., Tel-Or E., Gedanken A.; New approach for the removal of metal ions from water: adsorption onto aquatic plants and microwave reaction for the fabrication on nanometals, J. Phys. Chem. B., 109 (2005) 15179-15181.

150. Carrillo-Rivera J.J., Cardona A., Edmunds W.M.; Use of abstraction regime and knowledge of hydrogeological conditions to control high-fluoride concentration in abstracted groundwater: San Luis Potosi basin, Mexico, J. Hydrology 261 (2002) 24-47.